

Copyright
by
Jorge Wong
2007

**The Dissertation Committee for Jorge Wong Certifies that this is the approved
version of the following dissertation:**

Bead Based Microreactors for Sensing Applications

Committee:

John T. McDevitt, Supervisor

Jennifer S. Brodbelt

Christine Schmidt

Jonathan L. Sessler

Jason B. Shear

Bead Based Microreactors for Sensing Applications

by

Jorge Wong, B.S.

Dissertation

Presented to the Faculty of the Graduate School of

The University of Texas at Austin

in Partial Fulfillment

of the Requirements

for the Degree of

Doctor of Philosophy

The University of Texas at Austin

May, 2007

Dedication

In honor and in loving memory to Han Lin

Bead Based Microreactors for Sensing Applications

Publication No. _____

Jorge Wong, Ph. D.

The University of Texas at Austin, 2007

Supervisor: John T. McDevitt

The dissertation research described here focuses on the fabrication and modification of the polymeric beaded sensing elements, one of the many critical components of a Microbead Array Chip-Based Multianalyte Detection System. Detection of biomolecules including proteins and oligonucleotides are based on affinity interactions between carefully selected ligands immobilized on the sensing microspheres. The current work relies on microspheres made of agarose gel shaped into micron sized beads with intrinsic porosity associated to the concentration of agarose in the gel. The beaded material described is considered of a homogeneous nature with limited transport capabilities although superior to homogeneous latex beads. The microbead array system potentially benefits from structural modifications on the sensing elements and includes improvement on the mobile phase mass transport, capture of larger particles, faster assays, and the increase in

the multiplexing capabilities. Efforts are also directed to preferentially modify gels made of agarose to facilitate the transition from the existing sensing elements to the new beaded designs made of the same polysaccharide. As a result the chemistry utilized to attach affinity ligands to procure reactive sensing elements remained practically the same. Collectively, these research activities have resulted in a number of novel polymer-based reactive particles that have the potential to service a variety of new sensing applications.

Table of Contents

Chapter 1: Bead Based Solution Phase Multianalyte Detection System.....	1
1.1 Overview.....	1
1.2 Multianalyte Detection Platforms.....	3
1.3 The chip-based multianalyte detection system.....	17
1.4 Summary and Dissertation Overview.....	23
Chapter 2: Designing Beads Structures for the Chip Based Multianalyte System Technology	26
2.1 Overview.....	26
2.2 Background Introduction	27
2.2.1 Affinity Chromatography	27
2.2.2. Polymeric Matrices an Essential Component in the Chip Based Multi-analyte Detection System	35
2.2.3 Agarose Gels.....	38
2.3 Experimental.....	48
2.3.1 Reagents.....	48
2.3.2 Methods and Instrumentation	48
2.3.3 Preparation of 2% Homogeneous agarose beads 250-280 μ m diameter size.	49
2.3.4 Preparation of 4% Superporous Agarose Beads.....	50
2.3.5 Crosslinking of Agarose Beads	50
2.3.6 Glyoxal Activation of Agarose Beads	51
2.3.7 Selection of Crosslinking Degree through C-Reactive Protein Assay.....	51
2.3 Results and Discussion	53
2.3.1 Preparation of Homogeneous Beaded Agarose Gels - Motivation.....	53

2.3.2 Size and Shape Description of Beaded Product	59
2.3.3 Parameters affecting the Size Distribution of beads.....	66
2.3.4 Chemical Modification of Homogeneous Beads: Selection of Crosslinking Degree	73
2.3.5 Superporous Agarose Beads - Motivation.....	81
2.3.6 Morphological Features of Superporous Agarose Beads	86
2.4 Summary.....	107
Chapter 3: Superporous and Homogeneous Agarose Beads on a Chip-Based Multianalyte Detection System. A Comparison on the Mass Transport Anatomy	
3.1 Introduction.....	110
3.2 Experimental Section.....	113
3.2.1 Reagents.....	113
3.2.2 Preparation of Homogeneous 4% Agarose Beads	113
3.2.3 Preparation of Superporous 4% Agarose Beads.....	114
3.2.3 Instrumentation and Methodologies	114
3.2.4 Kinetics Studies with CRP.....	115
3.2.5 Kinetics Studies with DNA	116
3.2.6 CRP ‘Sandwich’ Detection Test.....	116
3.3 Results and discussion	117
3.3.1 Fluorescence Signal Response Rate Comparison.....	123
3.3.2 CRP Dose Response Test.	126
3.3.3 Diffusion Rate Comparison.	128
3.4 Summary and Conclusions	140
Chapter 4: Multifunctional and Multicompartment Beads for Sensor Applications.....	
4.1 Introduction.....	142
4.2 Experimental.....	149
4.2.1 Methods and Instrumentation	149
4.2.2 Reagents.....	149

4.2.3 Core-Shell Beads	150
4.2.4 Raspberry-Type Beads.....	152
4.2.5 Macroporous Polystyrene Beads	152
4.2.6 Homogeneous Agarose Beads: 20-32 μm	153
4.2.7 Avidin Functionalization of Agarose Beads.....	153
4.2.8 DNA Functionalization of 20-32 μm Agarose Beads	154
4.2.9 Agarose Beads with 20-32 μm Functionalized Agarose Inclusions.....	155
4.2.10 Sensor Application: Multiple Analyte Detection in Composite Beads Assay.....	156
4.3 Results and Discussion	157
4.3.1 Agarose in Agarose Core-Shell Beads	157
4.3.2 Polystyrene in Agarose Core-Shell Beads.....	163
4.3.3 Glass in Agarose Core-Shell Beads.....	167
4.3.4 Raspberry Coating Like.....	169
4.3.5 Macroporous Polystyrene Beads	171
4.3.6 Beads in Concentric Layers.....	174
4.3.7 Agarose Beads with 20-32 μm Randomly Dispersed Functionalized Agarose Inclusions.....	175
4.3.8 Protein Viability Test after Agarose Coating	178
4.3.9 Multiple Analyte Detection Assay on Multifunctional and Multicompartment Agarose Beads	180
4.4 Summary.....	203
References.....	205

Vita 213

Chapter 1: Bead Based Solution Phase Multianalyte Detection System

1.1 OVERVIEW

This introductory chapter is aimed to describe the role of polymeric microspheres in the development of solution phase multianalyte detection systems. Large advances including areas such as medicine, pharmacology, microbiology, home land defense and environmental science would be derived from the development of rapid array sensors with multiple analyte parallel detection capabilities. Over the past decade, the McDevitt group has sustained efforts that attempt to combine and adapt the tools of the nanomaterials and microelectronics for the practical implementation of miniaturized sensors that are suitable for a variety of important application areas. Here microbead arrays wherein micro-pits within a silicon wafer are populated with a variety of chemically sensitized bead “microreactors” have been created. Developed initially as an “electronic taste chip” system, this nano-bio-chip-based sensor platform has been adapted for a broad range of analyte classes including pH, electrolytes, metal cations, sugars, biological co-factors, toxins, proteins, antibodies, and oligonucleotides.¹⁻⁷

Created with many of the same microfabrication methods popularized by the electronics industry, such flexible sensor systems can be described as “chemical processing units”. More recently, the McDevitt group has pioneered a second class of miniaturized sensor system based on a membrane capture element that is integrated into a fluidics structure.⁸⁻¹⁰ These membrane microchip ensembles have

been adapted to service cell, spore, and bacteria separation and identification applications. These “cellular processing units” serve as miniaturized analysis systems that mimic flow cytometry instrumentation in their capacity to complete important cell counting applications.⁸

Importantly, the performance metrics of these miniaturized sensor systems have been shown to correlate closely with established macroscopic gold standard methods, making them suitable for use as subcomponents of highly functional detection systems for analysis of complex fluid samples. These efforts remain unique in terms of functional lab-on-a-chip (LOC) methods having a demonstrated capacity to meet or exceed the analytical characteristics (sensitivity, selectivity, assay variance, limit of detection) of mature macroscopic instrumentation for a variety of analyte systems including: pH, DNA oligonucleotides, metal cation, biological cofactors, and inflammation markers.¹⁻¹² In many cases, these mini-analysis systems show promise for use at the point-of-need, yet further reduction in analysis time would be required before this process is completed.

In an effort to improve further the time and analytical performance properties of the miniaturized sensor systems, an effort has been made to define new reactive polymer particles that can be used for the rapid capture and sensitive detection of a variety of analytes. Likewise, this dissertation focuses on the development of new bead-based ensembles that have the potential to be used in a variety of solution phase analytical applications. The goals of this dissertation are to develop new sensor ensembles that can be used to sequester analytes from microfluidic streams with high effectiveness. Since many future point-of need

sensor applications will require rapid analysis times, it is desirable to also be able to control the rate of the various steps. Thus, the second goal of this program is to explore various strategies for enhancing the transport of reagents and capture of the same. Third, the dissertation strives to achieve a molecular-level insight into the processes that occur within the confines of the bead sensor ensembles. This insight will be used to craft a new generation of reactive particles that can be used as a tool set to open up new options for sensing applications as well as to improve the performance of existing systems with respect to analysis time, capture surface area, sensitivity and selectivity. This initial chapter will provide an introduction to the key concepts that will be used later in the dissertation. Important here will be a discussion of the various prior bead-based assay systems. Finally, the chapter will end with a discussion of the specific content of the various chapters that will cover different themes related to the development and refinement of high functionality bead-based sensor ensembles.

1.2 MULTINANALYTE DETECTION PLATFORMS

Bead-based analytical techniques were introduced to the medical diagnostics technology date as early as 1956 when Singer and Plotz performed immunological assays with the Reumathoid factor on a suspension of sensitized latex microparticles. The Reumathoid factor induced the development of latex aggregates which were visible by naked eye. The results on Singer and Plotz early assays conduced to a powerful technique to be used in the decades to follow for the

detection of cancer, a diverse variety of infectious diseases and even the identification of substances such as drugs.

In a typical Latex Agglutination Test (LAT), the microspheres are coated with an antibody via adsorption or covalent immobilization. If the complementary antigen is present in the solution to be analyzed the coupling between antigen and antibody occurs. The antigen acts as a crosslinking agent between latex particles inducing the agglutination process, Figure 1.1. Evaluation of the test result is done by direct visual observation or by light scattering techniques such as turbidimetry and nephelometry, which provide information on the incident light intensity loss during scattering due to the presence of solid dispersed matter in solution.¹³ Additionally, with the introduction of dyed microspheres colorimetric detection was shown to be possible with LATs.

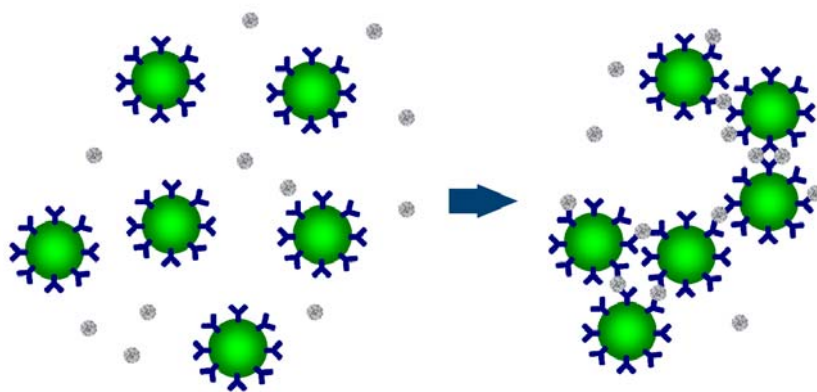


Figure 1.1. Schematic representation of agglutination of latex microspheres pre-coated with capturing ligand. The addition of polyvalent antigen molecules with specific affinity for the ligand induces the aggregation of the microspheres. The degree of aggregation can be measured by light scattering techniques.

Today many commercial LATs are available including tests for pregnancy and drug screens. The utilization of dyed microspheres facilitated the assay evaluation by direct visual observation adding also some limited capacity for multiple analyte detection (MAD) using different color spheres. The detection of multiple analytes with colorimetric LAT has been demonstrated on the discrimination of *Salmonella* strains where different antigen groups of the infectious disease were attached to different colored particles. The aggregation of colored particles are observed against a contrasting background color allowing the qualitative identification of a specific strain of the infectious disease of interest.¹⁴

Although some minimal amount of multiplexing is feasible in LATs, the synergistic dependence of latex microparticles to form bigger agglutinates makes the technique not practical for the simultaneous detection of analytes of different nature. The main difficulty here lies on the non-specific agglutination induced by the presence of substances within the mixture to be analyzed. Substances in the mixture, in addition to the analyte of interest, can cause agglutination. Such substances can also inhibit the agglutination. Thus, the result is either a false positive or false negative assay result. Each successful LATs available has been optimized individually for an specific analyte target and the non-specific interferences eliminated or their effect minimized. Any additional treatment to the test sample results frequently in a reduction on sensitivity and accuracy of the assay. Additionally, variations on the pH and ionic strength on the coated particles suspension also reduces the colloidal stability inducing self-aggregation in the

absence of the analyte of interest. This colloidal destabilization occurs even at pH and ionic strength close to physiological values.¹⁵

From the emerging solution-phase multianalyte detection systems the approach adopted by Diasorin, a company dedicated to the development of clinical diagnostics technology, through their Coupled particle light scattering (Copalis) multiplex technology, is the closest detection system to LATs design. Copalis utilizes an optical flow particle analyzer (flow cytometer) to measure changes in light scattering produced by latex agglutination due to immunochemical reaction. Single latex particles and aggregates are hydro-dynamically forced to travel individually through a finely focused laser beam, Figure 1.2. Low angle forward scatter light is collected with a photodiode, whereas a photomultiplier is positioned to collect wide angle light scatter. Light scatter profiles changes during agglutination providing the means to identify and quantify an analyte in the sample test.

The multiplexing capabilities of Copalis arise from the capacity to discriminate particle size as low as 0.1 μm . Thus, a combination of particles with different size can be mixed together for multianalyte detection. Different size particles are coated with different capturing moiety. The presence of a specific analyte is determined by monitoring the reduction of individual coated latex particles concentration due to analyte induced agglutination.

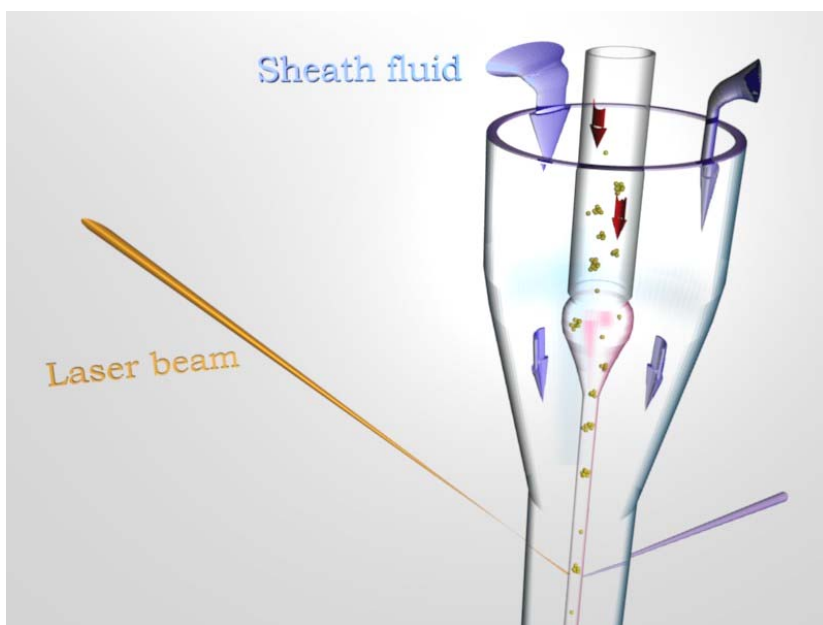


Figure 1.2. Illustration of a flow particle analyzer analysis region. The sample solution (red arrows path) containing microspheres is hydro-dynamically focused by proper adjustment of sheath fluid flow velocity (blue arrows path). Sample solution and sheath fluid do not mix and in ideal conditions a sample solution laminar flow is obtained. The individual microspheres and aggregates are forced to line up single file in the narrow stream to be eventually exposed to the interrogating laser beam. The light beam is scattered when in contact with particles and the scattering is detected by photodiodes or photomultipliers. The interaction between light and analyzed particles is used for a qualitative and/or quantitative presence testing of an analyte of interest.

There are two schemes for the Copalis approach. One format depends on the co-agglutination of latex microparticles. Consequently, the analyte concentration in the sample test can be correlated to the magnitude of latex aggregation. In the second configuration, Figure 1.3, the binding of colloidal metallic particles such as gold to the latex microspheres is mediated by the analyte of interest. The effect of the resulting ‘sandwich’ complex gold-analyte-latex is the broadening of the scattering histogram. The quantification of the analyte in the sample test is determined by the amplitude of the histogram broadening.¹⁶

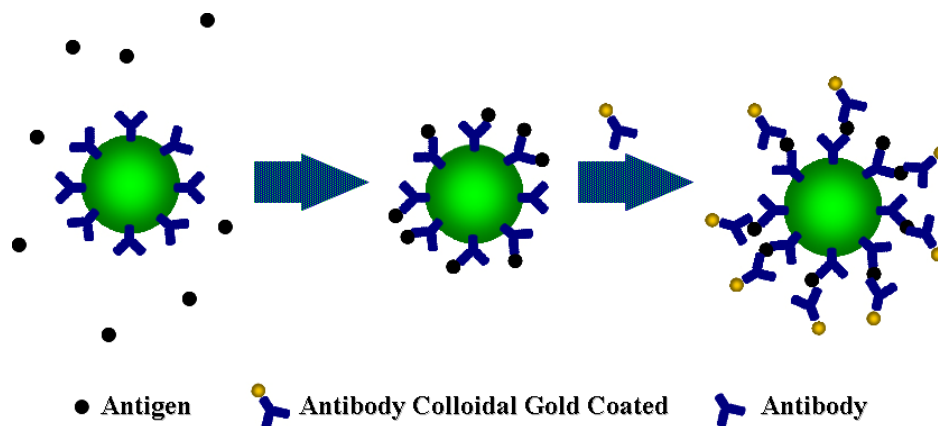


Figure 1.3. Schematic representation of Copalis gold immunoassay. Individual latex microspheres coated with capturing affinity ligand is exposed to the antigen. The unbound antigen is eliminated from the mixture. Colloidal gold coupled to a antibody specific to the antigen is added to complete a sandwich immunoassay. Gold immobilized on the latex particles provide characteristic light scattering profiles when examined with a flow particle analyzer.

Multiplexing applications with Copalis are found to be relatively narrow. For example it has been performed for the detection auto-antibodies associated to connective tissue diseases, hepatitis B surface antigen, antigens of human cytomegalovirus.¹⁶⁻¹⁸ Akin to LATs, agglutination is complicated by complex fluid samples making difficult the design of multiplexed assays. Further, the sensitivity of the approach has been found to be only modest compared to fluorescent techniques as well as the standard method of ELISA (see below).¹⁹

Although not a multianalyte platform *per se*, the commonly employed enzyme-linked immunosorbent assay (ELISA) is used as a standard in clinical immunoassays. The performance of multiplex bead array assays including the Luminex system are frequently compared to ELISA. Briefly, direct ELISA starts with the capture of an antigen on a solid support coated with a capturing antibody.

Unbound antigen is removed and a detecting primary antibody is added followed by removal of excess antibody. An enzyme-linked secondary antibody that binds the primary antibody is added and again the excess is removed. Finally, a substrate is reacted with the enzyme to produce a chromogenic or fluorescent signal. The intensity of the signal is proportional to the amount of antigen, Figure 1.4.

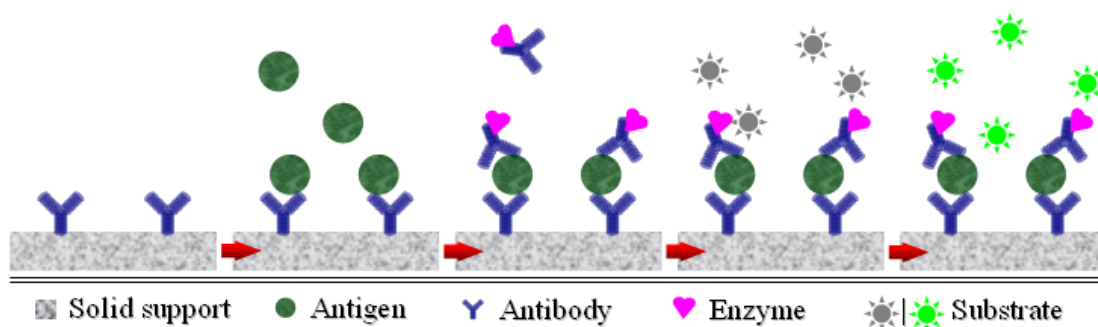


Figure 1.4. Schematic representation of direct ELISA test. Solid support is coated with capturing ligand. Antigen is added followed by removal of non-bounded antigen. Enzyme-linked antibody is added followed by removal of excess labeled antibody. Finally, the substrate is added which reacts with the enzyme to produce a chromogenic or fluorescent signal in a positive test result.

The elimination of particle aggregation as a necessary accessory for positive or negative analyte identification was accomplished with the introduction of individually addressable polymeric microspheres. An attractive and prominent route embraces colorimetric encoding of polymeric microspheres. The beads excited at determined wavelengths provide characteristic emissions that allow for the identification of different population of beads.

Luminex xMAP approach (LxMT) from Luminex Corporation takes advantage of the encoding identification regime. The LxMT shares similar features

to Copalis which include the use of latex microspheres and an optical flow particle analyzer. However, the Luminex approach differs though on the detection scheme. Luminex depends on fluorescence-based assays instead of particle size and agglutination processes. Luminex approach also produces different polystyrene bead populations which are encoded with dyes for their discrimination allowing multiple analyte detection. Today the company claims 100 distinct sets of encoded beads produced with red and infrared dyes in different proportion. Each set of beads can be coated with a reagent to target a specific bioassay. Two lasers are simultaneously focused on each individual bead as they are forced to line up in a single file when traversing the detection chamber of the flow particle analyzer. One laser at 633 nm particles is for particle identification and the other at 532 nm reports fluorescence. Thousands of beads can be analyzed in seconds.

Assays on LxMT are usually performed on a 96 well plate arrangement and on each well up to 100 tests to which the sample test is added. A 96 well microtiter plate reader adds automated sample delivery capabilities. ELISA on the other hand requires separate individual assays which is time consuming and also requires larger volume of sample test to complete the same amount of assays. In many cases, ELISA method leads to lower limits of detection relative to the Luminex approach. However, in selected cases the company claims comparable or better limit of detection and dynamic range.^{20, 21}

In these flow analyzer systems, the preparation of the sample is critical. The sample to be analyzed optimally requires single particles in suspension with good colloidal stability. As complex samples such as biological fluids are tested the

colloidal identity of the microsphere suspension can be compromised as the probability for the aggregation of particles is increased. The LxMT platform, thus, benefits significantly from the extensive studies performed on the parameters affecting LATs and ELISA which include size, surface charge, chemical functionality groups and hydrophilic or hydrophobic nature of the latex particles; pH and ionic strength of the colloidal media; the amount and mode of attachment of immunoreagents on the latex particles; and co-adsorption of other biomolecules.²²⁻²⁴

The LxMT, therefore, provides instrumentation optimized for their polystyrene particle size of 5.1 μm and the optics carefully aligned to focus properly on the sample stream. The sheath stream that surrounds the sample stream is also set to provide an optimal sample stream diameter. Despite the recommended or preset instrumentation settings and the filter included within the equipment to eliminate unwanted aggregated particles, particles of similar size to the polystyrene particles or smaller can still pass through the filter into the detection zone. The outcome is a disruption on the required laminar flow of the sample and in extreme conditions mixing of sample fluid with the sheath fluid leading to anomalous light scattering and decrease sample resolution can be obtained.²⁵

Undesired aggregation may also result in significant loss of analyte from the sample test since most of the aggregates will be eliminated through filtration. For instance, analysis of serum and plasma samples often require dilution to reduce non-specific particle interactions that lead to low recovery of microspheres, clogs and extraneous background signals.²⁶⁻²⁸ If the non-desired aggregation is not

minimized, the quantitation can lead to erroneous results which are important for sample tests with low analyte concentration and also critical in borderline values assigned to diagnose different states of a disease. Even though it is not of common practice in flow cytometry assays to report the formation of unwelcome aggregation of particles during sample preparation, the complication exist and it is a delicate balance of experimental conditions that has been reported frequently on LATs assays.^{29, 30}

The Luminex system offers 100 sets of encoded beads as mentioned above. The combination of 10 intensities of two colors furnishes the 100 different encoded populations of beads. The diversity in the sets of beads can be potentially 10-fold increased by the addition of 10 intensities provided by just one more dye, but the preparation of such beads is not easy.³¹ Dyes showing insignificant non-specific interaction with biomolecules and stability in storage and assay conditions are within the mostly desirable features for a proper encoding thus reducing greatly the selection. Besides, the classification of the existing encoded microspheres is already problematic in solutions with high ionic strength as broadening in the emission spectrum occurs; the discrimination of closely related population of beads is therefore complicated.

Detection systems depending on flow cytometry equipment still suffer from low flexibility for miniaturization. Flow analyzer platforms require a relatively large supply of sheath fluid to focus the sample into a narrow uniform stream of beads lined up in single file. The fluidics component also requires a vacuum system connected to a pump. The addition of optoelectronic components to the analyzer

platform makes it expensive and adds complexity to the instrument that requires high maintenance. Mobilization of the system is possible, but portability is constrained. For example, a mobile flow cytometry (Cylab) designed by Partec, a company dedicated to biotechnological innovations, is housed in a car with power requirements supplied by the car battery and solar panels. Water supply and waste water collection is also included in the mobile unit.^{20, 32, 33}

David Walt and coworkers introduced a MAD platform that also utilizes latex microbeads with colorimetric encoding similar to LxMT system, but departs from the use of a flow particle analyzer. Cross-reactivity due to higher multiplexing level is still present as well as the aggregation of particles, but composite particle clusters are effectively eliminated from the detection step as each microsphere is committed to be singly localized in pits prior to sample test exposure.

The Walt system consists on a set of individually etched fiber optics fused together to form a fiber imaging bundle. The collection of etched wells at one end of the imaging fiber bundle renders a high density microwell array, Figure 1.5. The reported wells dimension ranges between 3.6 μm to 200 nm which allow housing to beads of comparable size. A 500 μm diameter optical fiber bundle contains about 6000 cavities of 3.6 μm size.³⁴ Polystyrene beads with diameter size 3.1 μm are encoded with different concentrations of a dye such as an acetate europium complex or fluorescein which is physically entrapped in the beads by a solvent swelling stimulation process.³⁵ The beads are coated with a capturing affinity entity and loaded randomly by capillary action on the array by dipping the optic fiber bundle in a mixture of encoded beads suspension. The exposure of the array of

beads to a sample test solution leads to the entrapment of the analytes of interest. A xenon arc lamp is used as a source of excitation and an optoelectronic assembly that includes a charged couple device (CCD) camera is used to register the fluorescence generated on each bead.

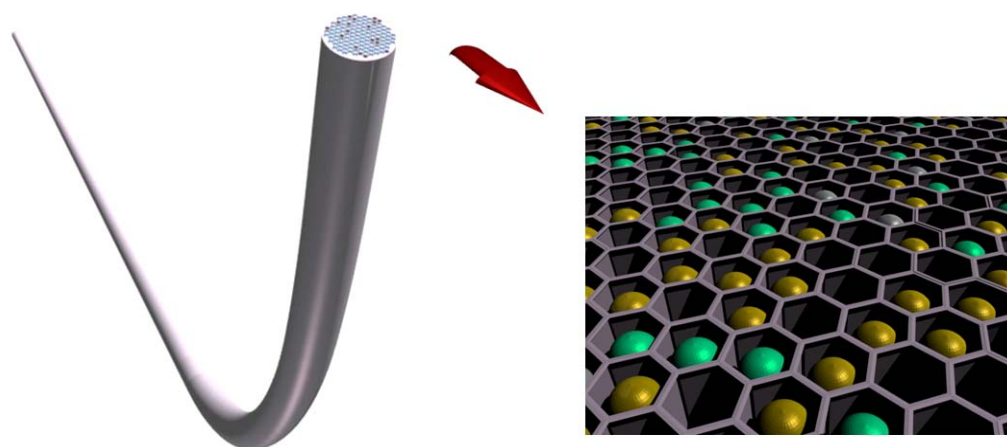


Figure 1.5. Illustration of etched fiber optics fused together to generate an array of pits. The pits are randomly loaded with different populations of latex beads by dipping the end of the bundled fiber optic in a solution containing the mixture of sensitized beads. Different bead populations contain different affinity ligands specific to different antigens. Different populations of encoded beads are represented with different colors. The actual identification of the microspheres depend on fluorescent indicators embedded within the beads which require light excitation followed by detection in a CCD camera located at the other end of the bundled fiber optic.

As opposed to a flow cytometer system, data collected with the fiber optic multiarray system (FOMAS) corresponds to the whole set of beads in the array at once. Due to the arbitrary loading position of beads, it is necessary to perform a bead decoding step prior to the sample test analysis. The decoding process is required not only to identify the beads' optical encoding signature, but also because

of possible loss or rearrangement of beads which is reported not being observed during assays.³⁴ It is likely that events such as the presence of empty wells and the occasional finding of two beads in a single well are due to loss or rearrangement of beads in the well. However, these findings seem not to be frequent.

A prominent attribute of the FOMAS is the capacity to collect and direct the signal of a single bead to the detector with reduced extraneous signal from neighboring beads in the array. Every single fiber ideally houses one single bead, thus, each bead has its own light transmission avenue. The signal intensity is also magnified by a high load of entrapped analyte in the bead localized in a small volume (typically 3.1 μm diameter microspheres). Detection of lower target concentrations is done at a expense of longer incubation times due to diffusion into stagnant solution and bead contained in the wells.³⁶ Another facet of this particular MAD system setup is the reduced array size which demands small sample test volumes, grants faster diffusion events due to small effective pathlengths allowing for relatively short assay times. Although sample test solutions as small as 10 μL can be used, care must be taken to avoid evaporation of the solvent as well as the drying of the arrays' surface.

The LxMT and FOMAS results reliability depends greatly upon the number of replicate beads. In FOMAS variability on the signal from bead to bead has been reported and it becomes significant when the concentration of target is reduced for a fixed amount of beads.³⁶ Replicates are therefore necessary to eliminate false positive or negatives and to increase the signal-to-noise ratio. As a result, at high multiplexing levels the number of replicates may need to be increased due to

crossover reactivity and it will also require a larger array size.³⁷ Higher multiplexing levels also imply diversity of capturing beads exhibiting different electrical and chemical properties originated from biomolecule coating properties. The surface interaction between the fiber optics' and the beads' exterior will bias the loading of beads. Thus, some bead populations will take over most of the available sites in the array and some with reduced replicate number may have their reliability compromised.

Despite the difference in design, the systems available for MAD share many common features in their instrumentation as well as the detection. Consequently, factors curtailing sensitivity and restricting multiplexing levels are also inherited. Limiting factors include non-specific interactions, availability and stability of reagents such as antibodies and oligonucleotides, crossreactivity at high multiplexing levels, ligand immobilization methodologies, the necessity for optimized conditions due to the nature of the reactions involved or the instrumentation, and the ambitious enterprise into miniaturization to produce a flexible portable stand-alone detection system.

In the next section, a short description of the bead-based detection system pioneered by the McDevitt laboratories will be provided. This integrated bead-array system is well-suited for multianalyte and multiclass applications as described below.

1.3 THE CHIP-BASED MULTIANALYTE DETECTION SYSTEM

Individually addressable microspheres that allow for MAD can also be accomplished by positional encoding. The concept involves a directed organized building of an array of selectively modified beads targeting a chosen bioassay. The concentrated effort on the development of a positional bead-based MAD system described below does not exclude the colorimetric encoding utilized in LxMT and FOMAS designs described before. In fact, a combination of both encoding approaches can be utilized if multiplexing in a single bead is desired. This new concept will be described in further detail later in the dissertation.

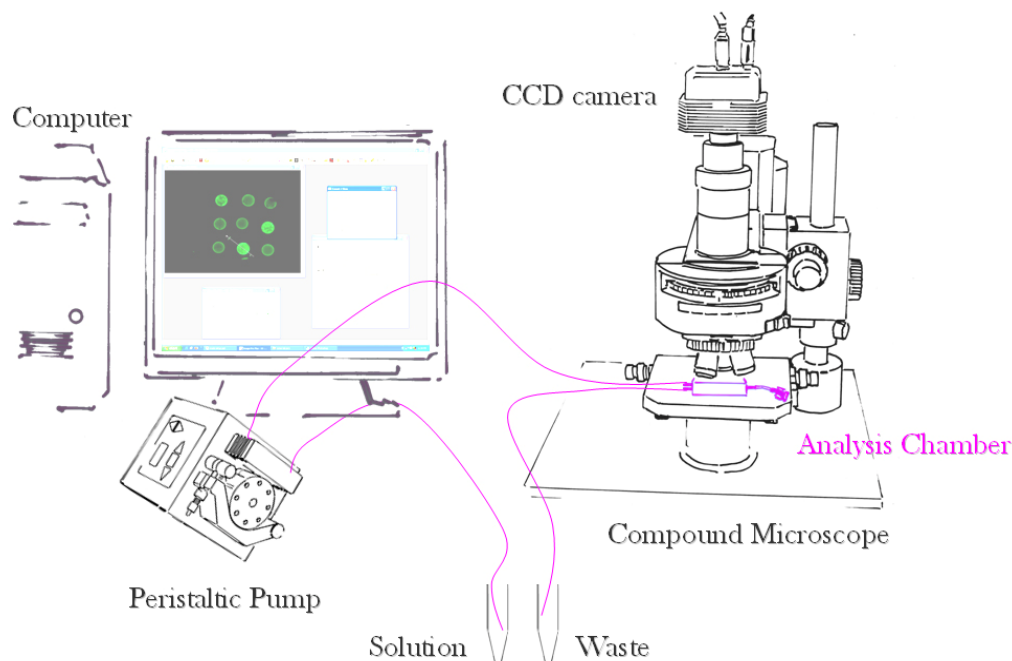


Figure 1.6. Schematic representation of the chip-based multianalyte detection platform basic components. The illustration shows the laboratory bench-top instrumentation used for the development of assays. Only one peristaltic pump is depicted which delivers the solutions to the analysis chamber positioned under the microscope. A computer and specialized software controls the pump and the camera coupled to the microscope allowing for automated assays.

The chip-based multianalyte detection system is comprised of polymeric sensing elements, an optical detection system, a microfluidics circuit and specialized computer software, Figure 1.6.

The micron-sized polymeric sensing elements are localized in wells chemically etched on silicon wafers displaying a squared array pattern. The wells on the silicon wafer possess trans-wafer which allow for the passage of fluids and of light, Figure 1.7.

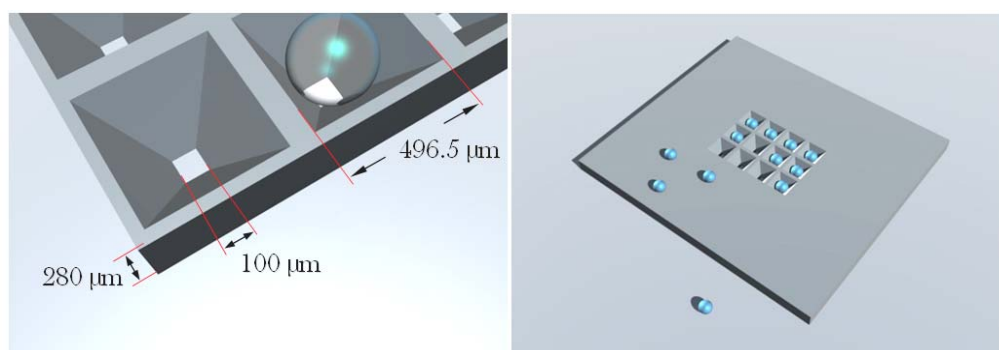


Figure 1.7. Silicon chip with trans- wafer openings. (Left) A section of the chip is shown and the dimensions of the wells are included. The dimensions shown may vary. Fluids passing through the openings bathe the beads forcing close contact of solution contents and ligand immobilized on the beads. The bead size to be used is limited by the bottom opening in the etched silicon chip.

The silicon wafer is enclosed in a metallic or plastic casing with openings where tubing is attached for the delivery and elimination of fluids, Figure 1.8. Mechanical peristaltic pumps put in motion the transit of fluids contained in one or more reservoirs through the analysis chamber where the sensing elements are. The circuit of fluids can be modified accordingly to the required needs such as different solution in a specific sequence either in a closed loop or in an open circuit format. Alternatively, several pumps can be used to deliver solutions in an automated

fashion through tubes that converge into a single line connected directly to the analysis chamber.

Beads can be loaded in the chip either manually or with a modified 96-well liquid dispensing system provided by BioDot (made through collaboration with the McDevitt laboratory). The automated plate reader selects specific beads contained on each of the 96-wells (or 384 plate format) and transfers them to the silicon chip to build the desired matrix of activated microspheres.

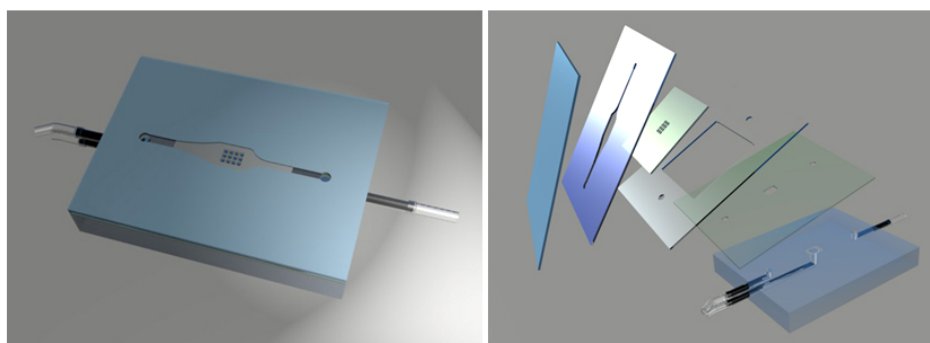


Figure 1.8. Illustration of one of multiple possible designs for the analysis chamber. The chamber here depicted consists of a polymethyl methacrylate base with microchannels to which metallic inserts and flexible plastic tubing is attached for the delivery and disposal of solutions. A series of intermediate double sided adhesive layers allows for the fitting of the silicon chip and defines the solution transit path to the wells containing the beads. A transparent glass or plastic top layer seals the chamber after it is loaded with beads.

The bead-populated analysis chamber is positioned under the optical path of a compound microscope equipped with appropriate light source, optical filters and a charged coupled device (CCD) camera. The camera captures images from the sensing elements and the digitized information is processed in a computer with specialized software.

The physical design of the MAD system described above has been shown to be highly versatile and amenable to structural modification to accommodate membrane filters instead of an etched silicon chip and if required even the complete elimination of microspheres from the detection system. The membrane MAD system variation is transformed into a 'cell processing unit' enabling the analysis of, for example, blood cell contents such as CD4⁺ T lymphocytes on the evaluation of HIV infected individuals.³⁸ Both assay systems exhibit excellent assay characteristics that surpass in many respects the detection capabilities of established (gold standards) macro technologies (see Table 1). Important applications that support and prove feasibility of this program include the development and complete validation of LOC assays for immune function (CD4 T-helper cells), detection of *Bacillus globigii* spores at the DNA, protein and cellular level, detection and measurement of aflatoxin-B1 and brevetoxin through a LOC competitive immunoassay format, detection of *E. coli* bacteria, and measurement of biomarkers of inflammation in human serum in a multiplexed format. Indeed, the multi-class, multi-analyte testing capacity of this LOC system represents one of its most powerful characteristics of these portable detection systems.

Analyte	Range of LOD	Gold Standard	Level of Agreement	Matrix
pH	$2 < \text{pH} < 12$	Glass electrode	± 0.02 pH units, $R^2=0.99$ correlation	Serum, buffer
Ca^{2+}	10^{-7} to 10^{-3} M	ISE	$R^2=0.999$ for dose dependent	Serum, buffer
CRP	10 – 100,000 ng/mL	ELISA	$R^2=0.987$	Human Serum
CRP	10 – 100,000 ng/mL	ELISA	N/A	Human Saliva
DNA-18 mer	10^{-13} M	PCR	N/A	Buffer
CD4, CD3, CD8, CD45 cells	50 – 15,000 cells/ μL	Flow Cytometry	$R^2=0.98$	Human Serum
Bacillus Spores	500	Culture	N/A	Bioaerosol samples

Table 1.1. Detection of a diverse collection of analytes on the chip-based MAD platform. The performance of the chip-based MAD technology is outstanding when compared to established ‘gold standard’ macro-technologies.^{1, 3, 5, 7, 8, 10}

The flexibility of the chip-based MAD system is not only restricted to the physical design of the analysis chamber. The silicon chip is suited to accommodate microspheres of larger size than the ones used in other bead-based MAD platforms. Microspheres ranging in size from 150 up to 300 μm with different composition such as polystyrene, copolymers of polystyrene-polyethyleneglycol or agarose have been used successfully in different assay types.^{1, 3, 11}

The capacity of sheltering larger microspheres is an invitation for beads structures that diverge from the conventionally used simple ‘homogeneous’ polymeric environment. For instance, it is possible to include variations in the pore size of the microspheres whereby the mass transport through the polymeric

skeleton is more efficient, to select analytes by size in addition to affinity, to entrap larger moieties inside the bead's body, to sustain live cells inside to be treated after.^{39, 40} Further, it is possible to use not only latex beads, but also a more friendly biological environment such as polysaccharides in which the adsorption processes of proteins can be reduced largely. A combination of beads not only with different chemical functionalities, but also with different structural characteristics, can be loaded in the same chip providing the contrasting separation styles used in large scale chromatographic techniques.

The integrity of the beads over time is an important factor to consider. The capturing capacity of the beads is subjected to the proper preservation of the affinity ligands activity. The perpetuation of the immobilized ligands activity is, thus, basically the same for both positional and colorimetric encoding schemes. The polymer matrix is also susceptible to degradation over time especially if made of polysaccharides such as agarose which is reported to show some matrix dissolution after 5 years of storage. An advantage, though, of a positional over colorimetric encoding lies in the fact that dyes tend to photobleach, thus, the encoding may be eventually lost. The encoding is also compromised by loss of dyes not bound covalently to the polymeric matrix. The dye progressively diffuses out of the microspheres and the rate of diffusion will depend on the buffer the beads are equilibrated in. Loss of fluorescence intensity on Eu-dye encoded beads are reported to occur as early as 1 to 6 months in storage conditions.³⁵ This loss of fluorescent intensity may difficult the differentiation of bead populations when the intensity gap between similarly encoded beads is small. As the density of the

polymeric matrix increases, the diffusion of dyes is hindered, but it also implies limiting the region close to the beads' surface to the immobilization of affinity ligands. The three-dimensional binding capacity of the microspheres is therefore more closely related to a 'two-dimensional' ELISA assay.

The chip-based MAD system is not only manifesting its competitive contribution on the detection arena, which include from simple ions to complex molecules, but also the high accessibility of its components to be miniaturized towards the development of a fully functional portable analytical device. The above description of the detection system setup presently is better described as a development platform where the assays are being optimized and the scope of assay nature broadened. The utilization of elements such as double adhesive layers to define the shape of the solution circuit transit can also be used to define chambers for solution confinement. Hence, fast design and testing of prototype cards that include washing buffers, detecting analyte solution, sample loading region and waste containment can be performed at a low budget.

1.4 SUMMARY AND DISSERTATION OVERVIEW

The above described LxMT and FOMAS are robust systems for the fast detection of multiple analytes. Color encoded microspheres are used as solid supports for the capture of analytes by affinity interactions. In addition, flow cytometer based systems are also suited to the analysis of particles other than microspheres such as cells. The multiplexing limitations associated to the microspheres context is mainly due to the bead encoding schemes and to the

crossreactivity in complex samples, with the latter a common issue to all analytical systems involving affinity recognition events. The chip-based MAD claims its seat within the highly competitive MAD systems as it introduces an alternative positional encoding format without excluding the colorimetric encoding approach which is frequently adopted by other bead-based platforms. The chip-based MAD original design is based on beads. Besides demonstrating capable of performing similar assays to LxMT and FOMAS with excellent results, has also shown to be flexible to modifications and easy miniaturization. Hence, it has grown to include variations in the analysis chamber that allow to probe directly into cellular structures similar to flow cytometer based instrumentation. An important feature of the chip-based MAD lies in the fact that it is still a young technology and the system allows for the direct integration of microfluidic systems to support tailored delivery of reagents under active control. Enhancements to the platform do not only involve expanding assays or perfecting them. Improvements come also from the design of the fluidic chamber and on the polymeric sensing elements to optimize both efficient mass transport and the chemical interaction between analytes and ligand.

This dissertation will focus on the development and refinement of high functionality polymer ensembles that may be used in integrated microfluidic sensor systems. The remaining chapters cover a series of themes related to the construction and characterization of these polymer reactive particles. Chapter 2 will be devoted to the fabrication of microspheres structures based on agarose. The introduction of the chemically tailored beads into the chip-based technology aims

towards the diversification of bead-based assay formats and to the potential improvement and optimization of the existing assays. Here a variety of methods will be explored to define the optimal methods to derivatize agarose beads so as to make them suitable as single particle sensor ensembles. Bead activation methodologies will be explored as well as methods to define single populations of sensor ensembles having similar size and reactivity characteristics.

In Chapter 3, methods are devised so as to control the surface area and porosity of the agarose bead ensembles. Care is taken here to devise new methods whereby the transport of bioanalytes into the reactive particles can be completed over a short time frame. Effective diffusion constants for protein and DNA analytes are measured for these systems.

In Chapter 4, a series of new sensor ensemble modalities are created and characterized. Here multifunction and multicompartment bead ensembles are examined. In selected cases for the promising new systems, new sensor ensembles are explored in the context of multiplexed detection within a single bead structure.

Chapter 2: Designing Beads Structures for the Chip Based Multianalyte System Technology

2.1 OVERVIEW

As mentioned in the introductory chapter, this dissertation focuses on the development, refinement and utilization of tailored polymer reactive ensembles suitable for sensing applications. Here it is essential for such particles to both sequester from fluid stream the analyte of interest as well as to support the detection of the same analyte. Bead particles having reactive and selective bio-ligands have been used previously by the McDevitt laboratory to serve both of these functions. In order to yield idealized analytical characteristics, it is important that analyte capture is completed with high specificity. The reduction of non-specific associations is key to realizing this idealized performance.

In many prior applications, separation events are completed using chromatographic procedures. For some time agarose has been used in the separation steps for a large variety of biomolecules through affinity interactions and size differentiation. Agarose is still used and preferred material in many chromatographic purification procedures or a media in which live cells can be studied due to the high biocompatibility and high hydrophilicity between other features. Interestingly, the standard sensing element used by the McDevitt laboratory is based on agarose shaped into beaded particles and with appropriate size to fit conveniently into the wells etched on a silicon chip. The chemistry used to extract target analyte from complex sample solutions relies on specific affinity

interactions. Consequently, the beaded agarose beads are modified to immobilize affinity ligands.

Prior to describing the development and optimization of agarose beads for multi-analyte detection, a brief introduction on the definition of affinity chromatography and on the description of agarose gels as an affinity matrix will be provided. Following the preparation of the beads, protocols used to chemically sensitize the beaded gels are also described. The basic sensing elements possess limited fluid transport capabilities through the microspherical internal volume, a characteristic of the gel explained with more details below.

2.2 BACKGROUND INTRODUCTION

2.2.1 Affinity Chromatography

Polymeric matrix supports have been used for decades in the separation and purification of molecules of diverse nature. In particular, chromatographic techniques introduced in the early 1900's by the Russian botanist Mikhail Semyonovich Tsvet have evolved to become a fundamental analytical tool for scientific areas such as medical research and medical diagnosis, environmental monitoring and safekeeping, and pharmacological development. The scope of chromatographic analytical approaches in terms of the separation mechanism of biomolecules, but not limited to molecules with biological origin or activity, has grown to include the partitioning of analytes based on their size (size exclusion chromatography),^{41, 42} hydrophobicity (hydrophobic interaction and reverse phase

chromatography),⁴³⁻⁴⁵ particle charge (ion exchange chromatography)^{46, 47} and biorecognition or ligand specificity (affinity chromatography).^{48, 49}

Parallel to the expansion in the variety of interaction mechanisms between the supporting matrix and the analytes of interest, the chromatographic support has transitioned from the utilization of large scale supports (columns) for high loading separation and purification capacity to the employment of individual micrometer sized particles for the analysis of minuscule sample volumes. Additionally, the polymeric matrix is either used as a ‘static interactive’ sequestering environment or a ‘dynamic interactive’ media in the production of complex molecules (solid phase synthesis).

Affinity chromatography developed in the 1960’s is one of the most powerful separation and purification techniques.^{50, 51} Affinity chromatography relies on the reversible interaction between a specific ligand coupled to the matrix and the analyte. The analyte can range from small molecules to large entities such as cells. The interactions in affinity chromatography involve competitive partitioning processes between the solutes and the immobilized affinity ligand, Figure 2.1.

The ligand in the classic definition of affinity needed to possess an *in-vivo* relationship to the biomolecule. The departure from the *in-vivo* molecular recognition requirement was originated from the observed binding of kinases to dyes with similar motifs to their respective coenzymes.⁵¹ The demand for the similar structural motifs to the analyte binding molecules was likewise eliminated with findings such as the linking of proteins to metal ions immobilized in the

support.⁵³ Thus, for a ligand to act as an affinity entity, it needs to show recognition capability with an optimum binding constant with the target biomolecule. The binding in the recognition processes result from one or a combination of a variety of arbitrary weak interactions including electrostatic or Van der Waals' forces, hydrophobic effects and hydrogen bonding.⁵⁴

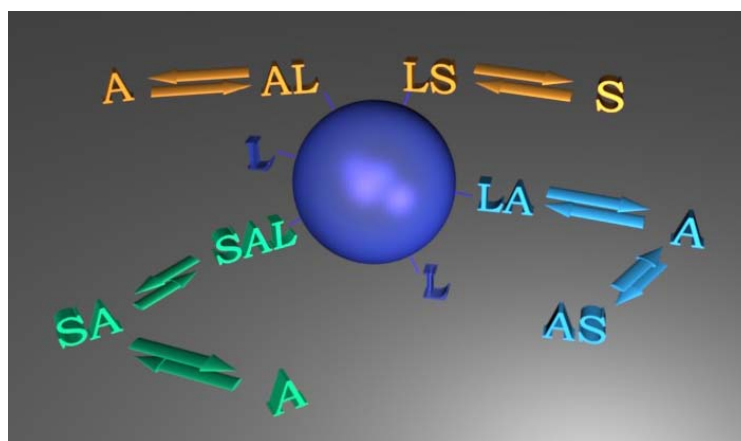


Figure 2.1. Simplified representation of interactions in affinity chromatography separation showing the competitive partitioning between analyte (A), immobilized affinity ligand (L) and a soluble ligand (S). A single binding site (univalence) is considered for all of the species in the sample. Three interaction types have been reported: in blue, soluble ligand and immobilized ligand compete for the analyte; in orange, soluble ligand and analyte compete for the immobilized ligand, and in green, the formation of a ternary complex as a result of the immobilization of a soluble ligand-analyte complex.⁵²

The progressive change in the perception of molecules acting as affinity ligands free of the specific structural constraints triggered the search for molecular motifs displaying exquisite recognition schemes. Dye-ligand affinity systems were the first type to be explored because of the large availability and variety that derived from textile industry. Dye-ligands are found to bind to a large number of proteins, in some instances with significant specificity.⁵⁵⁻⁵⁷ However, despite the

dye's capability to mimic natural ligands and stick to the reactive sites of a specific protein, usually non-specific adsorption of other proteins occur under the same experimental conditions.⁵⁸

The ligand selectivity is perhaps the most important parameter for any affinity separation process since the immobilization of biological active analyte depends on the degree of recognition and the strength of the interaction. The success of affinity separations for critical applications in the medical field had relied strongly on the high specific molecular recognition experienced between biomolecules *in-vivo*. However, biomacromolecules and their respective complement ligands encountered between enzyme-coenzymes, antibody-antigen, antibody-cell, lectin-polysaccharide, nucleic acid-complementary base sequence, hormone-receptor and other typical biological interactions that come from natural sources, are married to a high production cost. In addition, the purification steps are lengthy and copious coupled to the fastidious demand of biological activity retention.

The appealing characteristics of fine-tuned molecular recognition in the wide variety of configurations present in the biological *in-vivo* milieu are poorly restrained when depending only on natural sources and on the limited specificity of textile industrial dyes or other ligands. Deficiencies in the limited supply of a large growing variety of high specificity affinity ligands is partly alleviated by exercising synthetic pathways that include phage display technology and combinatorial peptide libraries synthesis, molecular modeling (biomimetic ligands)⁵⁷, ribosome display techniques^{59, 60}, systematic evolution of ligands by exponential enrichment

(SELEX)⁶¹⁻⁶³, affinity tags and fusion proteins.⁶⁴⁻⁶⁶ With the increase in the number of ligands by rational design based either on the structure or function of the target analyte,⁵⁰ there are still technological limitations that limit the speed and efficiency to sort out and select for the best performing affinity ligands from a vast pool of synthetic molecule prospects. Additionally, some purification and amplification steps are still necessary after potential candidates are identified.

Affinity separations are conventionally performed by attaching the ligand to a solid support. The classic chromatographic format setup is though not necessary.⁵¹ The molecular recognition process can be performed by anchoring the affinity ligands to porous membranes,⁶⁷⁻⁷⁰ in free solution linked to water soluble stimuli sensitive polymers^{71, 72} or to aqueous soluble macropolymer in a multi-phase system.⁷³⁻⁷⁵

In affinity separations where the immobilization of the ligand on a polymeric matrix is needed, the immobilization procedure in many cases is not a trivial procedure. To achieve high selectivity on the separation of the analyte from a mixture, non-specific interactions must be eliminated from the supporting matrix. In addition, high binding capacities require high density of immobilized ligand. However, the excessive localization of ligands can lead to hindered environments that does not allow for the proper binding of the analytes. In many cases, a spacer is recommended between the ligand and the matrix because of the steric effects imposed by the matrix itself. Likewise, the spacer should be selected carefully to avoid non-specific interactions with the sample.

To complicate the matter, the ligands must be oriented properly exposing the reactive sites of structural motifs that are responsible for the recognition process. The molecular orientation of immobilized ligands is of concern in both adsorption and covalent link to the polymer matrix. Hydrogen bonding, electrostatic, Van der Waals and hydrophobic forces affect the orientation of proteins as they approach the surface of the polymeric network. At low ionic strengths, the electrostatic interactions are enhanced, thus, controlling the pH and ionic strength of the media may direct antibodies to preferentially approach through its most hydrophilic regions (binding site regions) to the surface of the polymer, Figure 2.2. Depending on the antibody's charge distribution, regulated by ionic strength and the pH of the solvent, the regions of the protein that end up interacting directly with the polymer's surface can correspond to the antigen binding sites,⁷⁶⁻⁷⁸

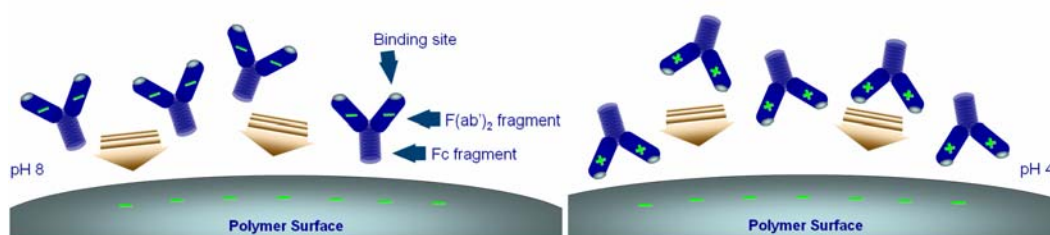


Figure 2.2. Schematic representation showing avian immunoglobulin IgY protein approaching a negatively charged polymer surface as a function of the pH.⁷⁶ Variations on the acidity of the solution can be used to regulate the charge distribution in the protein which is associated with its isoelectric point. Electrostatic interactions between the polymer surface and the protein 'induced dipole' configuration will favor a specific orientation of the protein during the adsorption process. At pH 8, the binding sites are 'active' and available to interact with antigens. At pH 4, the binding sites are 'inactive'.

Random orientation of the protein during covalent immobilization occurs due to the presence of many chemical functional groups on the surface of the protein, as illustrated in Figure 2.3. Here again the random orientation ushers proteins into decreased binding capacity. Typically, sulfhydryl, carboxyl or amino groups from the protein are used to chemically react with the supporting polymeric matrix. Several approaches grouped as site-directed protein immobilization methods are used to target a unique site in the protein for reproducible covalent linkage with the polymeric surface, Figure 2.4. The techniques used include, but are not limited to, targeting specific characteristic moieties on the protein structure such as the presence of one cysteine residue, immobilization through polypeptide affinity tags harvested by genetic engineering, and binding of Fc region of antibody to immobilized protein A or G.^{79, 80}

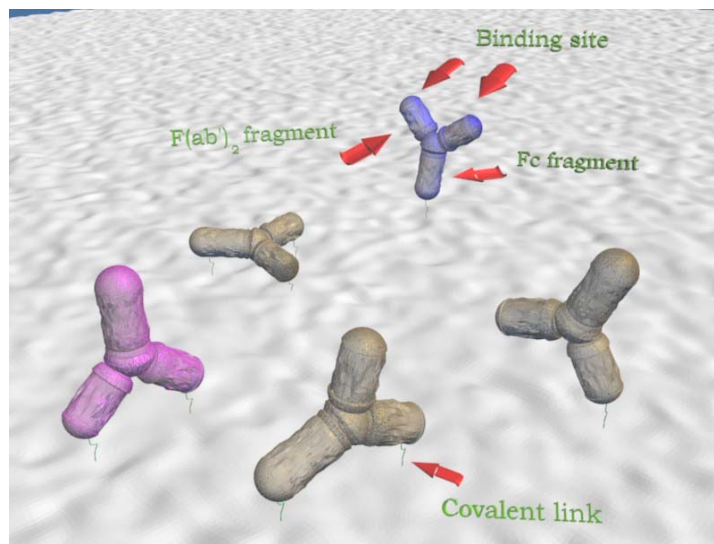


Figure 2.3. Illustration of antibody random covalent immobilization. Immobilization of protein occurs through single or multiple covalent links and at different protein surface regions. In blue, ‘active’ antibody showing the binding sites completely exposed for antigen coupling. In purple, inactive antibody with binding sites completely blocked. In grey, the binding sites are sterically hindered.

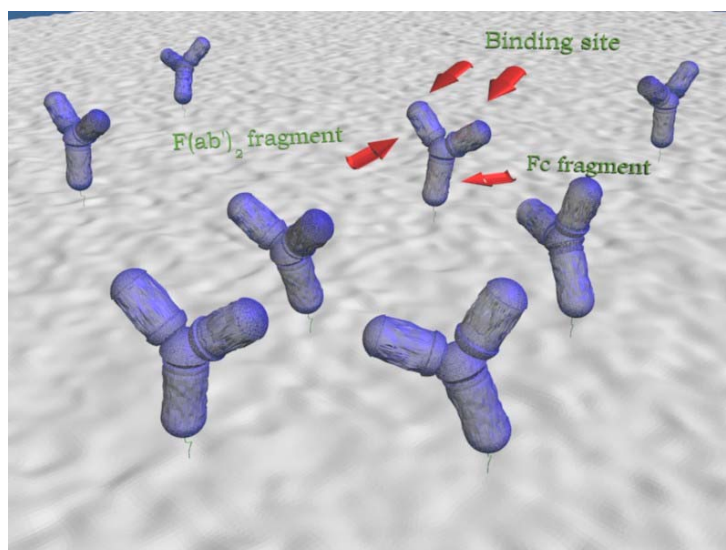


Figure 2.4. Illustration of antibody site directed immobilization showing the attachment of protein through a unique site and in a reproducible manner. Binding sites are ‘active’.

Apart from the isolation of an appropriate affinity ligand and the immobilization through an optimized protocol, the high specificity and selectivity can be lost if the molecule extraction experimental conditions are not tailored to target the analyte of interest. Important factors include the loading buffer (pH, ionic strength and composition) used to equilibrate the matrix and the sample, flow rates that allow for enough time for the binding to occur, and the temperature of the whole separation process. Thus, a delicate balance in the experimental settings must be attained to maximize the desired molecular recognition event.

2.2.2. Polymeric Matrices an Essential Component in the Chip Based Multi-analyte Detection System

Laboratory clinical assays have proven efficacious as a tool for the diagnosis of diseases in either qualitative or quantitative perspectives. The use of affinity assays are predominant and typically involve the extraction of a characteristic disease marker sequestered on a polymeric support. The polymeric support is usually in the form of micro-spherical particles and the mechanism by which the analyte is selectively seized off from a mixture of molecules is grounded on high specificity affinity interactions. Consequently, the polymer support framework is detailed with an affinity ligand.

An assorted number of polymeric micro-spheres are available commercially. The most common supports used in bioassays include latex, glass, and polysaccharide particles. Latex and polysaccharide supports are the preferred supports in most affinity detection system techniques. Although both can be prepared as spherical micro-particles, polysaccharides are mostly used for affinity purifications involving the use of relatively large volumes of the gel to prepare either a monolithic bed or columns of packed particles. On the other hand, latex polymers in addition to packed columns it is found to be frequently porous membranes and individual particles.

Latex beads vary in composition and repeatedly combine polymers like polystyrene or polyacrylates. It is customary to append certain chemical functional groups during the production of the latex beads as they will provide active spots in the polymeric matrix to anchor affinity themes. Latex is intrinsically hydrophobic.

The extent of hydrophobicity can be modulated by adding different proportions of monomers with hydrophilic extensions. Despite the enrichment in the hydrophilic constituents, there is a threshold above which the structural stability is lost. The remainder hydrophobicity contributes in large to adsorption phenomena of the biomolecules present in the sample test in addition to the species that are the object of focus. In latex beads, additional processing steps are rigorously necessary to eliminate the undesired adsorption of solutes other than the analyte of interest. For this purpose, many strategies were developed and optimized to mitigate hydrophobic interactions. In addition, latex polymers based on polystyrene or closely related structures contribute with background signal in fluorescence-based detection practices. Nonetheless, latex beads are used extensively in fluorescence-based procedures with exceptional results.^{36, 81}

The adoption of polysaccharides matrix supports can be traced back to the early developments in affinity chromatography. Agarose was the most popular owing to its inherent high hydrophilicity, relatively neutral, low non-specific interaction manifestation, controllable pore size, stability in a wide range of pH values and easy activation for ligand coupling. Furthermore, agarose, a naturally occurring polymer displays nearly perfect biocompatibility and makes it an ideal media in the separation of proteins, other polysaccharides and DNA without compromising their biological activity. The polysaccharide medium, however, is susceptible to high temperatures, microbial degradation and limited flow rates.

There has been considerable exploration of synthetic methods, by trial/error and rational design, on the production of latex polymers centered mindfully on

polymeric products with distinct properties to suit precise functions. The fruitful labor of many researchers has resulted in a colorful gamut of polymer morphologies dressed with a wide spectrum of chemical attires. As a consequence, simple and composite polymeric designs are available exhibiting from low to large active surface areas, flow restrained systems to efficient internal mass transport architectures, impervious skeletons to biodegradable scaffolds, and ‘static’ frame configurations to flexible stimuli-sensitive frameworks.

In contrast, agarose structural designs have remained virtually static. Modifications to the polysaccharide framework are restricted and include the increase in mechanical strength and the addition of large flow through channels that accommodate a more generous mobile phase mass transport.

Despite of the numerous latex morphologies available, the most simple design, ‘homogeneous’ spherical micrometer sized particles, is used preferentially in MAD systems. Those platforms include flow cytometry and fiber optic-based techniques. MADS based on latex particles owe their emergence to the encoding of beads with fluorophores that allow the identification of different populations of latex beads based on their ‘colorimetric fingerprint’.

Similarly, ‘homogeneous’ polysaccharide beads, in particular made of agarose, as well as latex beads were used in the development of the positional encoded bead-based format of the chip-based MAD technology pioneered by the McDevitt laboratory. Other agarose beaded design alternatives are practically non-existent when compared to the latex variety. In order to benefit from the polysaccharide innate features and to further expand the analytical capabilities of

the chip-based technology, novel beaded structures are to be fabricated as will be described later in this chapter.

2.2.3 Agarose Gels

Agarose is a natural linear polysaccharide extracted from marine red algae. The agarobiose unit, a disaccharide with 1,3 linked D-galactopyranose and 1,4-linked 3,6-anhydro- α -L-galactopyranose, represented in Figure 2.5, is repeated about 390 times per linear chain with an estimated average molecular weight of 120 kDa. Similar structures are also found in the algae which typically contain pyruvic acid ketal, methyl or sulfate residues. These structures as a group are named agaropectin and they typically constitute a large fraction of the polysaccharide content in the algae. Additionally, residues in general impart lower gelling capabilities, a non-neutral gel and minor capacity for custom chemical derivatization. The ideal structure shown in Figure 2.5 is therefore usually obtained through chemical modification rather than direct fractioning procedures from natural sources.⁸²

The gelation mechanism for agarose was proposed in the early 1970s by Reed and corroborated experimentally by Arnott et al.^{83, 84} Briefly, during the gelation process of an agarose solution in water, polymer chains in random coil configuration initially associate into double helices stabilized by water molecules contained in a cavity along the helix axis.

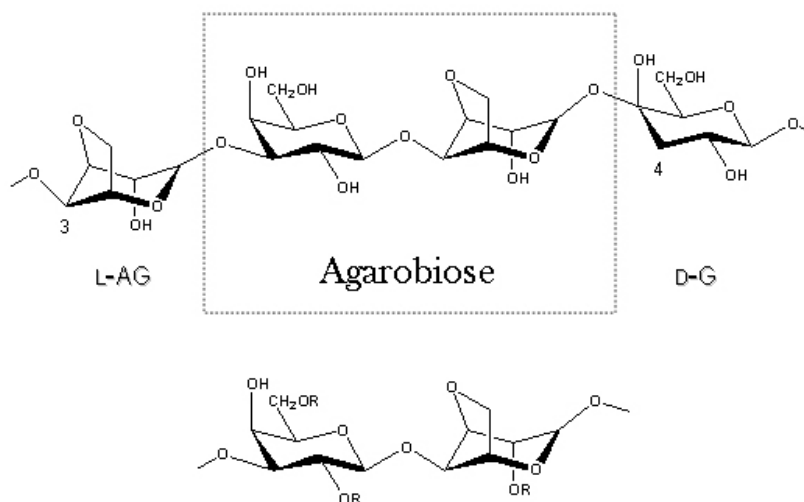


Figure 2.5. Illustration of basic agarobiose repeating unit. (Top-boxed) Ideal agarobiose unit structure: L-AG is 3,6 anhydro- α -L-galactopyranose and D-G is β -D-galactopyranose. Linking positions are indicated at position 3 in L-AG and position 4 at D-G. (Bottom) The residues are represented by “R”. Most common residues found in natural agarose are pyruvate, methyl and sulfate groups. The positions where “R” is shown are available for substitution in the ideal structure.

A single chain usually is not restrained to one double helix. Substitutions in the ideal agarobiose unit tend to disrupt the double helix formation introducing kinks that facilitate association with other chains. Three of the four hydroxyl groups point outwards from the helix cavity and are available for substitution. These hydroxyl groups are involved in the aggregation of helices via hydrogen bonding interactions to form bundles referred as *supra-fibers*, Figure 2.6. A supra-fiber has been found to contain as low as 7 and up to 10^4 helices. The assembly of supra-fibers renders a three-dimensional ‘rigid’ network, the gel, with large interconnected voids occupied by water.^{84, 85}

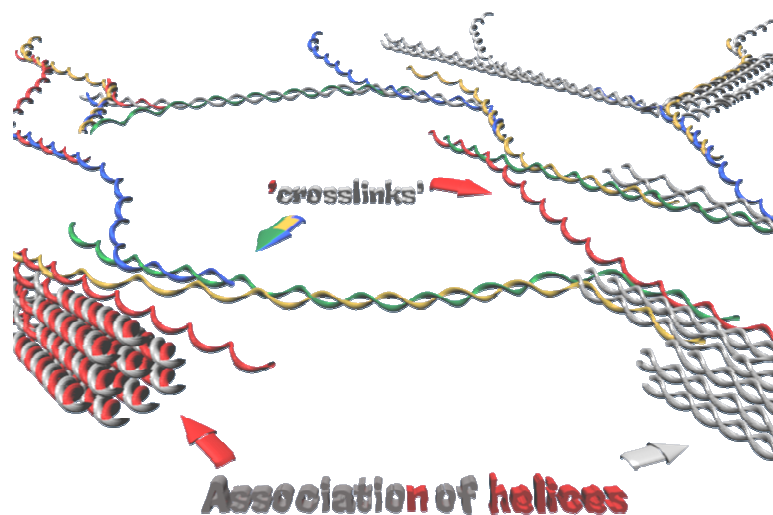


Figure 2.6. Illustration of agarose helices. Single agarose chains also participate in more than one helix acting as ‘crosslinks’ in a 3-dimensional network. Some crosslinks are depicted with different colors above. The helices also associate forming a ‘close-packed’ assembly called supra-fibers which can consist of up to 10^4 helices.

The characterization of agarose gels along with the pore size is not only complicated by the necessity to study the gel in unperturbed conditions where the gel is completely hydrated, but also by the fact that the gelation mechanism of agarose is rather quite complex. The transition from the liquid-like sol to the gel proceeds through conformational changes of random coils, convoluted physical interactions and association-dissociation of single chains via hydrogen bonds. Additionally, the gel characteristics are found to be intimately affiliated to its thermal history.^{85, 86} The gelation and the re-melting behavior usually show very marked hysteresis attributed to large aggregates stable at high temperatures upon heating the gel. The molten gel carries with it residual helix fractions.⁸⁷

The sol-gel transition temperature or gelation point is dramatically affected by factors such as the presence of residues or substitutions along the agarose chain, by the average-number molecular weight of the macromolecules, the concentration of the agarose solution and the solvent system from which the gel is cast. In addition to the thermal history, reproducibility in gel characteristics is indeed problematic.

The pore size is considered one of the most important features in separation and purification techniques. The pore diameter in a gel is subordinated to the concentration of the agarose solution. Certainly, under the same conditions a higher concentration of agarose produces a more dense gel which is linked to smaller pore diameters. In addition, the pore size distribution is narrower for concentrated solutions. In low ionic strength buffers different concentrations of agarose solutions will provide gels with pore diameter ranging from a few nanometers up to 900 nm.⁸⁸ The ionic strength of the buffer in which the gel is equilibrated will dictate the degree of association of chains into helices and on the extent of helices aggregation. At low ionic strength the aggregation of neutral agarose is not favored; the pores are therefore smaller and the size distribution is narrower than in high ionic strength buffers. For instance, by changing the ionic strength of the equilibrating buffer it is possible to increase the mean pore diameter in a 1% gel from 370 nm up to 1.8 μm with the broader size distribution containing pores up to 3 μm .⁸⁹

The stability of the gel relies on the cohesive forces between the chains in a helix and with neighboring helices, which in turn, build upon the length of each

agarose unit. Higher molecular weight of the individual chains supplies stronger gels more resistant to stress failure under both tension and compression. Individual chains participate in more than one helix resulting in a larger number of 'cross-links' per chain when the molecular weight is increased. Additionally, longer 'cross-links' with reduced rigid configuration contribute more actively to the elasticity of the network.⁹⁰

The agarose units in the gel maintain their discrete identities and the network may be broken without breaking any of the covalent bonds in a polysaccharide unit. Hence, the mechanical stability can be further improved by introducing actual crosslinking between chains. Typical crosslinkers used are divinyl sulfone, bisepoxy divinylsulfone and epychlorydrin. Crosslinking of agarose provides better resistance to compression under hydrodynamic pressure, allows heating above the melting point of non-crosslinked agarose, long term storage stability, resistant to dissolution under pH between 3 to 14, and better tolerance to denaturants or chaotropic agents, diverse solvents and mild oxidants.⁹¹

The rate at which the gelation proceeds has a significant impact on the gel microstructure. Rapid cooling forcing a rapid sol-gel transition invariably contributes to smaller average pore size as opposed to slow cooling.⁹² The pore size distribution is narrower and the supra-fibers are thinner with poorer mechanical stability. In rapid cooling processes the sol-gel transition temperature is lowered. It is presumed that proper rearrangement of coils do not proceed as fast as the temperature drop since the mobility is impaired. The association of chains and

aggregation of helices do not achieve a close packed configuration otherwise seen at slow cooling.⁹³

An agarose gel provides an abundant source of hydroxyl groups available for chemical substitution to facilitate the covalent attachment of affinity ligands. There are many chemical modifications or activation procedures from which to choose and pertinent literature is frequently provided by chemical and biochemical corporations. It is more attractive to perform the least amount of modifications to both the support and the ligands to prevent unpredicted interactions during a separation assay.

The immobilization of antibodies or other biomolecules on an agarose skeleton may be more advantageous than on a flat solid surface. Similar to other porous polymers, the available surface area for immobilization is large. The fibers, which can be approximated to cylinders in shape, Figure 2.7, offer a better exposure scheme of the activated spots in the gel for immobilization. The result is that the immobilized affinity ligands will be drawn apart along a circumference concentric to the cylinder as we depart away from the axis of the circumference. The steric hindrance is reduced for low or moderate affinity ligand density in the gel and the binding sites of the ligand will be more available for the target recognition process. The most desirable condition is undoubtedly to proceed with a ligand site directed immobilization, but the procedure is in many instances cost prohibitive and more laborious and not-practical for fast deployment.

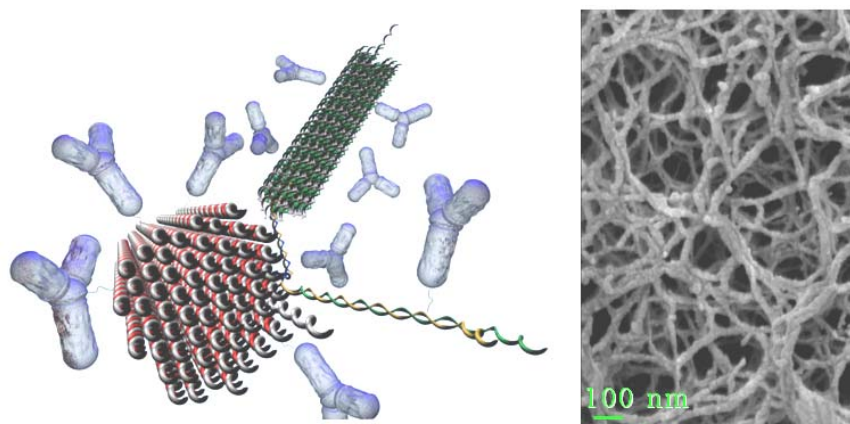
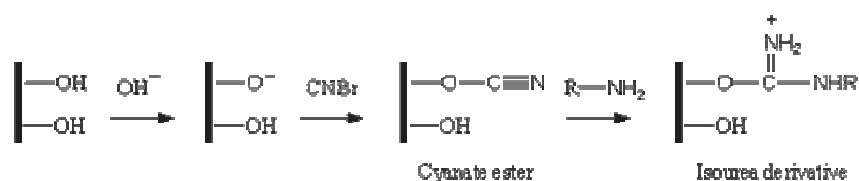


Figure 2.7. (Right) Depiction of antibody random immobilization on small bundles of associated agarose chains. (Left) Scanning electron micrograph showing network of agarose fibers from a 2% gel. Agarose was sputter coated with 15 nm gold. The average fiber diameter from the micrograph was found to be 11.9 ± 1.9 nm ($n = 100$). Gold deposited on the fibers does not correspond to the thickness indicated by the sputter microbalance. In addition to uneven gold coating, the thickness of fibers cannot be determined properly through the micrograph due to gel shrinkage during critical point drying. Nevertheless, IgG antibody typically 150 kDa is comparable in size to supra-fibers diameters. (SEM image were by courtesy of Dwight Romanovicks).

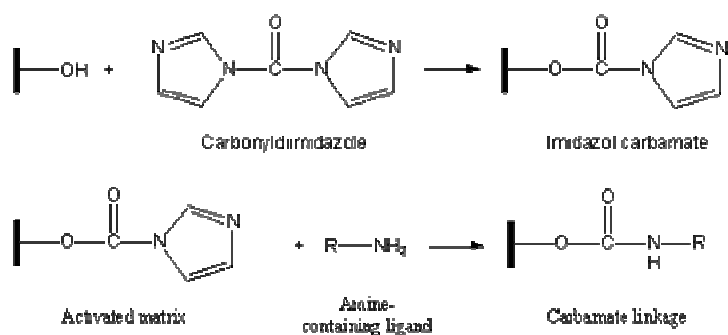
Pore size is frequently selected by varying the concentration of agarose in the gel although the pore diameter obtained is not uniform in size. A Gaussian distribution for pore diameter is frequently obtained which is narrower at high agarose concentration gels.⁸⁹ Frequently, for most applications such as sequencing of DNA the resolving power of the gel is appropriate. Also, the apparent pore size instead of the actual pore size distribution is an aspect more practical to look for when selecting gel concentration. The apparent pore size measurement is based on the measurement of the mobility of molecules through a gel to produce a fair separation.

The most common agarose gel activation procedures target the reactive chemistries available in the affinity ligands to be immobilized such as amine,

carboxyl or sulfhydryl groups in proteins. Cyanogen Bromide activation (CNBr) was introduced in the 1960s for the activation of polysaccharides or any support containing hydroxyl groups.⁹⁴ The reaction of hydroxyl groups with CNBr in basic media generates cyanate esters in agarose. The activated gel can be coupled to biomolecules with primary amine groups. The isourea bond formed though is unstable and the loss of ligands occurs gradually.



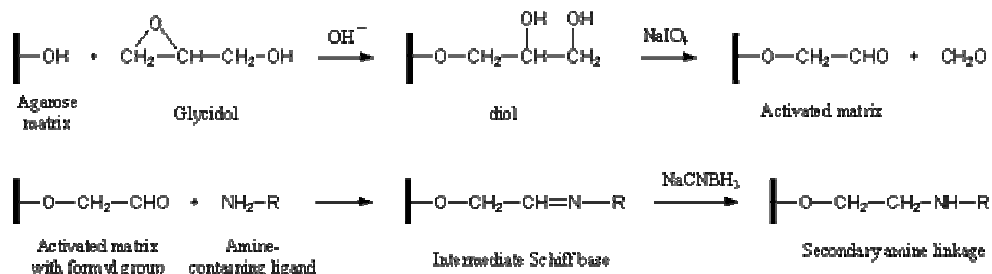
The N,N'-Carbonyl diimidazole is used to activate carboxyl and hydroxyl containing supports in non-aqueous solvents such as dimethyl sulfoxide.⁹⁵ With agarose an intermediate imidazolyl carbamate is formed. Stable amide linkage is formed upon addition of the amine containing molecule.



In non-aqueous media imidazole-activated gel is stable. In the presence of water the activated matrix eventually reverts to its original state. The gel charge is

not changed as a result of the activation and the coupling of amine containing compounds with poor solubility can be performed in organic solvents.

The coupling of primary and secondary amines to carbonyl groups may also be completed via reductive amination. The agarose gel has to be previously modified to contain carbonyl terminations. Aldehydes are procured by treating the gel with an epoxide such as glycidol, which adds a spacer terminated in vicinal diols, followed by mild oxidation. The activated gels are stable and can be stored for long periods if bacterial growth is prevented with the addition of a preservative such as sodium azide. The immobilization of an amine containing compound with the aldehyde produces an intermediate Schiff base which is subsequently reduced to produce a stable secondary amine.



The gel activation procedures described above are some representative techniques frequently used in both small and large scale.⁹¹ There are undoubtedly advantages of one over another depending on the desired final application. Activation reproducibility is fundamental. Long term storage with preserved reactivity and matrix integrity in a variety of solvent systems and a wide range of pH is often treasured. Other activation relevant attributes include efficient and fast coupling of affinity ligands especially when using sensitive, scarce and/or

expensive ligands. In some circumstances a specific activation procedure may introduce non-specific interactions with the sample to be evaluated. Such non-specific interactions may arise from changes in the matrix overall charge or in the gel hydrophilicity. The corrective measures to eliminate the non-specific interactions may unintentionally cause detrimental effects including adverse conformational changes in both affinity ligand and analyte.

Having provided a background for the activation and formation of agarose beads, in the remainder of this chapter studies targeting the development and understanding of customized reactive agarose particles will be described. Here activation chemistry, formation of beads, size selection and tailoring of micro and macro porous beads will be evaluated and discussed in detail.

2.3 EXPERIMENTAL

2.3.1 Reagents

Hexanes, n-heptane, hexadecane, decane were purchased from Fisher Sci. (Fair Lawn, NJ). Sorbitan triolate (Span 85), polyoxoethylenesorbitan monooleate (Tween 80), agarose type I-B, divinyl sulfone, sodium borohydride, tris-(hydroxymethyl)-aminomethane and sodium hydroxide were purchased from Sigma-Aldrich, Inc. (St. Louis, MO). Ethanol was purchased from AAPER Alcohol & Chemicals (Shelbyville, KC). Sodium periodate, D-(+)-mannitol, glycidol and sodium cyanoborohydride were obtained from ACROS organics. Potassium hydrogen phosphate was purchased from J.T. Baker (Phillipsburg, NJ). Carbonate-Bicarbonate buffer pack pH 9.4 and phosphate buffered saline pack pH 7.4 were purchased from Pierce Technologies (Rockford, IL). Rabbit anti-Human CRP was obtained from Accurate Chemical and Scientific Corp. (Westbury, NY). Purified human C-Reactive Protein was purchased from Cortex Biochem (San Leandro, CA). Alexa Fluor® 488 Protein Labeling Kit (A-10235) was purchased from Molecular Probes (Eugene, OR). 6% epychlorohydrin crosslinked agarose beads were purchased from Agarose Bead Technologies (Tampa, FL).

2.3.2 Methods and Instrumentation

Overhead Stirrer RW20 DzM.n was acquired from IKA Works Inc. (Wilmington, NC). The chip-based MAD system was described in Chapter 1. The optical interface included a compound microscope (Olympus America Inc.; Melville, NY) equipped for epifluorescent imaging with a 100 W Hg lamp, a 5x

objective, interchangeable filters including FITC and Pacific Blue (Chroma Technology Corp.; Brattleboro, VT) and a 12-bit charge-coupled device (CCD) color camera (DVC Company, Austin, TX). Data was processed using Image Pro Plus 4.5 software (Media Cybernetics; Carlsbad, CA). Fluid delivery to the analysis chamber was carried out with peristaltic pumps from FIA labs (Bellevue, WA) and controlled with FIA lab software. Confocal Laser Scanning (CLS) images were obtained with a Leica SP2 AOBS Confocal Microscope (Exton, PA) and Scanning Electron Microscope (SEM) pictures were obtained on a LEO Model-1530 scanning electron microscope (Carl Zeiss Inc., North America). Standardized metallic screens were purchased from W.S. Tyler (Mentor, OH) and Newark Wire Cloth Company (Clifton, NJ). Sample drying at the critical point (CPD) was performed on a Samdri 790 from Tousimis Research Corporation (Rockville, Maryland).

2.3.3 Preparation of 2% Homogeneous agarose beads 250-280 μm diameter size.

Homogeneous agarose beads were prepared by emulsifying a 2% agarose solution.⁹⁶ 1 g of agarose was dissolved in 50 mL water by heating the mixture to 86 °C in a boiling water bath. A suspending solution made of 9 mL Span 85 diluted to 100 mL in n-heptane was heated to 58 °C and stirred at 550 rpm. The polysaccharide solution was allowed to stabilize at 61 °C and then poured into the suspending solution. Stirring proceeded at 550 rpm at 58-59 °C for 1 min. Agarose was left to gel into small beads as the temperature dropped to 24 °C at 550 rpm. Beads were collected on a sieve and washed with water. Sorted through metal screens the 250-280 μm beads fraction was collected and washed with a mixture of

50/50 ethanol/water to eliminate surfactant and organic solvent residues and finally with water to properly rehydrate the gels. The beads were kept in water at 4°C.

2.3.4 Preparation of 4% Superporous Agarose Beads

Superporous agarose beads were prepared in a double emulsification procedure.⁹⁷ A 4% agarose solution containing 2g agarose in 50 mL water, and a mixture consisting of 0.7 mL Tween 80 in 20 mL hexanes were prepared and equilibrated at 50 °C. The mixture and the agarose solution were mixed and stirred at 1000 rpm for 2 min while keeping the reactor in a 50 °C thermostated bath. A 50 °C suspending solution was prepared by diluting 8.5 mL Span 85 to 150 mL in hexanes. The suspending solution was added to the stirred emulsion, stirred for an additional minute before readjusting the stirring speed to 600 rpm. The bath at 50 °C was removed and with continuous stirring the emulsions were left to cool to 25 °C. Stirring was stopped, the product collected in metallic sieves, washed and sorted by size with water and the size fraction 250-280 µm was separated. Additional washing of the beaded product was done with a 50% ethanolic solution followed by water and stored at 4 °C.

2.3.5 Crosslinking of Agarose Beads

A 1 mL 250-280 µm settled agarose beads was resuspended in K₂PO₄ 0.5 M pH 12.3 to 5 mL. Transferred to a conical test tube 30 µL divinyl sulfone and 2.56 mg NaBH₄ were added. The mixture was shaken 17 hours in a plate shaker ensuring the exposure of all the beads to the solution. The beads were washed 3 times with 5 mL of a solution prepared with 0.2 g NaBH₄ and 50 mL NaOH solution pH 12.37. An additional solution with 0.2 g NaBH₄, 0.225 g D-mannitol in

50 mL NaOH pH 12.6 was prepared to quench unreacted vinyl groups. The beads were resuspended in 5 mL NaOH pH 12.3 and 6 mL of D-mannitol solution was allowed to react with the beads for 4 h followed by extensive washing of beads with nanopure water.

2.3.6 Glyoxal Activation of Agarose Beads

A solution consisting of 10 mL NaOH, 0.027 g NaBH₄, and 3 mL glycidol was prepared. In a conical test tube 1 mL crosslinked beads was resuspended in 2 mL water and 1.2 mL glycidol solution was added. The mixture was shaken overnight. Afterwards, the beads were washed 3 times with 50 mL water, resuspended in 2.5 mL water and 0.7 mL NaIO₄ 0.2 M added and reacted for 1 h. Finally the beads were washed thoroughly with water, resuspended in carbonate buffer pH 9 and kept at 4°C.

2.3.7 Selection of Crosslinking Degree through C-Reactive Protein Assay

The immobilization of affinity ligand, anti-CRP, on the beads proceeded as follows: To 500 uL activated beads in a 2 mL eppendorf tube 1089 uL of anti-CRP (8.3 mg/mL) and 60 uL NaCNBH₃ 0.44 M was added. The mixture was rotated overnight. The beads were washed 3 times with nanopure water followed by the addition of 1 mL Trizma 50 mM buffer pH 7.15 and 60 uL NaCNBH₃ 0.44 M solution. The reaction proceeded for 1 h and the beads washed afterwards. Additionally the beads were exposed to 500 uL 1% BSA in PBS for 15 min and then washed with PBS buffer.

For the assay in the chip-based MAD system beads were loaded in a silicon chip and the analysis cell assembled and placed under the microscope. The flow

rate of the delivered solutions was set to 1.6 mL/min and 5 min for each solution. The microspheres were subjected in sequence to PBS buffer, 500 ng/mL CRP solution, washing with PBS, anti-CRP Alexa Fluor 488 conjugate and to a final rinse with PBS buffer previous to image capture of the beads with the CCD camera.

2.3 RESULTS AND DISCUSSION

2.3.1 Preparation of Homogeneous Beaded Agarose Gels - Motivation

An agarose gel is considered a homogeneous media when the agarose solution is set to gel without introducing porogenic agents in the embodiment. The resulting gel will have a relatively uniform pore size with dimensions small enough to reduce the mobility of diffusing molecules from 2 to 3 orders of magnitude moving from free solution into the gel network.⁹⁸ Agarose is generally prepared as a monolith or a continuous bed where the hot agarose solution is poured into a container and left to gel and adopt the shape detailed by the container. Other common format consists on the packaging of a relatively large amount of microspherical beads into a column. The beaded gel is prepared by emulsifying an agarose solution.⁹⁹ The agarose solution is dispersed in an organic solvent containing a surface active agent. The partitioning of agarose solution into fine droplets is usually achieved with mechanical stirring increasing dramatically the interfacial area between the two immiscible phases, Figure 2.8. With continuous stirring the heterogeneous system is allowed to cool letting the ‘stabilized’ droplets to transit from sol to gel state. With proper adjustment of experimental parameters beaded material is obtained.

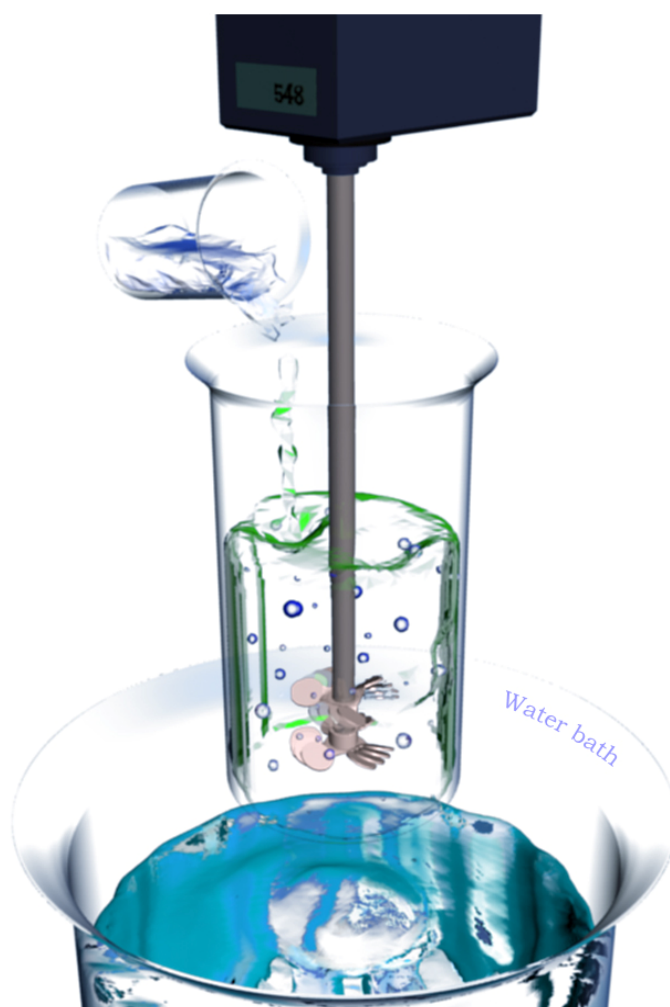


Figure 2.8. Illustration of Agarose solution emulsification. The suspending solution, an organic solution containing a surfactant, is stirred and the agarose solution added. A bath is used to stabilize the mixture while the interfacial area between aqueous and organic phases is increased. The stabilized agarose droplets are set to gel by allowing the temperature to drop below the gelation point. The thermometers, hot plates and additional baths are intentionally omitted.

The success on the application of the chip-based MAD system on bioassays such as the detection of cardiac markers like C-reactive protein (CRP) required the inspection and selection of antigens, antibodies and a combination of reagents from

diverse source of suppliers to obtain the highest signal-to-noise ratio on the fluorescence mode detection and to reduce the variability between bead duplicates loaded in the chip in a single or between several separate assays.

Inconsistencies on the reactivity of different proteins are undoubtedly not the unique source of error. The agarose beads from commercial origins were indeed contributing significantly to irreproducible assays. Before detailed studies of agarose beads tailored for sensor applications is provided, it is helpful to describe the behavior obtained from commercial sources of agarose that target the affinity purification applications. Here the requirements for the individual beads are less sophisticated than for the sensor application where signals from individual beads are extracted there from. Likewise, commercial beads were purchased and activated. These beads were then examined in CRP assays as will be described in more detail below. These beads exhibited large differences in activation levels and bead diameters, both of which influence the signal of the bead-based assays.

The bead diameter size variation was conveniently revealed by simple inspection under a microscope and partially corrected by utilizing metallic sieves. The desired bead sizes in the available etched silicon chips ranged between 250-300 μm . Unfortunately, after size screening through 300, 280 and 250 μm sieve openings the recovered volume of beads was severely restricted. Table 2.1 summarizes the volume of 250-300 μm beads fraction extracted from a few bottles of commercial agarose beads. Sieving was carried out after complete hydration of beads by exchanging the original preserving solvent with distilled water.

Agarose beads initially used were of 6% concentration. The selected 6% gels is very often the preferred choice for meticulous purification or separation of molecules. The higher concentration not only provides stronger beads, but also a better fractioning capability. The mobility through the gel is smaller because of the smaller pore sizes compared to lower agarose concentration. Table 2.2 is data obtained from agarose beads offered by Colloidal Science Solutions Inc. Bioscience Bead Division.¹⁰⁰ It is clear that a 6% gel will delay diffusion of analytes into the bead when compared to lower gel concentrations. To take advantage of the total volume of the 6% derivatized bead it would be necessary to resort to lengthy assays or to exercise high flow pressures to accelerate analyte deliverance.

Agarose Gel Concentration (%) and batch number	Advertised size range (µm) and volume (mL)	Fraction 250-300 µm (mL)	% Fraction utilizable* beads in the product
2% CL-G Lot #01220	250-350 / 125	13.8	11.04
4% CL-G Lot # 01228	250-350 / 125	19	15.2
6% CL-G Lot # 10325	250-350 / 125	3.2	2.56
6% CL Lot# 10325	Not specified / 1000	60	6

Table 2.1. Utilizable bead size fraction from commercial beads purchased from Agarose Bead Technologies. Crosslinked and glyoxal activated beads is indicated by CL and G respectively. *The actual size range recovered from the metallic sieves differs from the specified screen openings.

Agarose Gel Concentration (%)	Protein Fractioning (kDa)	Polysaccharide Fractioning (kDa)	Linear Nucleic Acid Fractioning (bp)
1	1000 to 150000	1000 to 150000	> 3000
2	80 to 40000	90 to 20000	1340
4	50 to 15000	40 to 5000	860
6	10 to 5000	10 to 1000	180

Table 2.2. Typical biomolecule size exclusion as a function of agarose gel concentration. Data applicable to agarose products manufactured by Colloidal Science Solutions Inc. Bioscience Bead Division.¹⁰⁰

From Tables 2.1 and 2.2, it would be logical to select for a lower agarose concentrations. After all the volume of beads of correct size and the pore diameters in the gels are both larger. Unfortunately, the commercial 2% and 4% beads were previously reported by McDevitt laboratory co-workers to show poor mechanical properties and frequently irregular shaped particles. Added to the low yield recovery of 250-300 μm beads tied to a time consuming screening process, fluctuations of pre-activated beads was found on chemical reactivity even within the same batch of the commercial product, Figure 2.9.

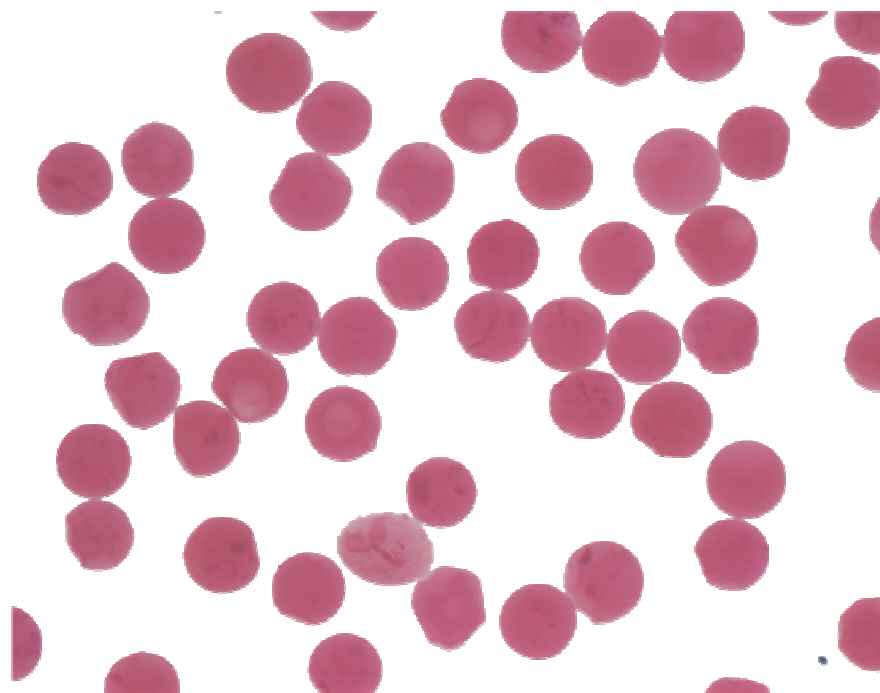


Figure 2.9. Commercial ABT glyoxal activated 2% agarose beads, fraction 250-280 μm . A random volume of beads was picked and tested for aldehyde reactivity with Schiff reagent. Regions within several beads containing most probably dense agarose domains and/or inclusions of organic solvent droplets originate the darker spots. Spherical and irregular shaped beads are found in a relatively large proportion. In addition, some of the particles exhibit large cavities.

Commercial agarose beads manufacturing and chemical derivatization are dedicated to affinity separations practices requiring large volume of particles used as a collective such as in packed beads columns. In those situations the variations in size, shape and reactivity recently described are seldom found not to be critical for reproducible and reliable assays.

It is reasonable then to reproduce the homogeneous agarose beads that are commercially available in a consistent manner to guarantee a reliable source of beaded product that will ensure the reproducibility of bioassays. As a result,

protocols for the production of beads and posterior chemical modification are also described here. It is necessary to point out that an exhaustive optimization of beads was not executed. In fact, a fast screening routine was necessary at the moment because of the necessity to replace the commercial source with a dependable supply of beads.

2.3.2 Size and Shape Description of Beaded Product

The above preparation procedure is intended for the preparation of homogeneous agarose beads with diameter ranging preferentially between 250 and 280 μm . That is, to yield a meaningful volume of utilizable beads in the specified range. Within the numerous experiments performed to identify and test the variables affecting the size, shape, and volume of settled agarose particles obtained by emulsification, the conditions described in the preparation procedure are not the optimal. The beaded product obtained as indicated above displays fair gel homogeneity, Figure 2.10. Oil or air inclusions and visible cracks or non-dissolved agarose regions may contribute to light scattering and irreproducible assays during a chip-based MAD assay.

Parameters such as stirring speed, temperature, amount of emulsifier, agarose solution concentration, geometry of the reaction vessel, emulsifier nature and organic solvent of the suspending media participate and compete strongly in defining shape, size and quantity of the final product

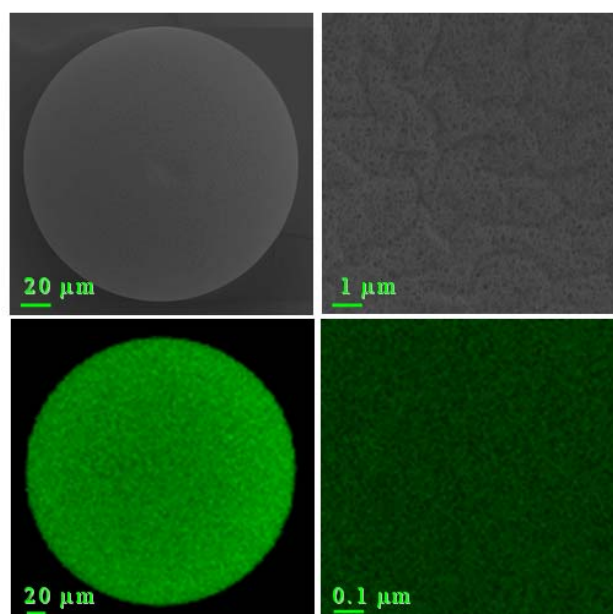


Figure 2.10. Scanning electron (top) and medial slice confocal scanning laser micrographs (bottom) of a homogeneous agarose bead. A magnification of the surface and the medial cross section of the beads is included at the right side. Critical point drying (CPD) of beads causes approximately 33% shrinkage in size. Agarose beads were stained with acridine orange for confocal images.

Shape was chosen as the initial feature to be controlled and reproduced. A starting point on experimental conditions were selected to be similar to the preparation procedures found in the literature.⁹⁶ Insufficient stabilization of the agarose solution produces mainly irregular shaped structures or coalescence of beads, Figure 2.11-B. Fractioning of beads due to excessive agitation also occur if the stirring speed is too high in poor stabilization conditions or excessive stirring, Figure 2.11-A. Excessive stabilization combined with high stirring speed contributes to the oil droplets and air bubbles inclusions, Figure 2.11-C. A complete description of factors that actually are involved in the many shapes of particles seen on the experimental maturation process to spherical beads is rather

cumbersome and will not be provided here. Rather, methods which yield desirable characteristics will be the focus of the discussion and tailored studies.

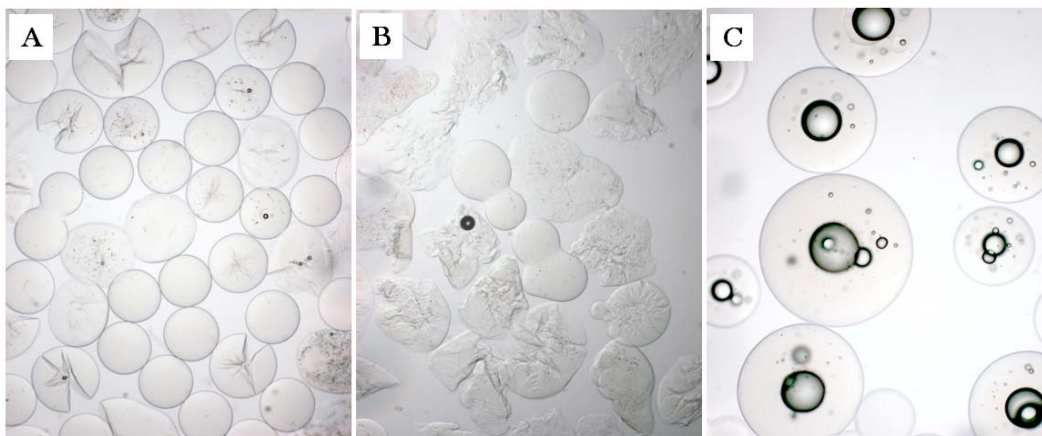


Figure 2.11. Irregular shaped ‘homogeneous’ agarose particles examples. (A) Broken and deformed agarose beads due mainly to excessive stirring. (B) Irregular shaped particles because of insufficient stabilization. (C) Excessive surfactant combined with fast stirring contributes to oil droplets and air bubbles inclusions in the gel.

In many situations spherical beads are obtained, but when deformed particles prevail, the separation of the beaded material is difficult. In conditions where most of the particles are beaded and free of defects size screening is necessary to separate particles fitting in the chip based MAD platform.

The beads are typically sorted with standardized metallic sieves producing populations ranging between the used sieves screen openings. The actual amount of beads for each range is an approximate value since the openings in the screens retain particles of comparable size which eventually clog the screen openings. Unintentionally, larger beads are included in the wrong fraction and in reality those occurrences are not isolated events taking into account the soft nature of agarose. Conversely, smaller beads are held into the wrong fraction due to clogging, fast

wash or large volume of beads to be separated. A relatively rapid cataloging of beads by size between 250 and 425 μm is summarized in Table 2.3 and Figure 2.12.

Sieve Range	Average Size (μm)	Standard Deviation	CV%
250-280 (n=114)	281	11.4	4
280-300 (n=69)	305	14	4.6
300-355 (n=70)	363	16.6	4.6
355-425 (n=49)	416	14.8	3.5

Table 2.3. Diameter length measurement of beads separated into batches of different sizes using screens with openings 250, 280, 300, 355 and 425 μm . (Measurements were kindly furnished by Dwight Romanovicz)

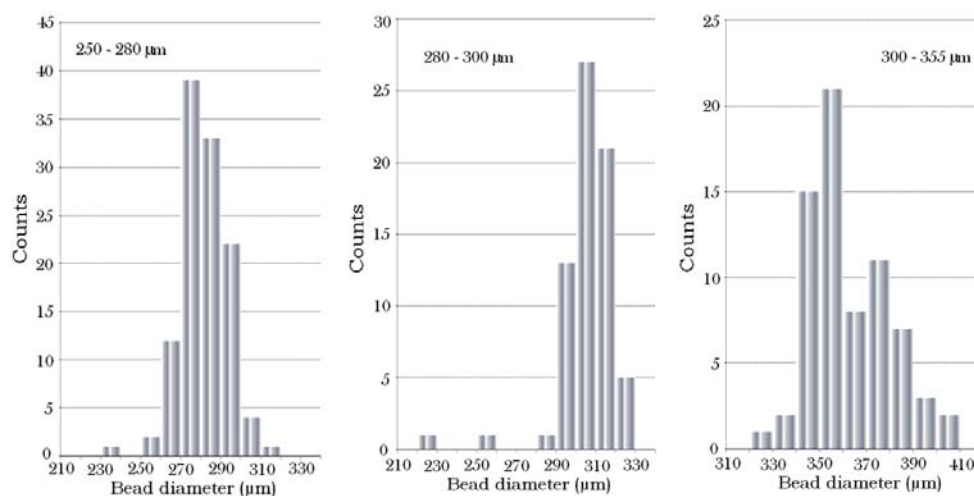


Figure 2.12. Diameter distribution of beads fractions between 250, 280, 300 and 355 μm recovered from size sorting with metallic screens. Diagrams correspond to data shown in Table 3.2. Relatively fast sorting was performed and beads out of the pretended size ranges are included in the fractions.

Cycling of beads into repeated washes and in small volumes can reduce significantly the tails in the bell-shaped distribution, Figure 2.13. The data shown below correspond to previously rehydrated beads with the first screening performed fast.

The sieving of gel microspheres with soft compressible bodies is somewhat complaisant to the passage of larger beads than the size openings specified on the metallic sieves. Thus, beads 250 μm and a few micrometers above 250 will be excluded from the 250-280 μm fraction and beads larger than 280 μm will be included in the specified range. As a matter of fact, the upper limit to the 250-280 μm fractions encompasses diameters close to 330 μm and a few even larger such as 400 μm are pushed down into our fraction during a single size cataloging.

One single simple and fast size sorting proves to be inadequate. A more accurate size range by systematic screening cycles concentrates the beads between 260 and 300 μm with a CV% below 3%. Further sorting of the same fraction after a certain amount of cycles is unfruitful and the propensity to loss of beads is augmented. The efficiency of separation and the number of cycles to accomplish a narrow distribution is sensitive to the volume of beads to be screened such as 10 mL against 200 mL of the mixture.

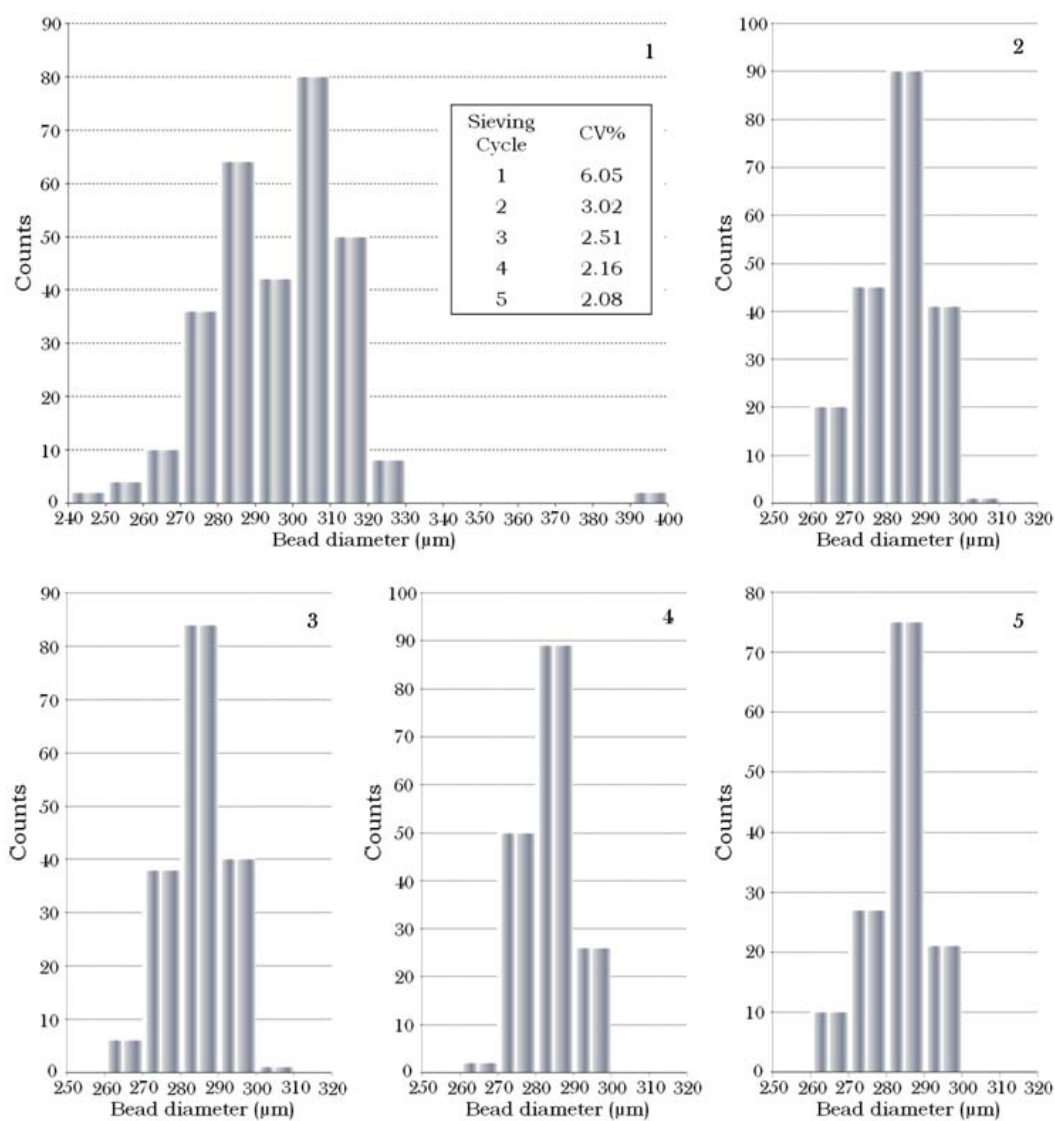


Figure 2.13. Isolation of 250-280 μm agarose beads fraction by size sorting with standardized metallic sieves. The size distribution is narrowed significantly. After the fourth cycle there is no further constriction of the distribution. The size range differs from the engraved value on the sieve frames because of the soft compressible characteristics of the gel. The number of sorting cycles depends on the volume of beads to be sorted.

Alternatively, a particle sorter instrument can be used in an automated fashion to narrow the diameter variation, but the automated sorter has an upper particle limit size that demands a previous screening through metallic sieves to avoid clogging of the instrument. Fraction 250-300 μm was subjected to an automated high-throughput particle analysis/sorting instrument from Union Biometrica (Sommerville, MA) and a diameter variation of about 5% is reported with bead diameter ranged between 225 and 290 μm linked to a CV% of 6.¹⁰¹ The reported value is then considered an improvement over the isolation of beads with metallic sieves. The fact is that the standardized metallic sieves require additional ‘normalization’ affiliated to the soft beads characteristics, amount of beads to be sorted and the handling or manipulation of sieves. To discard the user factor, automated wet sieving stations are also available in the market.

The diameter variation can be adjusted by changing sorting selection parameters in the automated system to produce a more uniform population or thinning the gap in the opening sizes of successive metallic screens. The scope of size processing into a realistic or practical diameter range to be applied in the MAD system has not been delimited yet. The actual magnitude of the error introduced due to size variation needs to be balanced adequately with the time and resources dedicated to minimize the deviation on particle sizes. Currently, the bead diameter in use has a CV% between 3.5 and 4%.

The porosity for agarose gels is conventionally reported as the volume fraction of water in the gel. Porosity for 2, 4 and 6% homogeneous gels shown in Table 2.4 was obtained for large pieces of gel equilibrated in nanopure water

instead of a set volume of settled beads. The volume of water contained in the gels is measured indirectly by measuring the wet weight and dry weight of the gel. It is assumed that all of the water forms part of the ‘free’ space within the matrix, ‘free’ space that is available for mobile phase movement. In fact, the drying process eliminates the water used to stabilize the matrix itself in both coil formation and association of coils to form supra-fibers.

Agarose Gel Concentration (%)	Volume fraction of water (mean \pm SD, $n = 3$)
2	0.9856 ± 0.0001
4	0.9745 ± 0.0015
6	0.9595 ± 0.0015

Table 2.4. Homogeneous agarose gel porosity as a function of gel concentration. The porosity is in inverse proportion to the gel concentration.

2.3.3 Parameters affecting the Size Distribution of beads

Sorting of beads through sieves manually or with automated instruments is important because of the troublesome control of experimental conditions in their preparation. A preferred distribution size with high yield in the desired range can be only corroborated with dependable isolation methodologies. Finally, the yield should be larger than the amount isolated from commercial sources. It is encouraging to be able to prepare a relatively large volume of utilizable beads despite the fact that the scrutiny into the optimal experimental conditions was not exhaustive, Figure 2.14.

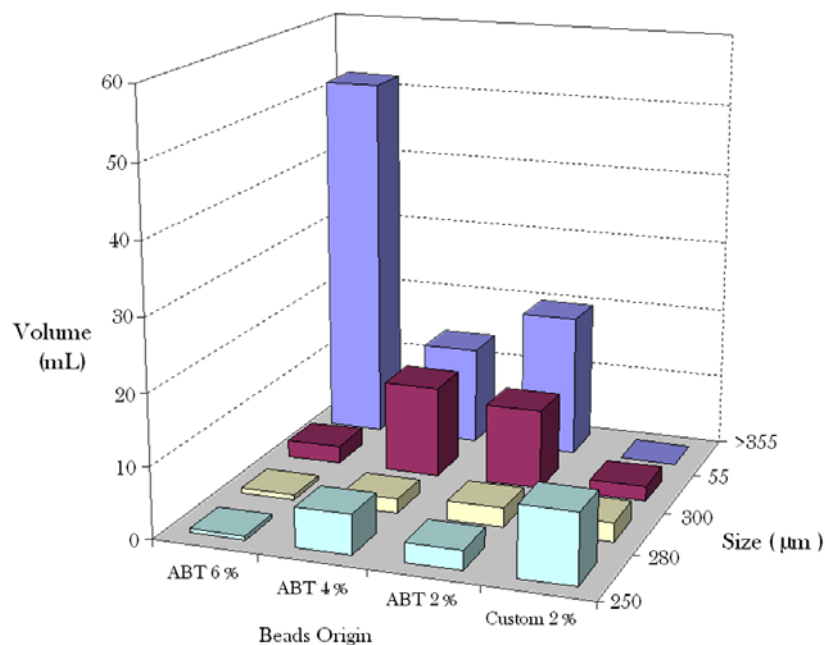


Figure 2.14. Size distribution comparison of ABT and custom made homogeneous beads depicting the volumes of 250-280 μm fractions relative to 50 mL sorted beads.

The following diagrams depict the influence of a few factors affecting the size distribution of beaded agarose. The general preparation procedure for 2% homogeneous agarose beads was used from which only one parameter was changed at a time. The targeted size is fraction 250-280 μm . The mixed population of beads were wet sorted through 355, 300, 280 and 250 μm meshes. The experimental conditions for the diagrams in general correspond to a maxima of the bell-shaped distribution shifted towards the 150-250 μm population (fraction volume not shown) thus the amount of beads above 355 μm is restricted and irregular particles are an unusual finding isolated to the biggest size fraction. The volume of produced mixed beads ranged between 55 and 60 mL of settled hydrated beads and sorting equivalent to three screening cycles (Figure 2.13) was performed on every 10-15

mL mixed beads. Sieves were washed between cycles to unclog openings and care was taken to recover the clogging beads to be added to its corresponding fraction. The beads were allowed to settle overnight and the volume registered next day. Figure 2.15 shows the size distribution of beads obtained at different surfactant concentrations in a fixed volume of suspending solution.

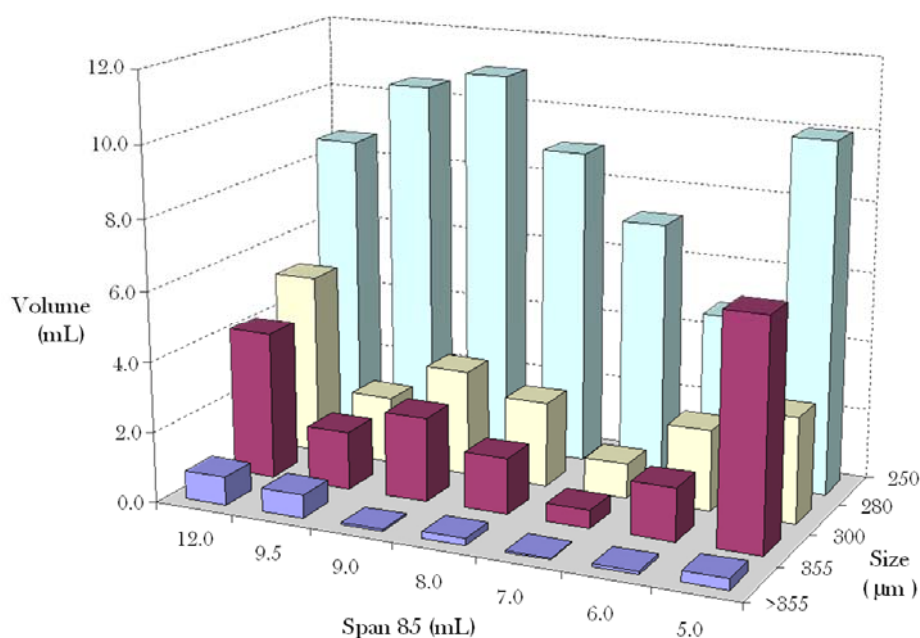


Figure 2.15. Size range distribution of 2% homogeneous agarose beads as a function of the amount of surfactant volume in the suspending solution. The volume of beads between 250-280 μm decrease if the volume of Span 85 is lower than 5 mL Span 85 and shifts the average size of the beads towards larger beads (data not shown).

An increase in the stirring speed invariably leads to a decrease in size of suspended particles, Figure 2.16. An excessive speed overcomes the stabilization of suspended droplets and recombination of particles occur forming deformed particles.

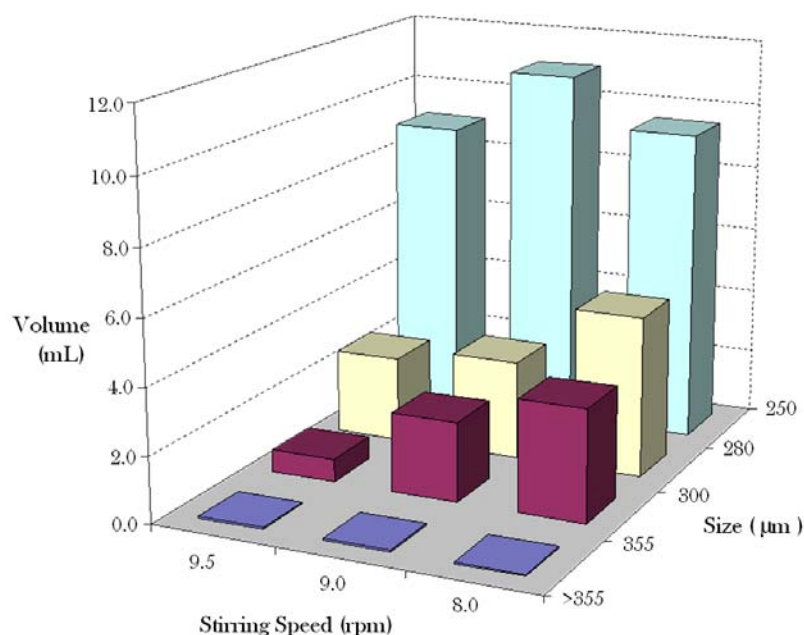


Figure 2.16. Size range distribution of 2% homogeneous agarose beads. Size dependency on the stirring speed.

The concentration of agarose solution increases the viscosity of the solution. Parameters need to be adjusted to obtain a reasonable volume of beads in the expected fraction. In general, under the same conditions, the volume of beads obtained is smaller and the maximum of the distribution is displaced to larger bead diameters (data not shown). The mean volume of the beads thus is bigger than 300 μm . The more viscous agarose solution is more difficult to break down into smaller droplets and it usually requires faster stirring speeds accompanied by larger amounts of surfactant. Working with higher temperatures compensates part of the higher viscosity effect. The viscosity of agarose solutions increases when the temperature is lowered. Alternatively, an increase in the ionic strength of the

solution also reduces the viscosity of the solution, but in addition to rearrangements of the coiled chains of agarose the porosity will also be affected.

The organic solvent and in a more general context the suspending media helps in the stabilization of suspended particles in part by limiting the mobility of the particles. The viscosity and surface tension imparted by the suspending media can favor or hinder the fragmentation and recombination of the suspended solution. It is usually found that suspending media with high viscosity and of opposite nature to the internal phase frequently renders highly stabilized droplets that remain suspended for long periods of time. The aid coming from stabilizing compounds such as surfactant is frequently still required. The choice of suspending media is preferred to be accompanied by easy and safe cleaning procedure. Hexadecane is a better solvent for the suspending solution because of the higher viscosity and in addition due to the higher boiling point. The added stabilization of suspended particles added to the surfactant contribution accounts partially for smaller microbeads and also a larger count of the same. The characteristics of the beads is expected to show some differences in gel strength and in pore size going from hexanes to hexadecane in Figure 2.17. The expected variation arises from differences in cooling rates⁹³ which are approximately 0.23, 0.47, 1.17 and 1.32 °C/min for hexanes, n-heptane, decane and hexadecane. The cooling rate here changes because of the different vapor pressures of the organic solvents. The data shown in figure 3 are partially optimized for n-heptane. Hexanes provides a larger volume of the desired beads (up to 15 mL 250-280 µm fraction compared to 11 mL in n-heptane), but the reproducibility is more susceptible to experimental variations

especially in temperature. Small changes in the cooling rate and/or the loss of the solvent during the temperature stabilization step can reduce the volume of the suspending solution to one half of its original value, and in some occasions more than half of the initial volume leaving behind a thick dense liquid with poor mixing properties.

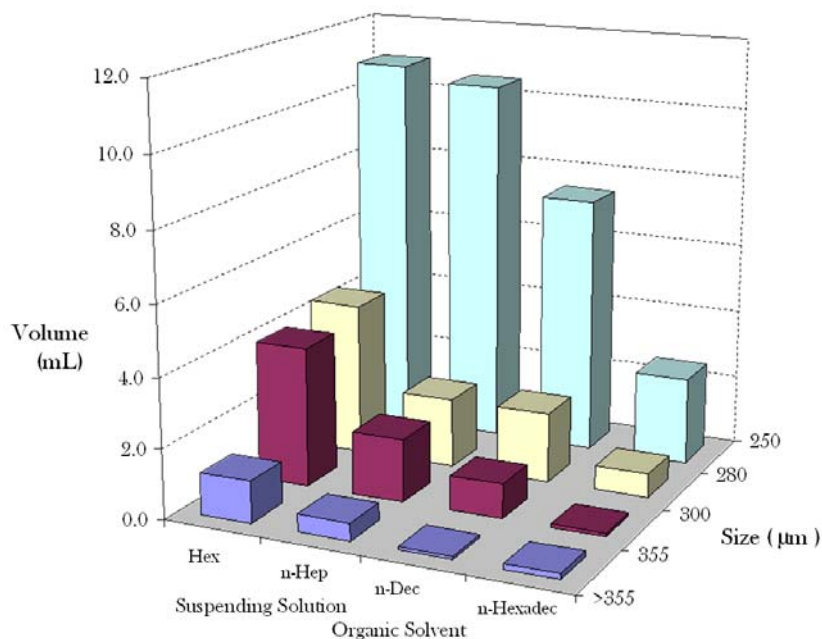


Figure 2.17. Size range distribution of 2% homogeneous agarose beads as a function of the organic solvent type used in the suspending solution. Fractions below 250 μm are not shown. The density, boiling point and viscosity of the solvent are found to be roughly proportional to the molecular weight of the solvent. Interestingly, the stabilization of the suspended particles also follows the same trend.

Fast mixing drags air into the suspending solution adding bubbles inside a large portion of the beads. The beads with bubbles and/or oil phase embedded tend to float after washing with water and the floating layer can be separated easily. Under nitrogen or argon atmosphere prior to adding agarose solution and during

stirring moderates the dissolution of gas in the suspending solution. In hexanes, the amount of floating material is larger and can form up to 6 mL. The volume of floating beads does not correspond to a volume of settled beads because degassing occurs. The layer is thinner with increasing molecular weight of the solvent and under heavier atmosphere. The use of a heavy gas stream accelerates the evaporation of the solvent which occurs faster if hexanes is chosen.

The study with solvents other than hexanes and n-heptane was not performed. Additional tests may be performed to compare the density of gels as well as the porosity due to the change in solvent. This work is outside the scope of this dissertation. There is a slight increase in opacity of the beads when going to hexanes to n-heptane and is more noticeable when using hexadecane. The slight added opacity to the beads when using heavier oils seem to correspond to a larger amount of agarose chains 'crosslinks' to form the more compact packages of supra-fibers and between them. A slight loss in beads transparency is noted when a real crosslinker is used to strengthen the beaded gels.

The change in one of the parameters requires the adjustment of the remainder to produce an analogous volume of beads targeting a specific size range. A unique single combination of parameters that lead to a noteworthy amount of beads has not been established and it is believed exist more than one. It is important to keep in mind that variations in experimental conditions also lead to variations in structural characteristics and even chemical reactivity more specifically related to steric hindrance.

2.3.4 Chemical Modification of Homogeneous Beads: Selection of Crosslinking Degree

Crosslinking of agarose with divinylsulfone (DVS) was first applied by Porath et al. to enhance mechanical properties of agarose gels in high performance liquid chromatography.¹⁰² A modified procedure was later proposed by Hjerten et al. to increase the stability of the gel up to pH 13 and also to reduce irreversible adsorption of some proteins reported to occur with DVS crosslinked agarose supports.¹⁰³ The method proposed by Hjerten et al. additionally eliminates the unreacted vinyl terminations with hydrophilic compounds rich in hydroxyl groups such as D-mannitol, galactose or dextran. The incorporation of such compounds adds more strength to the gel by bridging between close unreacted vinyl groups and compensates for the loss of hydrophilicity and of hydroxyl groups for posterior bead chemical derivatization.

Utilizing the crosslinking procedure previously described, 1 mL of settled 250-280 μm diameter beads were exposed to 25, 50, 75, and 200 μL DVS. If the highest average density is assumed for the packing of the spherical beads, the volume occupied by the beads is ~ 0.74 mL.¹⁰⁴⁻¹⁰⁶ In addition, the measured density of a homogeneous 2% agarose gel is ~ 1.0075 g/mL. Therefore, the calculated mass of the gel modified is ~ 0.73 g per 1 mL of settled beads. The crosslinker volumes, thus, correspond to 4, 8, 12 and 20 wt% of the available gel. Strength of gel studies were not performed on the crosslinked beads. At a first glance, the crosslinker increased the opacity of the gels when a larger amount of DVS is used. A line profile of transmitted light is shown in Figure 2.18. It can be discerned here that a

sharp loss of transparency for highly crosslinked gels is observed as a result of the use of DVS.

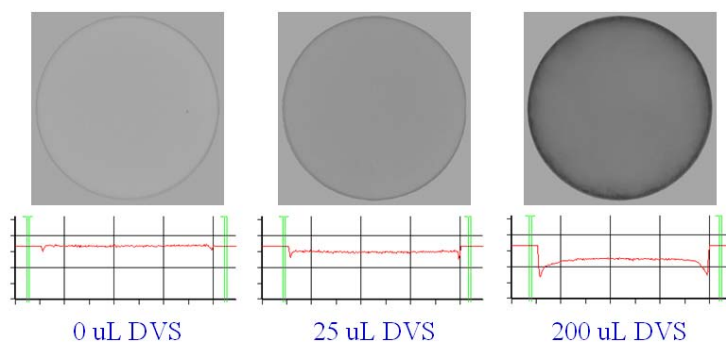


Figure 2.18. Relative opacity of crosslinked beads compared to non-crosslinked gel. The line profile is shown across the bead. The Y axis of the line profile diagrams represent the intensity of transmitted light which decreases as the crosslinking is increased.

Followed by glyoxal activation the reactivity throughout the microsphere is more consistent and the shape is also corrected when compared to commercial beads, Figure 2.19.

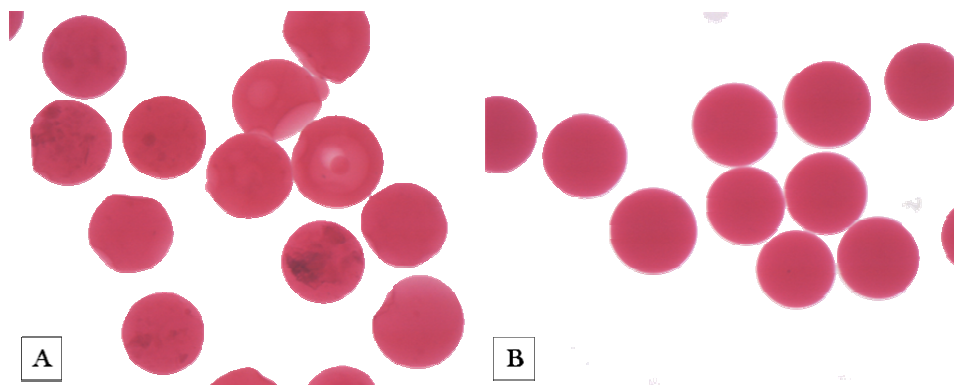


Figure 2.19. Bright field images of crosslinked glyoxal 2% agarose beads. Schiff reagent added to test for aldehyde presence. (Left) Commercial ABT beads and (right) home made beads. The elimination of gel incongruities in reactivity is secured by producing a more homogeneous gel and correcting the lack of symmetry.

A 'sandwich' format immunoassay was performed on home made homogeneous beads coated with anti-CRP protein. A 50 μL volume of settled capture beads in phosphate buffer saline pH 7.4 were exposed 100 μL 500 ng/mL antigen CRP solution for 5 min in an eppendorf tube. Following a rinse with the buffer, the detecting antibody was delivered. The fluorescence signal was measured on the beads after a final rinse with the buffer to eliminate free detecting antibody, Figure 2.20.

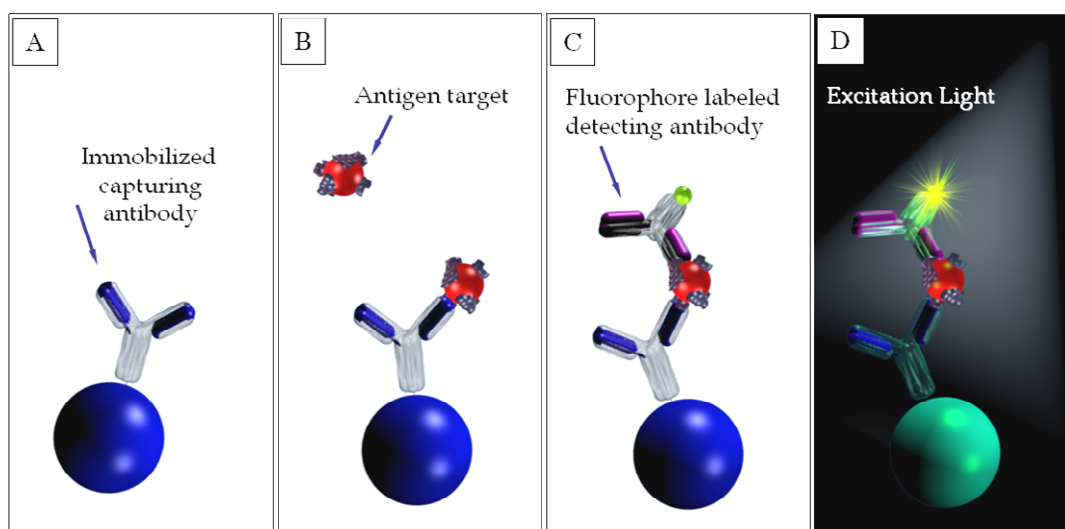


Figure 2.20. Detection of CRP in a sandwich format assay. (A) agarose bead with CRP covalently immobilized on its matrix, (B) Delivery of antigen CRP and capture of target by bead, (C) Following the elimination of excess of antigen, the target/ligand complex is exposed to detecting antibody, (D) after the elimination of unbound detecting antibody, the beads are exposed to appropriate excitation light, and the emitted fluorescence is measured with a CCD camera and the data processes.

The population of 2% agarose beads used for the assay described above, wet-sorted by size with metal screens, comprised microspheres with diameter ranging from 270 to 300 μm . The measured average size, 282 μm , is associated to a coefficient of variance value(CV) of 3.3%. An average fluorescent count of 1800

with a 4.0% CV (n=33) was observed for the beads used on the detection of CRP, Figure 2.21.

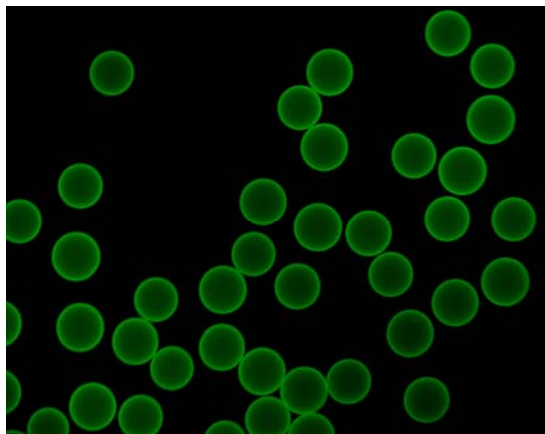


Figure 2.21. Fluorescence signal of a random set of homogeneous beads prepared at the McDevitt laboratory. The fluorescence corresponds to the detection of CRP through a sandwich format immunoassay performed in a test tube. The signal count average is associated to a 4.0 coefficient of variance. The average size of the population of beads used is 282 μm with a 3.3% CV (n=33)

Similar studies of signal variation on the detection of CRP were performed previously by other members from the McDevitt research group. Figure 2.22, taken from the laboratory database archive, show the commercial ABT 6% glyoxal activated and 6% plain non-glyoxilated homogeneous agarose beads. Both bead populations belonged to the same vendor. The objective of the study was to characterize the variability of size and reactivity of the beads obtained from commercial sources. The non-activated beads were subjected to glyoxal activation and wet-sorted by size with an automated high-throughput particle analysis/sorting instrument from Union Biometrica (Sommerville, MA). A CV of 61% and 9% was found for the diameter of the beads before and after size sorting respectively. Correspondingly, CV values of 28% and 6% was observed for the fluorescent

signal count on the non-sorted vendor-activated beads and in-house sorted activated beads respectively.¹⁰¹ These previous studies have shown that the variability in signal response in an immunoassay can be dramatically reduced by controlling certain parameters more carefully. For instance, selection of size and customized activation procedures depicted above in Figure 2.22.

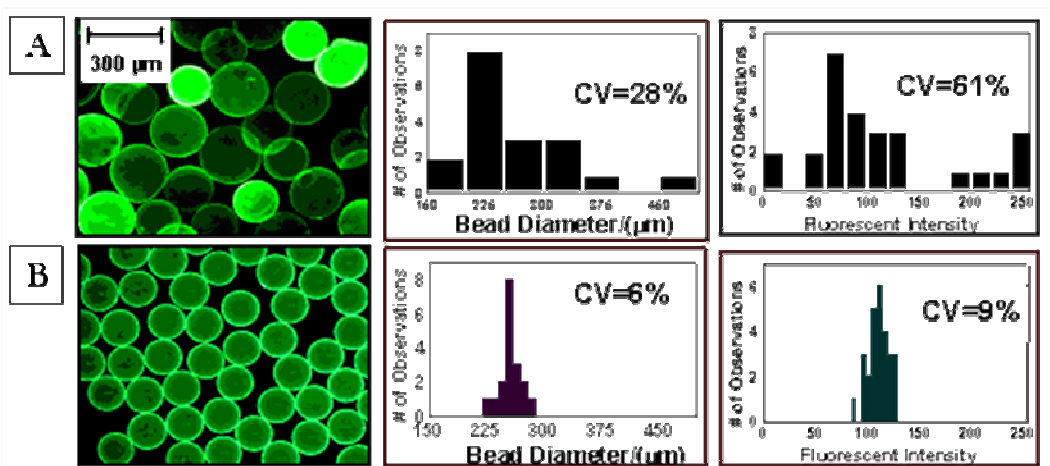


Figure 2.22. Size distribution and fluorescence immunoassay signal variability of cross-linked agarose beads obtained from a commercial source, same vendor. (A) Beads were purchased already glyoxal activated. It is observed a 28% CV for the fluorescent count and a 61% CV for the particle size. The particles were not size-sorted previous to evaluation of the diameter variability. (B) Beads purchased from vendor, but activated at the McDevitt laboratory. The beads were size-sorted with an automated high-throughput particle analysis/sorting instrument. The observed CV for the fluorescent signal and diameter particle size are 6% and 9% respectively.

By preparing and customizing the beads in-house, it is possible to follow closely the experimental conditions used during the preparation of beads procedure and the chemical modification to follow. Not only, was it possible to obtain a relatively large volume of beads homogeneous in size and reactivity with a relatively lower CV, but also, it is possible to narrow the experimental factors contributing to non-reproducible experiments during the development of assays.

An additional bioassay on the capture of CRP in a microchip with ABT and custom made homogeneous beads was performed to help on the performance evaluation of beads crosslinked with variable amounts of DVS. The commercial ABT beads used here belong to a batch of agarose verified to behave satisfactorily in former bioassays. The typical performance of the customized agarose beads within the context of immunoassay is show for these beads as well as similar beads derived from a commercial source ABT, Figure 2.23.

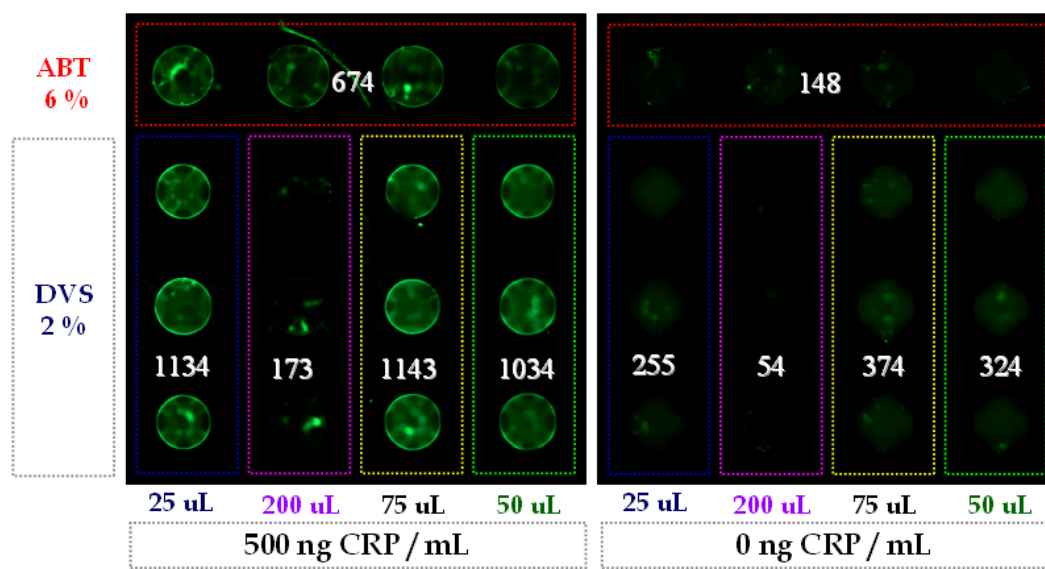


Figure 2.23. Capture and detection of CRP on chip-based MAD system. Beads fluorescence signal before (right) and after (left) detection assay at 80 ms exposure. Beads crosslinked with 25, 50, 75 and 200 µL DVS are compared to ABT beads. The average intensity signal is represented in white. Note a comparable performance of 25 µL DVS to ABT microspheres. The signal ratio of 25 µL DVS to ABT before and after is approximately the same (1.68 and 1.73).

A quick visual observation and the fluorescence intensity measurement of the area of interest aid in the recognition of the highest signal to noise ratio comparable to ABT beads. An initial value of 4 wt% of DVS relative to the amount

of beads was used in bioassays by member of the research group and contributed to adjusting the DVS to a level of ~4.8 wt% (or 30 μ L per 1 mL settled beads).

The data shown in Figure 2.23 shows a decrease in the signal to noise ratio as the crosslinker volume is increased. The crosslinking of agarose involves the bridging of adjacent hydroxyl groups. In addition, the crosslinker will react with any of the hydroxyl terminations available in the matrix. Thus, following excessive crosslinking, the number of sites available for gel activation is drastically reduced. The excessive crosslinking effect is observed going from 75 to 200 μ L DVS per 1 mL settled beads in Figure 2.23. Interestingly, the lowest fluorescence count is seen for 200 μ L DVS for the capture of CRP at 500 ng/mL antigen concentration, but the same highly crosslinked beads exhibit the lowest background levels. As the hydrophilicity of the bead is reduced due to the loss of hydroxyl groups, non-specific adsorption of protein is expected to rise. The expected increase in background levels is observed from 25 to 75 μ L DVS. Interestingly, there is a slight increase in fluorescence signal from 50 to 75 μ L DVS. In addition, the highly crosslinked beads corresponding to 200 μ L DVS shows the lowest background levels indicative of low non-specific interactions. An analysis of the commercial 6% agarose beads, show a relatively low signal count for the detection of CRP considering the gel is 3 times more concentrated than the home made 2% beads. The crosslinking degree in the 6% beads is high since the fluorescence count is similar to a 2% bead. The factors affecting the detection capacity of the 6% beads is not only because of a higher crosslinking degree, but also include the smaller pores and higher density of capturing ligand immobilized on the matrix. A large volume

of capture protein per unit volume may add steric constraints to the immobilization of analyte since the binding sites are obstructed by neighboring capture proteins. The inability to secure the analyte contributes to a “faster” diffusion of free analyte into the interior of the bead. For instance, in Chapter 4 it is seen that the “apparent mobility” of a 50 bp oligonucleotide through agarose media with a capturing probe is $\sim 2 \mu\text{m}/\text{min}$ while the mobility without a capturing probe $\sim 35 \mu\text{m}/\text{min}$. The analyte in an environment with sequestering abilities is not actually “free” to move around, thus the “apparent mobility” here is referred to the erratic movement of the analyte though a restricted distance, temporarily slowed down by a capturing ligand because of unsuccessful immobilization. The analyte then resumes its path towards deeper into the bead. These mobility values are not applicable to the detection of CRP here considered. The analytes involved in this section are much larger than a 50 bp oligonucleotide sequence and the charges of the molecules are also different. The enhanced mobility of analytes makes the internal volume of the bead more available to be used in short assay times and it is discussed in more detail in Chapter 3. The slight increase in the fluorescence at 75 μL DVS with respect to 25 μL DVS may be attributed, in part, to the slight enhancement on the analyte “mobility”.

2.3.5 Superporous Agarose Beads - Motivation

Homogeneous gels provide limited mobility to analytes owing to pore diameters of comparable size. Similar to chromatographic separations, the immobilization of analytes by affinity interaction or adsorption entails the transport of solute to the reactive surfaces of the solid support. Solutes are transported in the bulk of the solution through dominant convective movements which in the chip-based MAD system is furnished by pumps. Within the bead the liquid is of a stagnant nature when compared to the bulk of the solution and diffusive movement of mobile phase is prevalent. The diffusion in agarose cannot be eliminated for it will require a significant transformation of the biomolecule basic structure. The scope of the diffusion transport can be scaled down with large interconnected flow-through pores within the bead, Figure 2.24.

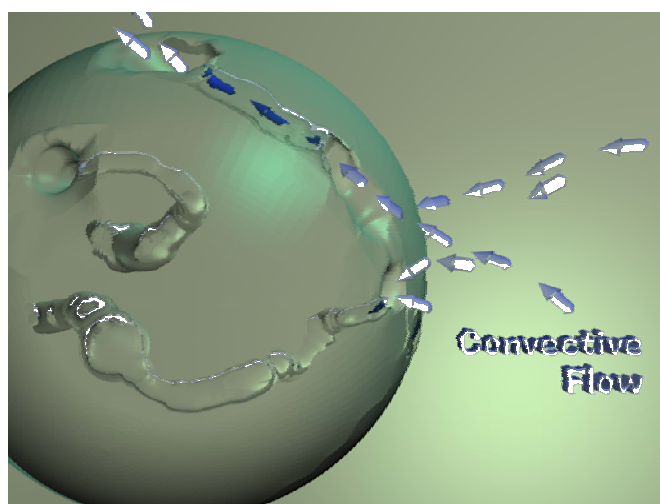


Figure 2.24. Illustration of superporous beads external surface showing large openings (left) that brings mobile phase convective movement into the bead (right). Only a few flow-through channels are shown.

Instead, the gel is partitioned into smaller homogeneous regions surrounded by large pores that bring convective fluid motion throughout the bead. Accompanying the facilitated mobile phase transport, the inclusion of enlarged cavities or ‘superpores’ accommodates larger particles to be immobilized within the bead.¹⁰⁷

Typical procedures for the preparation of superporous include the addition of a porogenic agent such as calcium carbonate solid particles to the agarose solution to be emulsified. The solid particles embedded in the beaded gel are dissolved afterwards leaving the empty interconnected large cavities.⁹⁸ Alternatively, a liquid hydrophobe can be used as the porogenic agent in a double emulsification of an agarose solution. Space occupied by the organic solvent will form interconnected channels as agarose is set to gel.¹⁰⁸

The superporous spherical particles, prepared frequently through a double emulsification process, show a large size distribution. The separation of beads into fractions with graded sieves to produce relatively narrow populations of beads in size is a common practice. The beads are usually packed into columns for high speed protein chromatographic separations. Within this context, separation of proteins has been reported where the matrix is modified directly by attaching a hydrophobe or an affinity ligand to perform hydrophobic and affinity interaction chromatography respectively^{96, 97} Also, diethylaminoethyl derivatized columns were used in ion exchange chromatography.⁹⁸ In addition, affinity chromatography was performed using red blood cell membranes as the affinity ligand. In this immobilized biomembrane affinity chromatography modality a suspension of red

blood cells were sequestered in the superpores of the beads relying on the sieving capacity (size exclusion) of the superporous gel.³⁹ Typically, the preferred particle size diameters in the chromatographic separations above range from 100 to 500 μm , and the populations used are further narrowed down to show a variation of up to 200 μm diameter. A narrow size range eliminates the possibility of a dense packing of the gel since the smaller particles tend to occupy interstitial spaces between larger beads. In packed columns of superporous beads, both the superpores and the interstitial spaces contribute to the mobile phase transport to enhance the speed of chromatographic separations.

The homogeneous bead pores are relatively small, typically below 500 nm. In superporous bead, the superpores may vary in size depending on the experimental conditions. The superpores are surrounded by dense homogenous agarose regions and these large channels are interconnected in the internal volume of the bead, Figure 2.25.

In simple emulsification techniques two immiscible phases are ‘mixed’ and one of them usually referred as the ‘internal phase’ is dispersed as fine droplets in the ‘continuous phase’. Under these conditions and oil-in water or water-in-oil emulsion is formed and routinely homogeneous particles with a relatively uniform set of micropores are obtained. Under the strict definition of polymerization, homogeneous beads result. Alternatively, gels such as agarose where no actual polymerization is involved provide the homogeneous beaded gels described earlier.

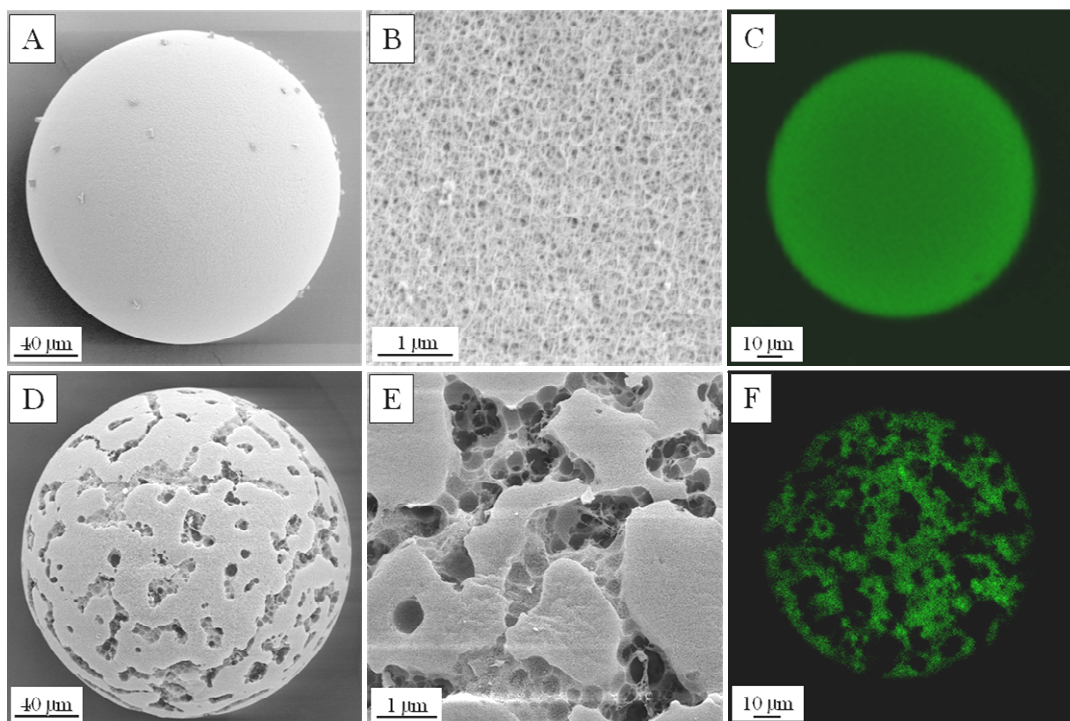


Figure 2.25. Scanning electron micrograph of (A) conventional agarose bead, (B) close-up of surface in homogeneous agarose bead, (D) superporous agarose bead, (E) close-up of superporous agarose bead showing superpores. Confocal laser scanning micrograph showing the medial slice section of (C) conventional homogeneous agarose bead and (F) superporous agarose bead showing the large flow through channels. The beads were stained with a dilute solution of acridine orange for confocal images.

The preparation of beaded macroporous structures usually follows a double emulsification procedure. Thus, ‘oil-in-water in-oil’ or ‘water-in-oil in-water’ emulsions are formed. If the proportion of internal-to-continuous phase in any emulsion is not less than 70%, it is then considered a high internal phase emulsion (HIPE). Low internal phase emulsions (LIPE) will contain no more than 30% internal phase.¹⁰⁹

The superpores in an agarose gel involve the formation of a medium internal phase emulsion (MIPE) considering the classification just described. Here

the MIPE is an oil-in-water emulsion where the organic solvent or porogenic agent is stabilized by an appropriate surfactant into small droplets in the aqueous phase. The relative amount of oil-to-water phases is set to obtain a thick foamy ‘liquid’ after stirring is applied. A second emulsion, a water-in-oil emulsion, is obtained when the foamy MIPE is suspended in organic solvent and broken down into stabilized MIPE blocks.¹¹⁰

Within each suspended MIPE fraction the gelation of agarose brings together the individual sugar chains reducing the liquid like properties of the agarose solution. Water and agarose ‘separate’ into two phases as agarose becomes insoluble. The oil phase in the foam concentrates forming “arteries” within the agarose network in a process similar to creaming, Figure 2.26.

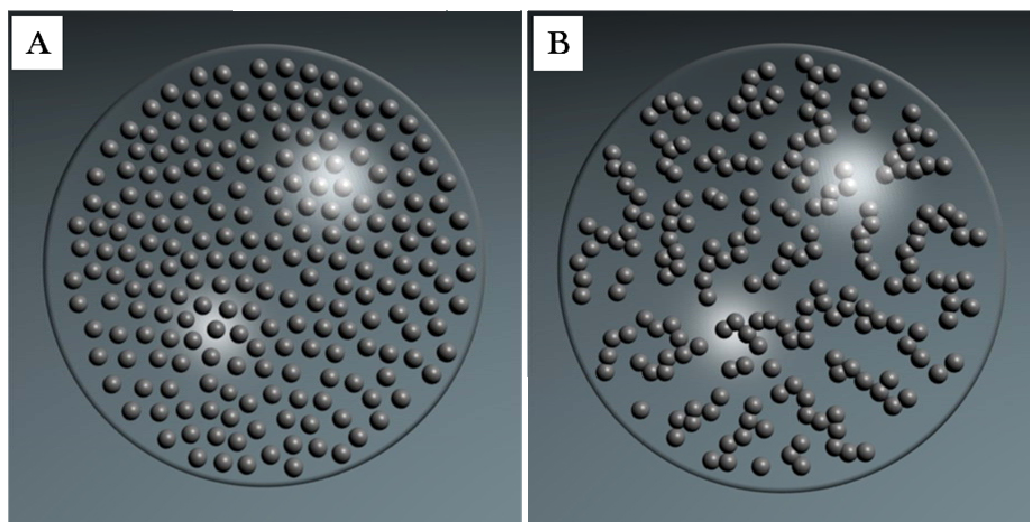


Figure 2.26. (A) Illustration of a stabilized droplet of medium internal phase emulsion (MIPE). Here the MIPE is an oil-in-water emulsion where the oil phase is suspended in an agarose solution. (B) The oil phase in the MIPE accumulates to form larger pools which when interconnected generate arteries that later constitute the superpores in the agarose bead once the aqueous phase gels. The segregation of the oil phase is accelerated by the gelation process when agarose chains aggregate.

As the oil phase droplets in the foam are brought together flocculation, Ostwald ripening and coalescence occur to some degree. The extent at which the arteries grow in size and count depends on the speed at which agarose is set to gel. Faster cooling of the mixture will reduce the time and speed at which oil droplets in the foam will come together and smaller arteries will be formed through the gel matrix. Slow cooling will allow migration of oil droplets in the foam into larger pools that will constitute larger arteries.

2.3.6 Morphological Features of Superporous Agarose Beads

As a matter of fact the pore size control and the mechanism involved in the formation of pores has proven to be much more complicated than described above. The cooling rate is only one factor that affects the structural characteristics of the bead in terms of large channels as well as the homogeneous gel regions the bead will end up with. In addition to increased controlled porosity the shape and the amount of beads of proper size cannot be forgotten in order to be used in the chip-based MAD system.

The shape follows the same trend as homogeneous gels as there is a tendency to deviate from spheres as particles grow larger in size. Even at experimental conditions here considered extremely similar there have been many circumstances in which the product obtained is completely different and the success in correlating to a specific cause was not accompanied by fortune. The unexpected mishaps are at the same time a healthy and a disconcerting reminder of the puzzling combination of agarose and emulsions systems.

A textured appearance is observed under a microscope in brightfield mode (pictures not shown). To some degree variation in pore size is detailed on beads obtained at different experimental conditions. A more accurate and complete characterization of the final product includes surface imaging through scanning electron microscopy and a more visceral view with confocal laser scanning microscopy.

Significant insight into the internal pore structures of the superporous beads can be achieved from confocal measurements. Images of bead sections obtained with confocal micrographs on fluorophore labeled superporous microspheres show interconnected conduits and agarose pocket voids of different diameter, Figure 2.27.

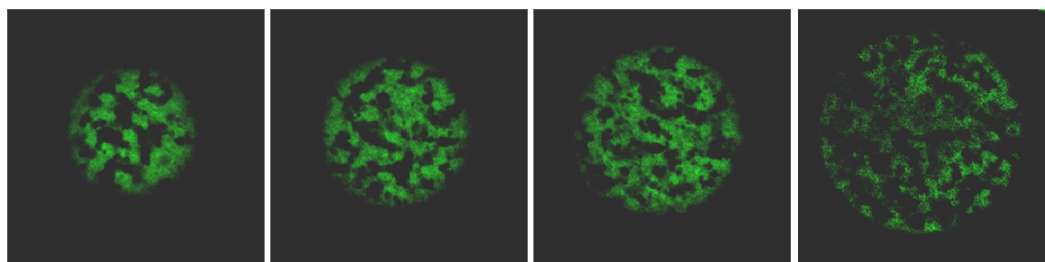


Figure 2.27. Confocal Laser Scanning micrographs showing slices of a superporous bead illustrates large interconnected channels within the bead. Beads prepared as described in the preparation procedure above. Volume void of agarose accounts for at least 35% of the total volume of the bead contributing to pores with diameter size ranging from 4 to 50 μm . The MIPE hydrophobe to agarose solution ratio used is 40% for the 4% superporous agarose beads.

The cross-section of pores on individual beads can be measured to estimate the average superpore size and the contribution or large pores to the total void volume in the bead. Void volume is estimated from different slices of the bead by applying a mask through Image Pro Plus v.4.5 software. The area of bright regions

is measured in the area of interest and subtracted from the total area of the region of interest. For the experimental conditions described in the preparation procedure, the estimated void volume accounts for at least 35% of the total volume of the bead with pore size diameter measured between 4 and 50 μm . The volume ratio of hydrophobe to agarose solution used is 20 to 50 mL or 40%. It is, therefore, concluded that most of the hydrophobe in the MIPE intervenes in the formation of large pores. Confocal images of specimens with similar internal porosity features do not necessarily illustrate unmistakably connectivity of the pores extending all the way up to the surface. Complementary SEM images show distinct cavities on the surface of the beads, Figure 2.28. Likewise, cavities on the surface do not guarantee the existence or a internal set of interconnected large pores.

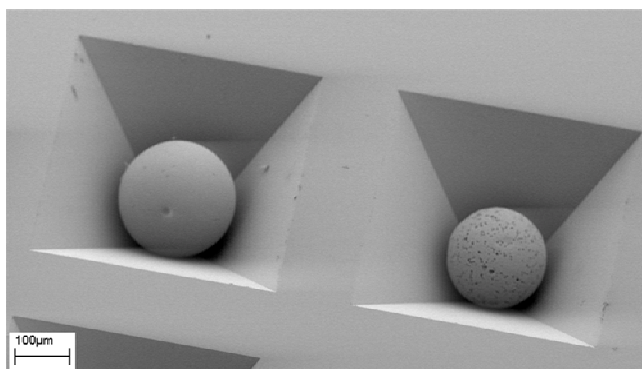


Figure 2.28. SEM picture showing homogeneous (left) and superporous (right) beads on wells etched in a silicon chip. The black dots on the superporous beads are the superpores cavities. The beads are 250-280 μm in diameter. The dent in the homogeneous bead is because of manipulation with a sharp hard object.

Similar to confocal images, the size measurement of the holes cannot be converted back faithfully to the real cavity dimensions found in the hydrated gel. The drying of agarose does not yield consistent degree of shrinkage. The

superporous beads (250-280 fraction) contract to about one third of its original size after critical point drying (CPD). In contrast, 2% homogeneous agarose beads shrink to about two thirds of the hydrated gel size. The exchange of solvent to eliminate water from the structure prior to CPD does not produce a significant difference in size between the hydrated and ‘dehydrated’ forms of the gels. The dehydration is not complete in ethanol and water involved in the stabilization of the gel structure through hydrogen bonding is not lost completely during the solvent exchange. The extraction of water during the exchange of water with ethanol produces an irreversible change in the volume of the gel and it is attributed to the same phase separation process that occurs during the transition from solution to gel.¹¹¹ The total elimination of water and ethanol during CPD takes the gel through the critical point where ethanol and liquid carbon dioxide coexist as a single phase (41°C and 1200 psi).¹¹²

Fluctuations in pore size of dried agarose in part derive from the distribution of pores, the breadth of the cavities and the density of the gel which in some experimental conditions are substantially different, Figure 2.29.

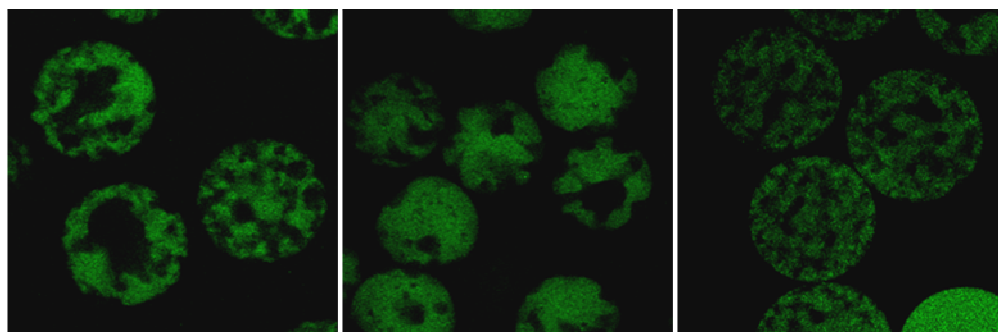


Figure 2.29. Confocal images of bead medial cross section depicting variations in shape and size in the pores or cavities inside beads.

Nevertheless, surface images provide valuable qualitative structural information and in conjunction with confocal images it is possible to ascertain the presence of ‘large’ channels not restricted strictly to the internal volume of the beads, Figure 2.30.

The amount of surfactant (Span 85) in the suspending solution affects the surface of the SA beads, Figure 2.30. In addition to separating the volume of the MIPE into smaller fractions they are stabilized into spherical particles as the surface tension is minimized. The dissolved agarose transits into the gel and purges the hydrophobe contained within. The isolation of the hydrophobe is not confined to the inside of the developing bead. It also occurs at the surface level where the second surfactant is still ‘protecting’ the disintegrating MIPE. The protection of the MIPE is not perfect. The hydrophobe in the MIPE is soluble in the suspending solution and although surrounded by a surfactant (Tween 80) part of the hydrophobe escapes into the suspending solution. There are two possible paths for the hydrophobe: to join the bulk of the suspending solution which in this case is exactly the same media, that is hexanes. Alternatively, it can stay as isolated hydrophobe surrounded by two layers of surfactant forming micelles (Tween 80 sandwiched between hexanes and Span 85).

Figures 2.30-A and 2.30-B suggest the hydrophobe from the HIPE stays with the bead and there is limited diffusion of the hydrophobe into the suspending solution at least until the gel is formed.

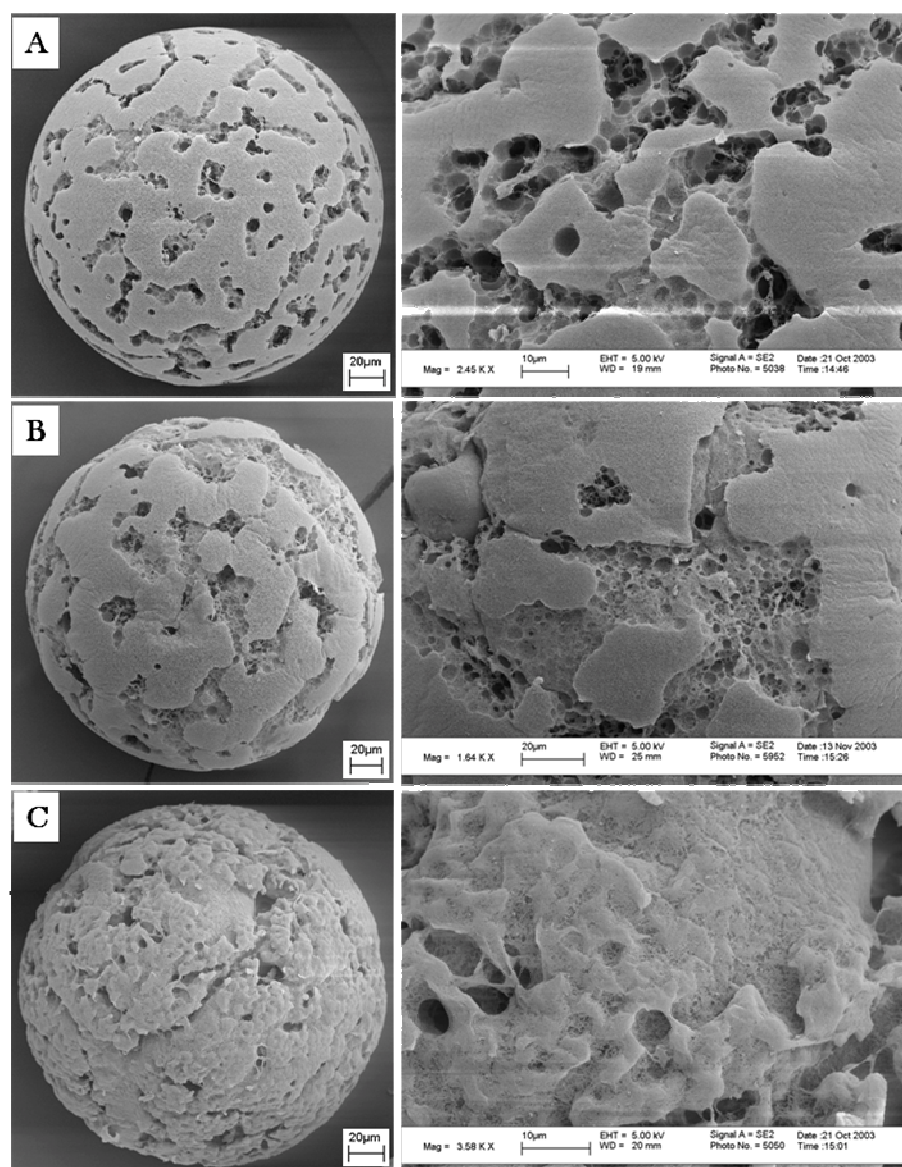


Figure 2.30. SEM micrographs of superporous beads depicting the surface morphology as a function of surfactant agent Span 85 in suspending solution. From (A) to (C), 10, 8 and 7 mL Span 85 was used respectively. Surfactant Tween 80 in the MIPE was set to 1.4 mL for all of them and the stabilization temperatures set between 58 and 60°C. The surface is smooth for beads in (A) and (C) similar to homogeneous bead if enough surfactant is added. The cavities edges are ‘sharply’ defined but as Span 85 is lowered the surface exposes less of the pores to the surface. In (B) an agarose coating is building up on the surface. In (C) the extent of the coating proceeds further and the thin homogeneous agarose layer reduces the access to the bead.

Stable droplets of the HIPE hydrophobe can be seen imprinted on the agarose surface in the channels. It is not possible though to determine from the pictures the degree of association of small hydrophobe droplets into bigger ones resulting from simple flocculation or any other process characteristic of emulsions. In Figure 2.30-B, the grooves are found to be wider, but the surface apparently shows less cavities connecting to the interior of the beads. Further reduction of surfactant in the suspending solution leads to a completely irregular surface with no fingerprint of the HIPE hydrophobe droplets on the immediately visible surface. The cavities conducting to the interior of the bead with amorphous surface, Figure 2.30-C, are covered by an agarose veil of loosely threaded fiber providing the gooey appearance when compared to Figures 2.30-A and 2.30-B.

Beads depicted in Figure 2.31 are suggestive of the presence of superporous spherical beads similar to the ones shown in Figure 2.27. Changes in experimental conditions from Figure 2.27 to 2.31 include an attempt to down-scale to one fourth the reagents used and faster cooling rate. The volume reduction factors in the cooling rate, but also places more acute shearing stress to the suspended MIPE fragments connected directly to the smaller reactor volume. The aftermath is far more frequent finding of deformed particles even in the 250-280 μm fraction. Cleaning of the sample was limited to washing with water during size sorting with metallic sieves. The particles were dyed with acridine orange. It is expected to find smaller particles swallowed up by larger ones during the stirring process. Excessive

shearing and lack of stabilization incites coalescence and in the process of stabilizing the larger particle a smaller one is pushed in. In localized events vesicles are also formed with agarose between a double layer of surfactant resulting in pockets of suspending solution in the bead.

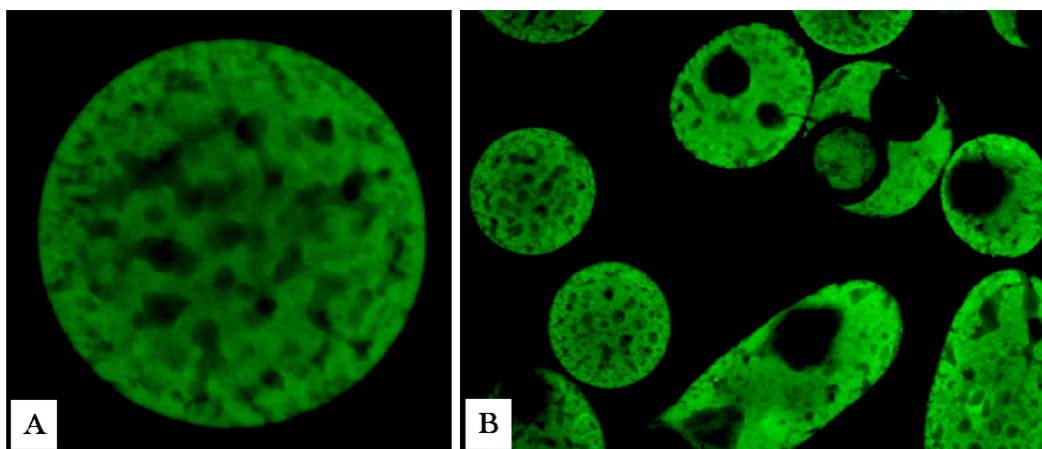


Figure 2.31. Superporous agarose confocal images. Note the spherical symmetry on the superporous bead shown in (A) and a couple of beads in (B). Particles between 250-280 μm were collected, washed with water and dyed with acridine orange. The cavities found in the particles are either originated by segregation of the hydrophobe from the MIPE, engulfing smaller beads or of a large amount of organic solvent from the suspending solution. The characteristics of the agarose gel below the surface of the beads are not predictable through confocal images. Experimental conditions similar to beads from Figure 2.27, but the amounts of reagents used were scaled down to one fourth. Additionally, the cooling rate was increased by submerging the reactor in a bath of cold water at room temperature.

Returning to the surface analysis of the beads, SEM images of particles belonging to Figure 2.31 are illustrated in Figure 2.32. A soft smooth surface is revealed on some beads plagued with small cavities. It is plainly captivating when the shy ones still keep part of their coating and as particles of the same party strip away their garments they disclose a little more about their origin.

The formation of the thin delicate agarose membrane regulates the loss of hydrophobe from the HIPE into the suspending solution and provides enough time for agarose to gel before the porogenic agent is lost. The surfactant in the suspending solution provides protection to this thin veil.

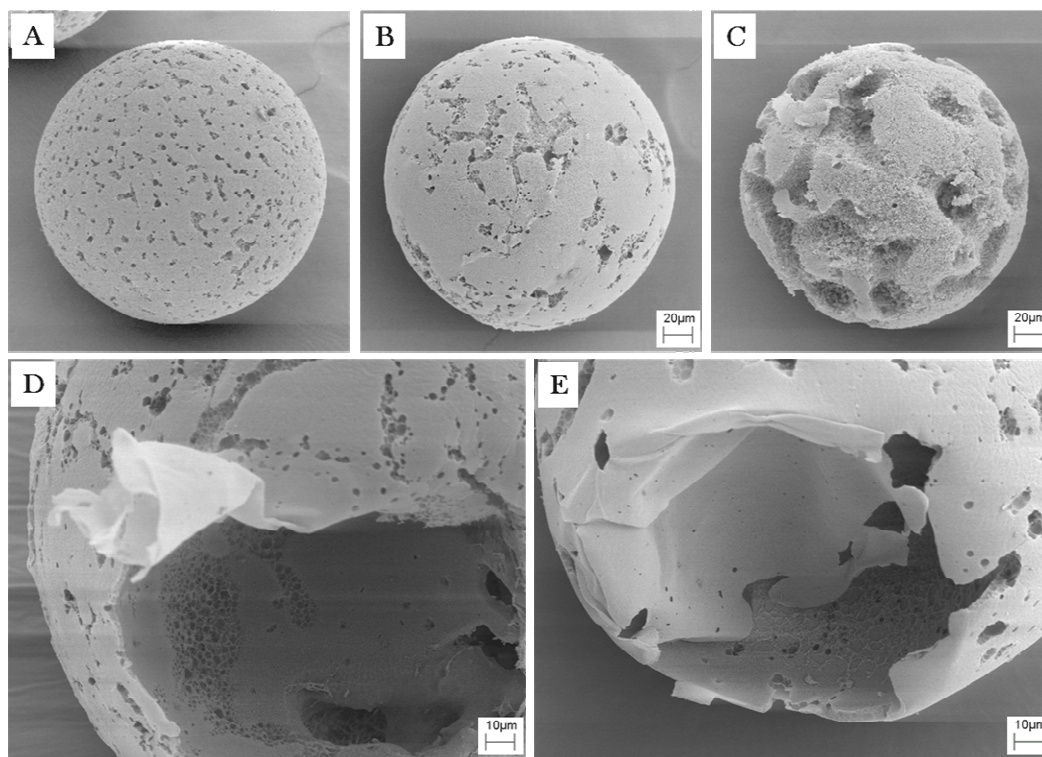


Figure 2.32. SEM images show same ‘superporous’ agarose bead depicted in Figure 2.31. (A) Spherical bead with smooth surface showing a copious amount of cavities. (B) Agarose surface layer peeling off the bead. (C) Bead without agarose layer coating showing large grooves and a ‘sandy’ like texture of agarose. The presence of traces of the agarose veil is still present. (D and E) Large cavity on ‘superporous’ particles. Note the delicate thin agarose membrane.

Image 2.30-C is probably an extreme condition equivalent to image 2.32-C. The veil is held so loosely by a few crosslinks that is lost easily either due to shearing forces in the stirring of the mixture or during the washing and sieving of

the beads. Confocal images do not reveal the presence of the thin layer and large cavities may be actually just isolated pockets void of agarose.

The effect of fast against slow cooling over the pore size is not easily discernible by confocal microscopy unless the destabilization of the MIPE is high enough to produce pores in which the size in average shows a significant variation. The MIPE evolves from fast stirring of a mixture of hydrophobe, surfactant and agarose solution. The mixture turns into a foamy ‘liquid’ and the mixing is less efficient. The volumes of foamy liquid localized farther from the stirrer shaft do not flow easily towards the propellers. The result will be a non-completely homogeneous break-down of the mixture and slight broadening of the pore size distribution from bead to bead in the same batch. The broadening of the pore size distribution is large enough to difficult weighing the contribution of the hydrophobe migration to form bigger pockets of hydrophobe.

It is intriguing to find out that the surface in beads obtained with a fast cooling process can provide a surface of such a smooth consistency as seen in Figure 2.32. The hidden agarose below the smooth surface shows on the other hand a ‘sandy’ like texture, image 2.32-C. A magnified view of the network exhibits a disordered association of agarose chains as opposed to a woven network of fiber found frequently when the agarose is left to gel slower, Figure 2.33.

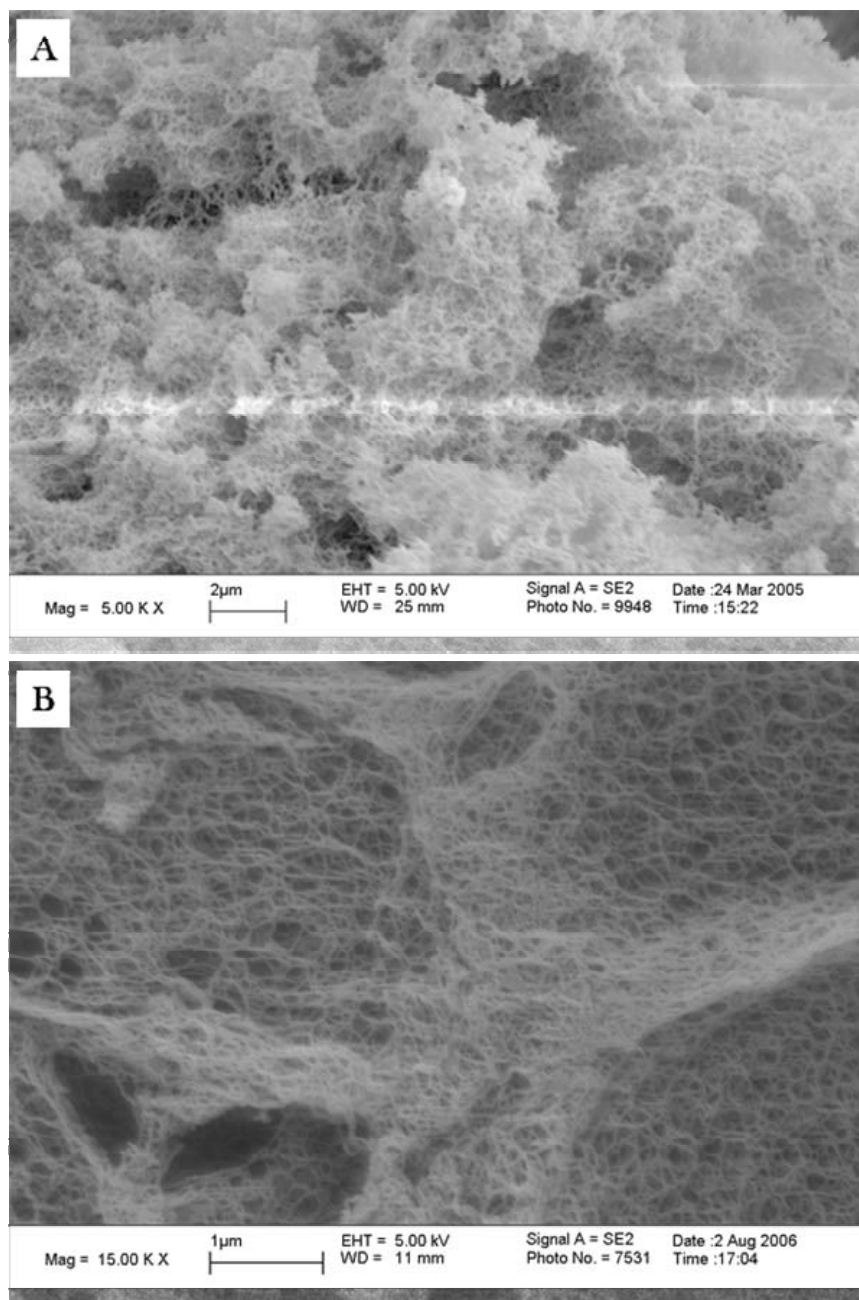


Figure 2.33. (A) Agarose forced to cool fast yields a disordered network similar to glass wool seen at naked eye. Image corresponds to beads from Figure 2.32. (B) A more detailed woven network of agarose fibers is seen when the agarose is gelled more slowly. Note the length of the fibers between the two networks.

The mixture is usually cooled down faster by submerging in a large pool of water bath at room temperature or slower by simply exposing the container to room temperature. The heat transfer efficiency is of course better when the container is in contact with water. What here is considered fast or slow does not seem to be strikingly different, but the temperature at which gelation starts decreases with increasing cooling rate. For instance, a drop from 56°C to 25°C ($\Delta T = 31^\circ\text{C}$) in 15 min or alternatively in 2 min correspond to a cooling rate change from 2 to 10 $^\circ\text{C}\cdot\text{min}^{-1}$. For a 3% agarose solution, this represents at least 1°C difference in the onset gelation temperature.⁹³

The “woven fabric-like network” of agarose is observed frequently in homogeneous gel media even when ‘rapidly’ cooled. In reality, the SEM micrographs can be very misleading and a look at the surface of the bead is not telling what is going behind the scenes. There is unequivocally a profound effect of the stabilizing agents on the surface morphology of the beads and of fast vs. slow transition to the gel state of agarose beyond changes on the onset gelation temperature. Thinking back on the role of porogenic agent, fast cooling affects the speed at which the porogenic agent is squeezed out from the agarose skeleton. At the surface of the bead the loose fluffy consistency of fibers giving the gooey feel of the veil emerges from a delicate local combination of stabilizing surfactants where a dynamic exchange of hydrophobe from the MIPE and from the suspending solution occur. Yet, the dynamic exchange is affected by temperature variations, shearing forces which are more prominent at the droplet surface level and the evolution of the agarose chain association also at the surface level. The exchange of

surfactant is also a latent possibility. After all, the rapid stirring breaks down the MIPE. Fractions of the MIPE are broken further into smaller pieces and recombination occurs until a delicate compromise is reached between the many components in the mixture.

The loosely woven agarose veil at the surface from Figure 2.30-C may also be obtained in conditions similar to the ones used in Figure 2.30-A without changing the amount of reagents or the cooling rate. For instance, in Figure 2.34, the particles were prepared using 9.5 mL Span 85 in the suspending solution. This concentration stands between cases A and B in Figure 2.30. Instead of a smooth surface the particles resemble more case C in Figure 2.30. Leaving aside the obvious fact that the batch of superporous particles exhibited poor overall morphologies, the manipulation of the solutions was inverted during the agarose bead formation procedure. To detail more the change in experimental conditions, the general preparation procedure entails a MIPE continuously stirred and during that time frame the suspending solution is equilibrated to 60 °C and then added to the stirred MIPE. In contrast the MIPE after being formed was warmed up in a separate bath without stirring while the suspending solution was stirred and equilibrated to 60 °C. The simple change in order inadvertently added minutes to the MIPE sitting ‘still’ in a warm bath and favored minuscule separation of phases. The hydrophobe droplets conglomerate either into larger pools of individual entities or merge to form larger single droplets.

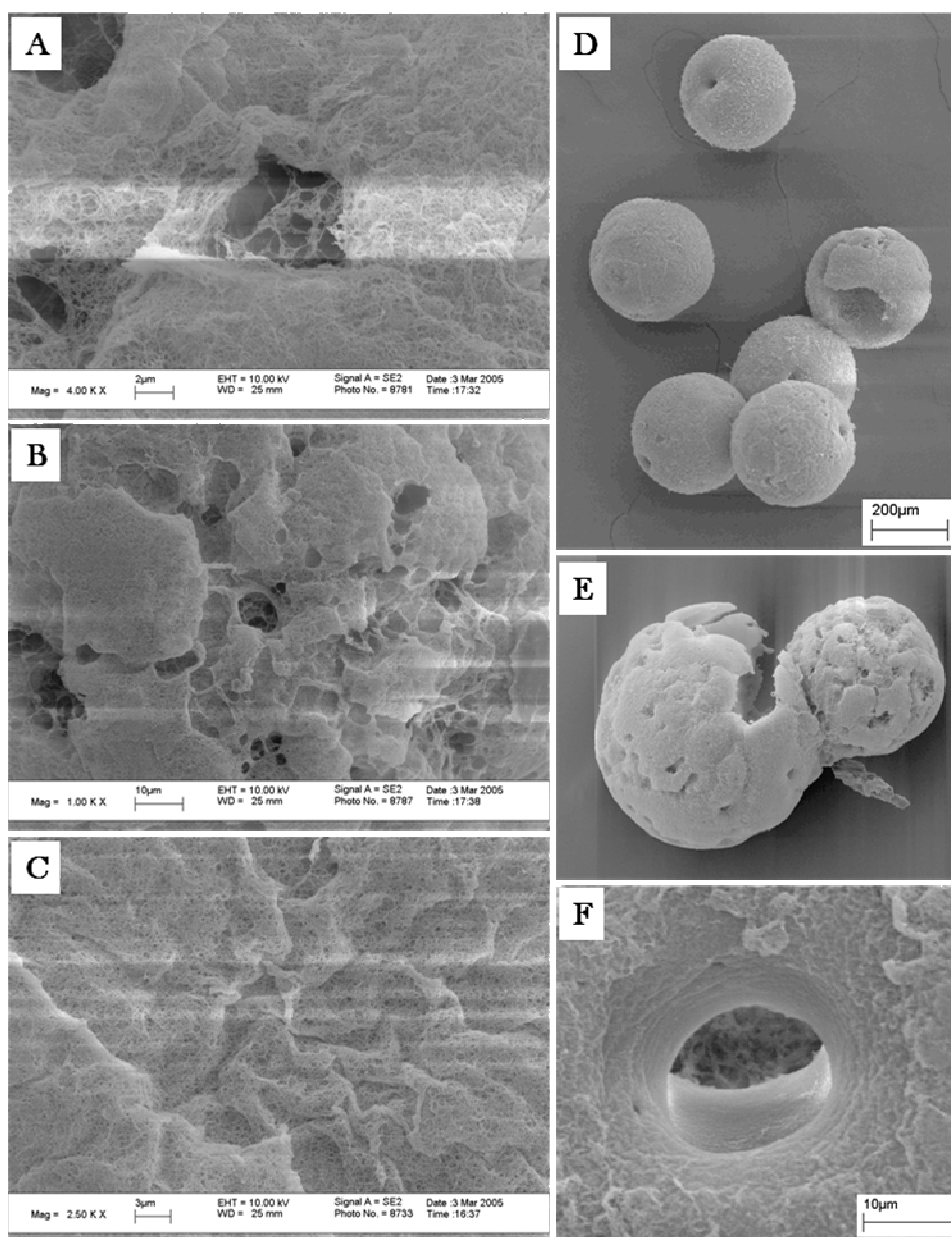


Figure 2.34. (A to C) Different growth stages of thin veil of loosely threaded agarose. (D) Complete coverage of holes with thin film of agarose. The film is not a densely packed form of agarose. (E) Deformed ‘superporous’ particles coated with thin veil of agarose. The particles have surface morphology similar to beads shown in Figure 2.30-C. (F) Illustration of a large cannel that leads into a large cavity in the particle. The experimental conditions are similar to the particles in Figure 2.30-A

The destabilization of the MIPE was initially constrained to the interval of time given by the cooling rate of the final mixture. The additional destabilization period accounts for larger channels or cavities in the bead observed in Figure 2.32. The larger cavities connecting the interior of the transforming MIPE and the suspending solution supports exchange of surfactants and hydrophobe in and out. The stabilized hydrophobe from the MIPE by Tween 80 have a hydrophobic surface and preferentially stays in the stabilized region containing agarose. The exchange may involve transferring hydrophobe around the surface of the forming bead which in addition to isolated hydrophobe droplets explains the low density fluffy consistency of the surface.

The stability of the MIPE was briefly tested by leaving it for longer periods of time at 60°C. It was found indeed a thin layer of hydrophobe accumulating between the glass container and the body of the MIPE. The time length required for the hydrophobe droplets to grow to a size observable by naked eye was not measured or registered, but it was certainly more than 30 min. The time required for a droplet to grow to a diameter on the order of 100ths of microns is certainly much shorter than the stability test performed. Despite the already known fact of the instability of most emulsions the test was performed to quiet an unnerving faint voice deep down in the subconscious mind.

To support the existence of larger isolated droplets near the surface more formally, the experiment was performed again, but with faster cooling rate. The MIPE was kept again in a separate bath at 60°C under 8 min instead of about 15 min. The results are shown in Figure 2.35. The surface of the chosen particle show

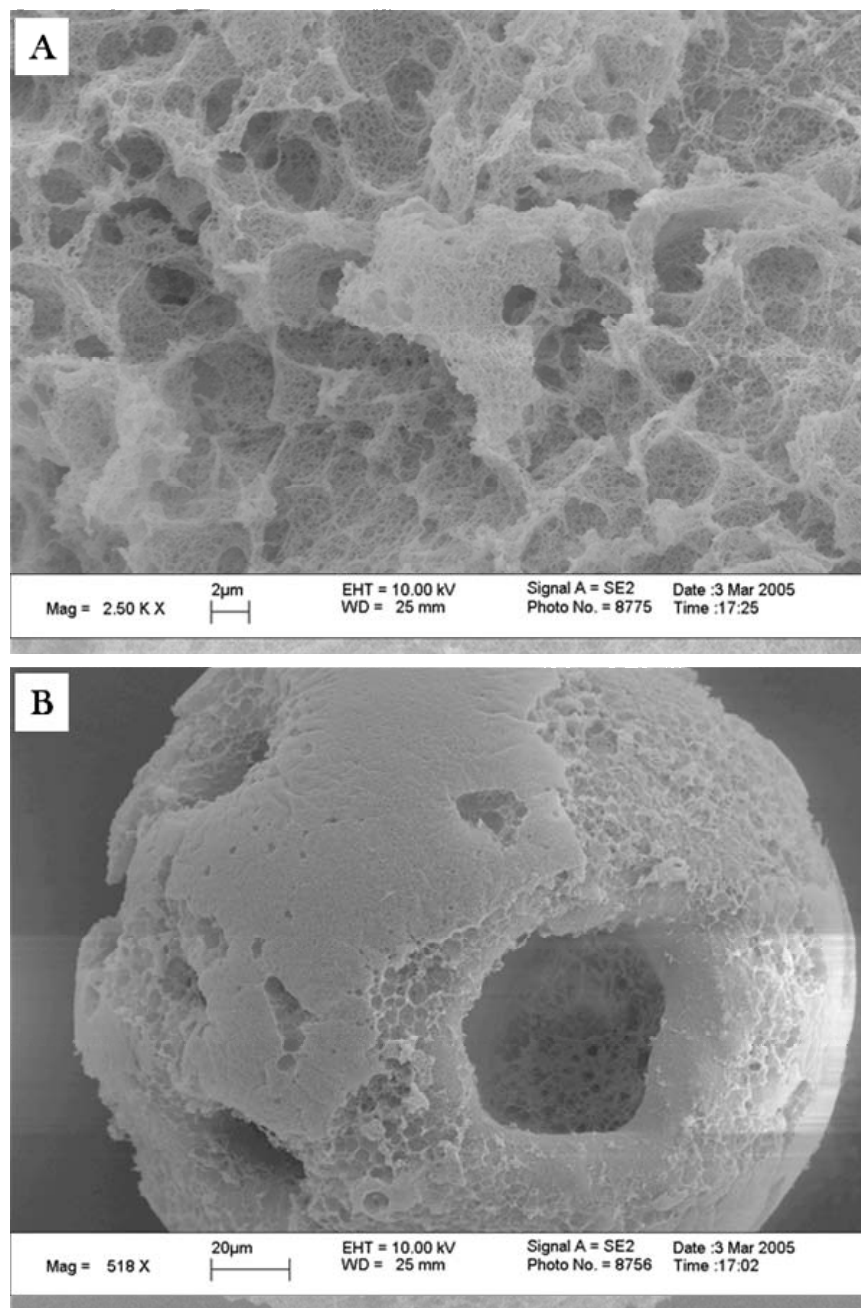


Figure 2.35. (Bottom) A ‘superporous’ bead showing large cavities and a surface with partial smooth agarose covering and a less dense agarose structure. (Top) a close up of the surface illustrating what is remainder after a thin coating layer is loss. The loose agarose fibers conform to the spherical shape of hydrophobe droplets up to a few micrometers.

both the smooth coating layer and ‘superporous’ features with low density agarose. The main body of the bead shows agarose with the close packed characteristics of regular homogeneous gels indicating successful displacement of the hydrophobe. The loose accumulation of fiber and large cavities at the surface also evidences the dwelling of hydrophobe droplets and the size of the droplets spans up to a few micrometers in diameter in the dried gel.

The accumulation of hydrophobe from the MIPE to forms larger droplets is analogous to using a smaller amount of surfactant in the MIPE. The result should be the formation of larger stabilized hydrophobe droplets, but smaller in count. To a certain degree this assumption is correct, but the larger hydrophobe droplets do not necessarily form the desired interconnected channels if the volume of surfactant is too low, Figure 2.36. The particles compared here were cooled fast in a water bath at room temperature to reduce the mobility of the hydrophobe droplets. The particles with a larger amount of the surfactant contained a larger amount of larger interconnected pores as well as a surface populated with cavities. The reduction of the surfactant in the MIPE on the other hand formed substantially thinner channels and fewer in quantity. The extent of pore connectivity cannot be distinguished clearly with confocal imaging. In addition, most of the particles possessed a few amount of cavities in the surface and they are mostly oval instead of spherical. The reduction in the volume of the reagents requires the utilization of a smaller reactor resulting in pronounced shearing. A fair amount of spherical particles is produced for the beads containing a larger amount of surfactant in the MIPE, but the amount of deformed particles also constitutes a larger percentage of the final product.

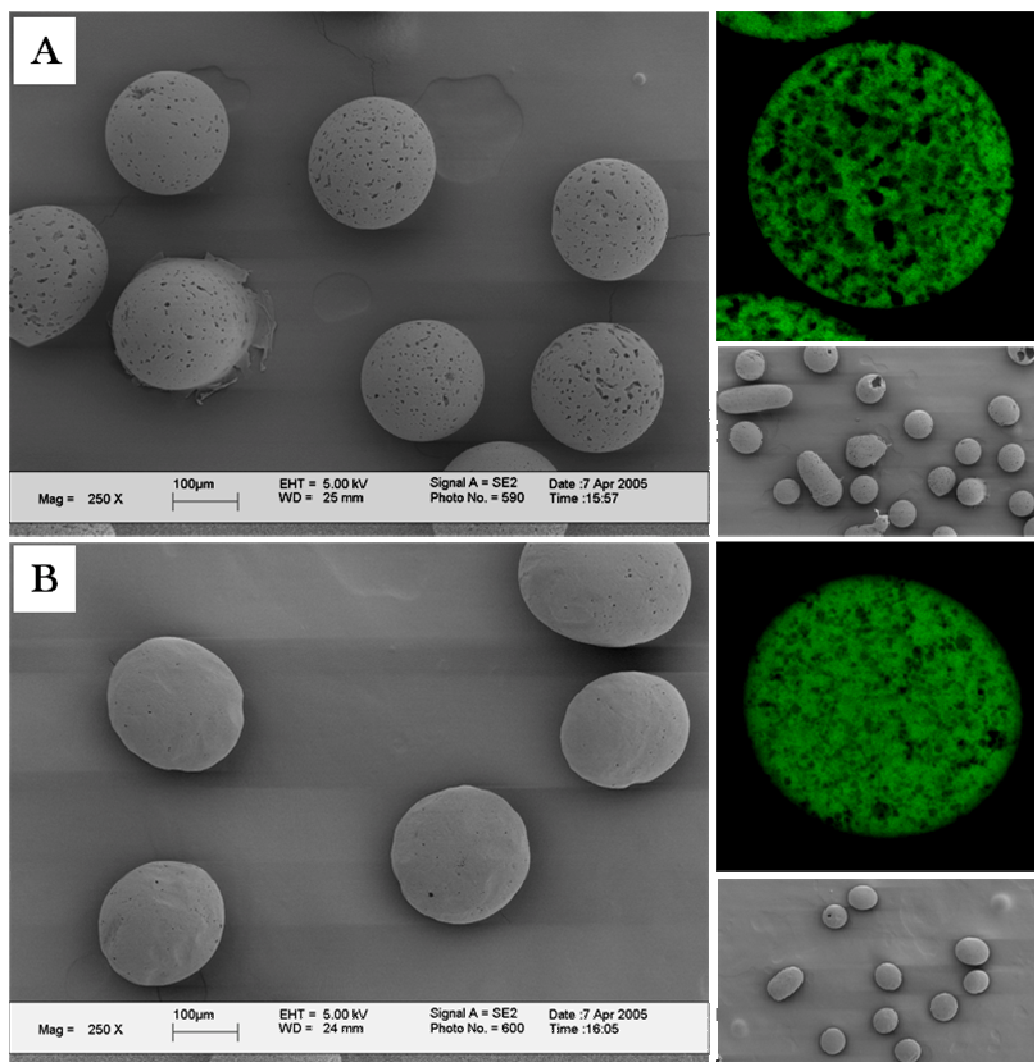


Figure 2.36. SEM and LCSM images showing the effect of stabilizing surfactant in the MIPE. Experimental conditions similar to (A) was prepared with a larger amount of surfactant in the MIPE (0.25 mL Tween 80) when compared (B) (0.1 mL Tween 80). The superpores are bigger in (A) and the connectivity of pores can be appreciated. . The channels in (B) are thinner and the connectivity is not obvious as many spherical cavities seem to be isolated. The experimental conditions are similar to the beads illustrated in Figure 2.37.

The amount of surfactant Span 85 from 7 to 10 mL in the suspending solution has shown to be adequate in the preparation of superporous beads although

the effect in the surface morphology varies. Keeping the same amount of emulsifier, but reducing the total volume of the suspending solution amplifies the shearing forces as the stabilized droplets are brought closer to each other. The utilization of an excess of surfactant necessary to produce spherical beads should be enough to overcome excessive shearing, but the volume solvent in which it is dissolved does affect the superficial appearance. The same amount of Span 85 was dissolved in 100 and 150 mL hexanes and the other components kept constant. The amount of pores obtained is about the same for both conditions and the cavities on the surface are of the same size in average. The grooves on the other hand are deep and dominant on the more diluted suspending solution, Figure 2.37. It is presumably the excess of solvent will be involved in the formation of vesicles with plain suspending solution inside when the suspending solution is more diluted. The vesicles do not survive the shearing stress in a smaller volume of suspending solution because they are more fragile than MIPE.

For a proper understanding of surface and internal morphological features of beaded superporous agarose gels it is necessary to control carefully the variables that affect the stabilization of the spherical particles both in the MIPE and in the suspending solution. The system is without any doubt more complex than the preparation of homogeneous beaded gels. Here the stabilization of two emulsions must be controlled. One of which, the MIPE, is annihilated and triggered mainly by the ‘solidification’ of one of the phases.

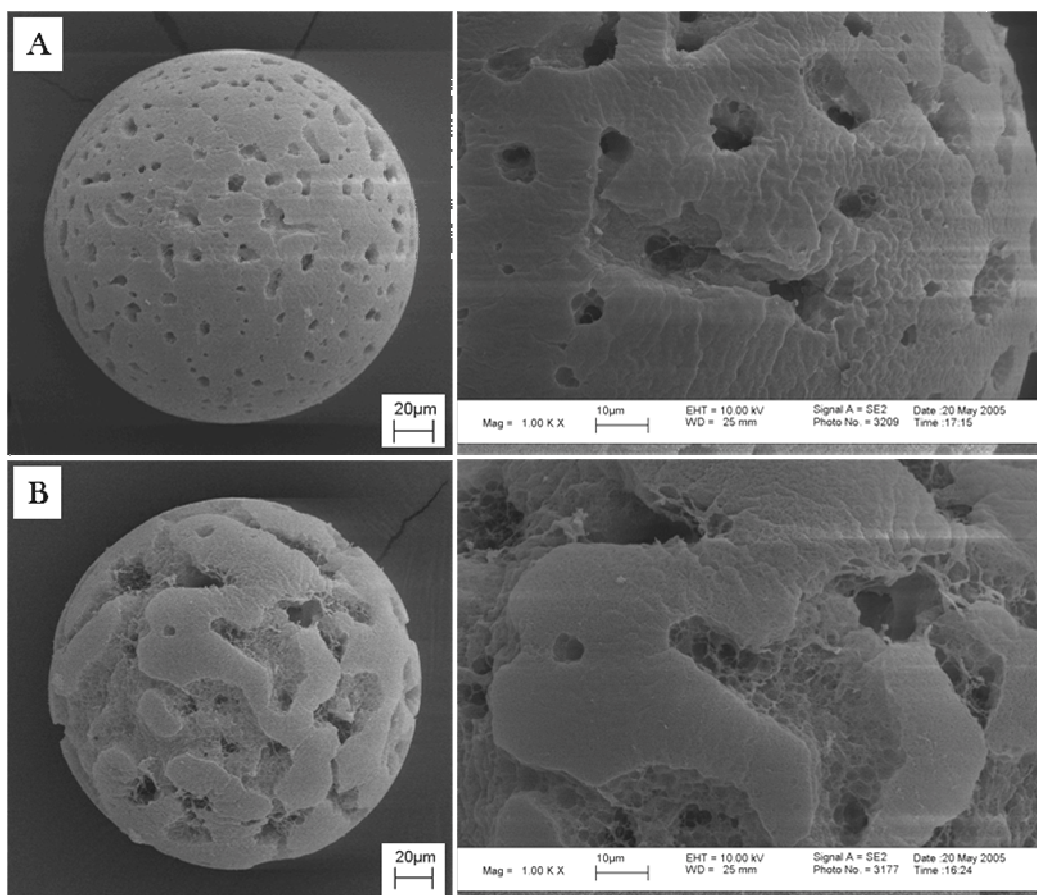


Figure 2.37. Scanning electron micrograph of superporous beads obtained using suspending solutions with same amount of surfactant, 9 mL Span 85, but diluted in hexanes to 100 mL in image (A), and 150 mL on image (B). Other experimental conditions are the same. The shearing forces are enlarged for beads in (A) and the surfactant is enough to protect the forming bead. Note the large grooves on (B) and the absence on (A) even though they have the same excess of stabilizing surfactant. A close examination of the surface shows apparently the same amount of cavities on the surface.

The speed at which the segregation of the hydrophobe from the MIPE must be in concordance with the rate at which agarose gels in order to produce interconnected arteries inside the bead and extending out to the surface. The arteries that provide physical access or fluid flow from bead exterior into bead

interior can be seen with confocal microscopy, but the surface must be inspected to secure the presence of cavities that will allow facilitated flow through of mobile phase. The SEM images indicate that in certain conditions a layer of agarose is built up on the surface covering the cavities. The film of agarose can be thick and dense enough to resemble the homogeneous agarose regions which will hinder mass transport into the bead. In addition to easy access and the presence of arteries, it is also desirable to gain complete control on the size of the channels and on a more uniform distribution of interconnected channels that will expedite delivery of fluid to the total volume of the bead. The blocking of pores is not necessarily an inopportune happening since it can be used to isolate efficiently relatively large particulate matter within the channels or cavities formed within the microsphere. The 'automatic' sealing of the cavities which in adequate conditions occurs as part of the bead formation process frees from post-processing of the bead in order to contain the particulate matter.

The addition of any molecule or agent that will interact with the agarose chains will also affect the association mechanism. The study and characterization of agarose and its gelation mechanism has proven to be challenging as it is reported frequently in the literature. The probing of agarose forming part of an unstable heterogeneous media such as emulsions does not certainly facilitate an understanding of the system. In addition, the reproducibility of experimental conditions is crucial to obtain consistent results that will guide confidently to correct conclusions. Several key variables were identified here to affect profoundly the physical appearance of the beads and include mainly the stabilization of the

suspending solutions and the interaction between the stabilizing agents, the agarose solution and the hydrophobe. Further characterization of the system is undoubtedly necessary to elucidate the mechanism by which the pores are formed, a continuous or partial interconnected artery system is obtained, and the gelation mechanism in such environment.

2.4 SUMMARY

In this chapter, methods have been developed an optimized so as to create a series of customized agarose reactive particles that are suitable for bead-based assay microreactors. Here agarose beads in spherical form are created with diameters of 260 to 300 μm , with a coefficient variance as low as 2%, that are ideal for sensing applications. Post-manufacture processing of the beads through crosslinking, has provided the capability to further enhance the mechanical stability of the gels to accommodate high flow rates of mobile phase, within the microarray context, without compromising the structural characteristics of the sensing element. In addition, the chemical activation of the gels has been adjusted to eliminate the inhomogeneities in chemical reactivity within a single bead, and from bead to bead, found in commercial sources. Most important of all, is the added ability to control each step during the preparation and chemical modification of the sensing elements. As a result, not only reliable and reproducible sensing elements are fabricated within the context of the microbead array system, but also, with an understanding of the key parameters in the production of the sensing elements, it is now possible to build the microsphere according to individual specifications. The exploration on the several key factors affecting the physical characteristics of the sensing elements

presented here, made possible the inception of new beaded ensembles with a high potential for application in sensing technology. The novel beaded ensembles are presented in Chapter 4.

Also, within this chapter, with selected experimental conditions, continuous interconnected pores with diameters of 4 to 45 μm are found to be included in the sensing elements as visualized by scanning electron microscopy and laser confocal scanning microscopy. These systems, refereed here as superporous microspheres, exhibit up to 35% internal porosity making them ideal candidates to serve as sensing ensembles. While there has been much prior work using bead in bioassays, nearly all such works used monolithic beads with no internal volume contribution. Even in a conventional homogeneous agarose bead, which has a relatively high permeability when compared to other materials such as latexes, the internal volume is practically untouched in short assay times. The addition of a system of large interconnected cavities, to an already highly permeable gel, enhances dramatically the mobile mass transport and, hence, an efficient delivery of analyte to the binding sites in the homogeneous domains of the superporous system. The large pores allow for convective fluid flow to be included in the internal volume of the microspheres. As a result, the length of the assays in the bead-based microarray system can be significantly reduced if used instead of the conventional homogeneous systems, as it will be described in chapter 3. Additionally, the superporous system has potential applications in the direct immobilization of larger particles than conventional analytes used in other bead-based sensing systems such as those described in Chapter 1. Larger particles may include cells and utilize the

natural membrane cell-expressed receptors for the evaluation of diseased individuals. Studies of such nature with whole cells has been reported viable utilizing packed columns of superporous beads.³⁹ A similar system can be imagined in the bead-based microarray platform.

Chapter 3: Superporous and Homogeneous Agarose Beads on a Chip-Based Multianalyte Detection System. A Comparison on the Mass Transport Anatomy

3.1 INTRODUCTION

Successful immunological assays in previous publications addressed the utilization of homogeneous agarose microbeads in the chip based detection machinery. The homogeneous gel media displays interconnecting pores of diameters comparable to the size of the diffusing molecules. The diffusion speed of analytes is in part attenuated due to steric interactions with the agarose matrix. In the present work, the incorporation of large interconnecting pores into the homogeneous beads body shows improved analyte transport to the agarose reactive sites. The chip based detection system profits from the increased analyte capturing capacity in a short span of time. In contrast substantial internal volume of homogeneous beads with only homogeneous moiety remains untouched in the time frame of the assay. Coupling of specific fluorophore tagged binding molecules used for analyte detection is accomplished in a likewise timely fashion. Superporous agarose (SA) beads compared against homogeneous agarose (HA) beads are shown here to elicit a more intense and faster fluorescence measurable response on the detection of a small DNA molecule (MW 7.1 kDa) and a bigger analyte, namely C-reactive protein (MW 120 kDa). The superporous substitute gel candidate is a plausible upgrade to the chip-based multianalyte detection system and most important of all, the analyte detection diversity is not compromised.

Multianalyte detection systems are a pivotal tool on medical, military and environmental applications.¹¹³⁻¹¹⁶ The necessity to obtain rapid reliable data on for example the diagnosis of diseases, determent of bioterrorism, and protection of the environment inspired and procured the development of smart chemical and biological sensor designs. On the development of a particular novel chip-based multianalyte detection system designed by McDevitt and co-workers, individually addressable spherical polymeric units are altered to recognize and sequester specific analytes. Refinement on the recognition phenomenon catapulted detection and quantitation of analytes from ordinary ions such as calcium, to pH measurement to complex immunological assays that differentiate proteins such as C-reactive protein (CRP) and interleukin IL, and even to differentiate DNA chains varying on 1 base pair.^{1, 3, 5, 7, 9, 117}

The chip-based multianalyte detection system, described with more detail in previous publications, takes advantage of chromatographic properties characteristic of homogeneous gel-type beads (HA). The legacy of homogeneous gel type assays in the current evolution of a still blossoming chip-based system requires not only expanding the analyte detection diversity but also improving on the bead's architecture beyond the fine tuning of specific chemical reactivity of the supporting bead frame.

The polysaccharide beads sitting at the wells of a chemically etched silicon chip wafer constitute a small but an essential element in the detection system. Agarose, well known to be a friendly environment for biomolecules is undoubtedly a good choice in the design scheme of the detection system. The natural

polysaccharide is cast to form porous spherical gels of micrometer size. Additional meticulous selection of active molecules to be immobilized on the beads play the role of mobile phase sequestering agents in the detection scheme.

Agarose gels referred as of homogeneous type exhibit small interconnected pores typically smaller than 900 nm. The pore size distribution will vary with the concentration of agarose solution from which the gel is cast, the buffer in which it is equilibrated and on its thermal history.^{87, 89, 93} Despite the preparation methodology, homogeneous gels will reduce molecules mobility up to 3 orders of magnitude as they transition from free solution into the gel network. In contrast, agarose gels of superporous type in addition to homogeneous gel dominions contain large interconnecting flow pores which improve the transport phenomena in the gel. Many authors report a better performance in liquid chromatographic separations of SA over HA either by packing beads into continuous gels or by preparing monolithic agarose beds.^{98, 118, 119} Here SA and HA microspheres of same diameter size are used as individual microreactors on the capture and detection of DNA and CRP. SA and HA beads are compared to address the impact of a more efficient mobile phase mass transport on the chip-based detection machinery.¹²⁰ Superporous gels as well as the homogeneous type can be cast in the form of spherical beads of micrometer size.¹⁰⁸

3.2 EXPERIMENTAL SECTION

3.2.1 Reagents

Rabbit anti-Human CRP was purchased from Accurate Chemical and Scientific Corp. (Westbury, NY). Purified human C-reactive protein (CRP) was obtained from Cortex Biochem (San Leandro, CA). Rabbit anti-Human IgE was purchased from Bethyl Laboratories Inc. (Montgomery, TX). Alexa Fluor® 488 Protein Labeling Kit (A-10235) was purchased from Molecular Probes (Eugene, OR). Neutravidin™ Biotin-Binding Protein was purchased from Pierce Biotechnology (Rockford, IL). The 20 base-pair DNA capture sequences (MW 6.8 kDa, biotinylated DNA probe sequence: CCGTCAGACTTTCGTCCATT-biotin) and the complement (MW 7.1 kDa, fluorophore labeled DNA target sequence: AATGGACGAAAGTCTGACGG-FAM6) were purchased from Integrated DNA Technologies Inc. (Coralville, IA). Agarose powder type I-B, sorbitan trioleate (Span 85) and polyoxyethylenesorbitanmonooleate (Tween 80) were obtained from Sigma-Aldrich (St. Louis, MO). Sodium borohydride, hexanes, sodium cyanoborohydride and sodium periodate were obtained Fisher Scientific (Fair Lawn, NJ).

3.2.2 Preparation of Homogeneous 4% Agarose Beads

HA beads were prepared by emulsifying 4% agarose solutions.⁹⁶ 2g of agarose was dissolved in 50 mL water by boiling the mixture for a few minutes and with occasional stirring. A suspending solution made of 10 mL Span 85 and 90 mL hexanes was heated to 60 °C and stirred at 900 rpm. The polysaccharide solution

was allowed to stabilize at 60 °C and then poured into the suspending solution. Stirring proceeded at 900 rpm at 59 °C. After 1 min the stirring speed was adjusted to 600 rpm, heating stopped and the agarose left to gel into small beads as the temperature dropped to 25 °C. Beads were collected on a sieve and washed with a 50/50 mixture of ethanol/water and water. Sorted by size with metal screens the 250-280 um fraction was collected for further modification.

3.2.3 Preparation of Superporous 4% Agarose Beads

SA beads were prepared by a double emulsification of a 4% agarose solution.⁹⁶ A solution of agarose was prepared as described for HA beads above. The agarose solution was transferred to a 50 °C bath and stirred at 1000 rpm. A mixture of 0.7 mL Tween 80 and 20 mL hexanes stabilized at 50 °C was added to the agarose solution and stirring proceeded for 2 min. A 50 °C suspending solution prepared by dissolving 8.5 mL Span 85 to 150 mL with hexanes was added to the agarose suspension. Stirring continued for 1 min at 1000 rpm then set to 600 rpm and the mixture allowed cooling to 25 °C. Beads were collected and washed in a similar fashion as described for HA beads.

3.2.3 Instrumentation and Methodologies

Overhead Stirrer RW20 DzM.n utilized on the emulsifications was acquired from IKA Works Inc. (Wilmington, NC). The chip-based MAD system was described previously. HA and SP beads and corresponding control beads were positioned in an array of microcavities on a silicon wafer chip. The chip is placed in a plastic flow cell and held together either by an aluminum casing or by double sided adhesive layers. Target sample solutions were introduced using peristaltic

pumps from Alitea AB (Stockholm, Sweden) or Instech Laboratories Inc. (Plymouth Meeting, PA) and contained within a circulation loop. Pump settings were adjusted to deliver the same volume of fluid per unit time. Positioned properly under an Olympus (Melville, NY) epifluorescent microscope station the development of fluorescence signal is captured using a DVC 1312C (Austin, TX) 12-bit charged-coupled device monochrome camera and processed with Image Pro-Plus 4.5 software from Media Cybernetics (Carlsbad, CA). In a similar fashion confocal studies on beads medial cross-sections were performed with a Leica SP2 AOBS Confocal Microscope. Assay conditions for each of the tests, described below, on either microscope are the same unless indicated otherwise. Scanning electron micrograph images of HA and SA dried beads were obtained with a LEO Model-1530 scanning electron microscope (Carl Zeiss Inc., North America).

3.2.4 Kinetics Studies with CRP

Aldehyde functionalized SA and HA beads¹²¹ were covalently coupled to anti-CRP antibody by reductive amination.¹²² Rabbit anti-Human IgE was immobilized in a similar fashion to render control beads. The loading of anti-CRP antibody on SA and HA beads measured at 280 nm OD were found to be 3.94 and 3.01 mg per 200 μ L of beads. A protein labeling kit is used to link Alexa Fluor 488 to CRP. Concentrations between 0.065 (8000 ng/mL) and 0.104 μ M (12500 ng/mL) of labeled-CRP diluted with PBS from a 3.9 μ M stock solution were used. The delivery of 1.5 mL target labeled-CRP solution was set at 1.6 mL/min. At regular intervals of time the development of fluorescence signal was collected.

3.2.5 Kinetics Studies with DNA

Biotin binding protein is attached to aldehyde functionalized beads via reductive amination followed by 18 h incubation on a biotinylated-DNA 20 base-pair sequence solution. Details on lyophilized handling was previously reported.⁵ The loading concentration of DNA per 10 μL of beads at 260 nm OD was found to be 8.95 and 10.20 μM for SA and HA beads respectively. A 1 μM target-DNA solution was recirculated at 1.5 mL/min and data collected until signal equilibration.

3.2.6 CRP ‘Sandwich’ Detection Test

Here the same kind “kinetic studies with CRP” beads are used. CRP concentrations ranging between 0.1 and 5000 ng/mL were obtained with dilutions with PBS. Sequentially target-CRP, PBS and labeled anti-CRP were delivered at 1.6 mL/min flow rate to complete a “sandwich” format immunoassay.¹ Each solution was looped for 5 min before the next was introduced. Data was collected after a final wash with PBS.

3.3 RESULTS AND DISCUSSION

The utilization of single beads in the chip-based technology presented here mimics classic affinity and size exclusion chromatography separations. The fractioning process can be observed in real time via the development of fluorescence if the analyte of interest is present in the examined sample solution. The micron sized beaded support inspects the sample solution on the fly without actually probing all the volume of solution as it passes through it in a short span of time. The assay therefore relies at first instance on the architectural surrounding environment that steers fluids towards the reactive sites of the beads.

The agarose beads reside in wells etched on a silicon chip and placed within a laminate structure, Figure 3.1. The sealed chamber has defined microchannels which will guide the delivered solutions to the beads. Inserts attached to the base of the chamber are used to couple flexible tubing for the intake and proper disposal of fluid. The silicon chip with trans-wafer openings contribute to the passage of fluid bathing the beads from the top and exiting at the smaller bottom aperture. The top cover of the chamber is transparent to light consenting direct probing of the assay development through fluorescence signal development.

A typical array used in this report consisted on HA, SA and their respective control beads. Beads were prepared from a 4% agarose solution and the average diameter of beads used was 290 μm . HA gels prepared from 4% agarose solutions show a volume fraction of water of typically 0.96.¹²³ For a 4% agarose gel the

pores have an average value of 250 nm although it will change accordingly depending on the ionic strength of the buffer where it is equilibrated.⁸⁹

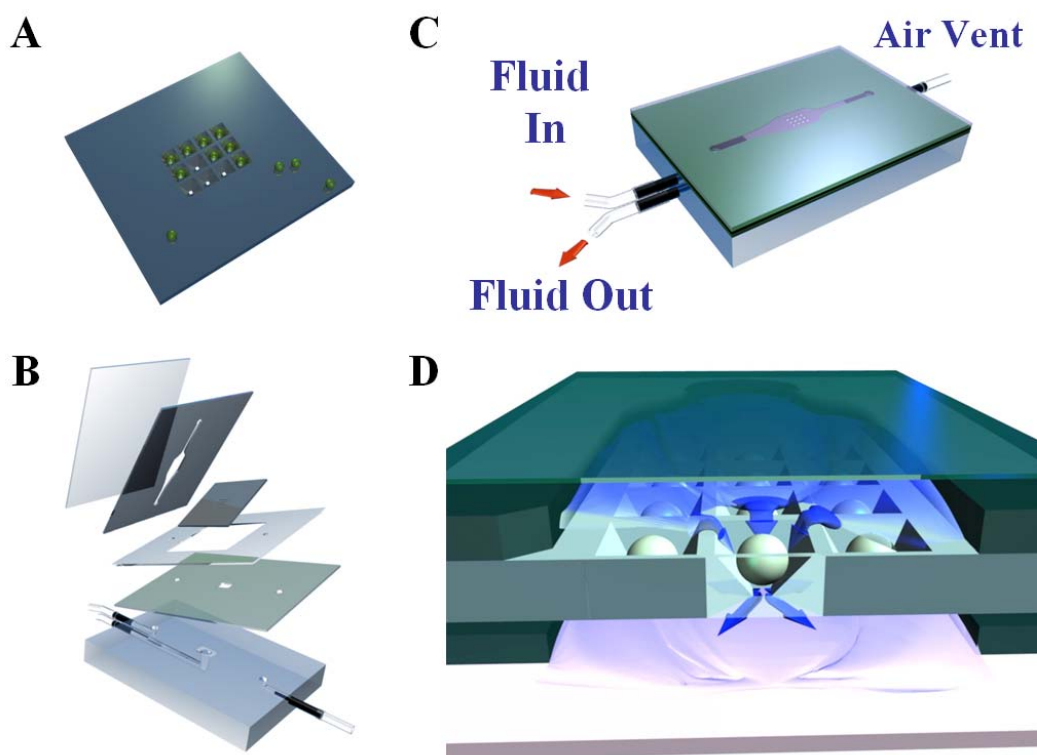


Figure 3.1. (A) Silicon chip with trans-wafer openings and beads in etched-wells of comparable size. (B) The analysis chamber is composed of polymethylmethacrylate base with microchannels. Metallic inserts and flexible tubing are attached to the plastic base. A series of double sided adhesive layers are used to hold the silicon chip wafer and define a circuit for fluid delivery to the beads. A plastic or glass cover transparent to light seals the chamber. (C) Illustration of assembled analysis chamber with conduits dedicated to fluid delivery and disposal as well as facilitated displacement of air contained in the chamber. The air vent is eventually sealed before the assay is run. (D) Analysis chamber sectioned to show fluid flowing through the well from top to bottom. The layered structure is designed to effectively separate regions above and below the chip to ensure transit of fluids through the beads.

SA contains HA regions as well as large flow pores also known as superpores. Confocal micrographs on SA beads used in this report showed that superpores with diameter size between 4 and 50 μm account for about 38% of the total volume of the bead. Thus the amount of gel available in HA beads is at least 38% larger than in SA beads. Confocal and SEM images of SA and HA beads are shown in Figure 3.2

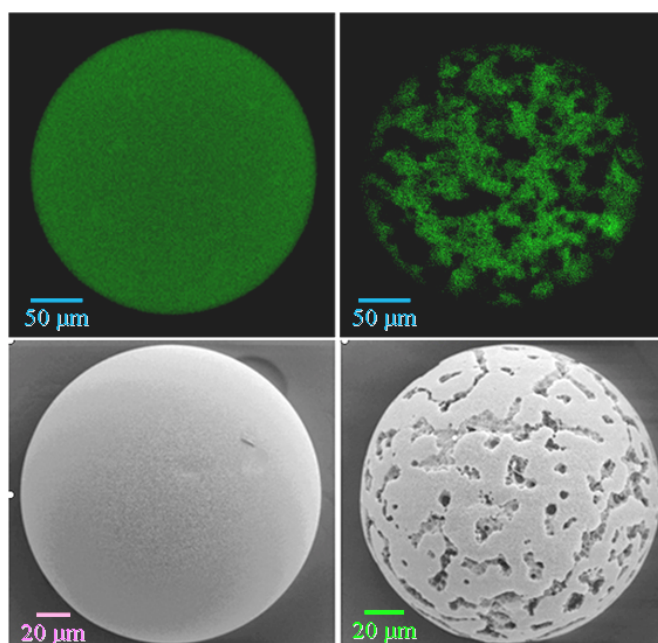


Figure 3.2. (Top) Confocal micrographs of medial cross-section HA and SA beads. HA and SA beads have immobilized oligonucleotide and CRP respectively, labeled with fluorophore. (Bottom) Scanning electron micrographs of dried HA and SA beads.

Despite the buffer in which the beads are equilibrated in, the introduction of fluid containing the target molecule reaches the beads through convective movement facilitated mainly by the pump action. From the bulk solution the target is transported across a ‘stagnant’ layer of liquid surrounding the beads. From this

point and further on, the supply of target through the stagnant layer and to the reactive sites of the bead is dominated by diffusion.

Due to the spherical geometry of the support, the mobilization of the target inside the bead is expected to proceed radially towards its center delineating concentric spheres as a moving boundary. This ideal situation is obtained for a homogeneous beaded material in free solution with fluid pressure exerted evenly around the microsphere. Apparently this ‘ideal’ case occurs also for a HA bead sitting on the chip as shown in Figure 3.3.

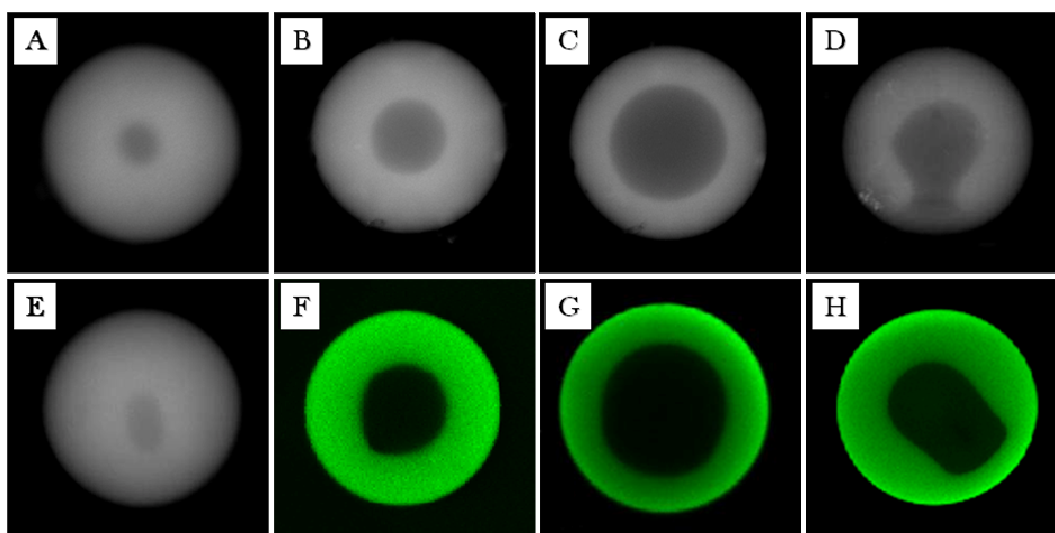


Figure 3.3. Epifluorescence and Confocal Scanning micrographs of immobilized CRP-Alexa 488 on HA beads (gray and green respectively). Pictures (A to C) show symmetrical fluorescence ring at a plane parallel to the silicon chip surface. Pictures (D to H) reveal the non-circular fluorescence band at a plane almost perpendicular to the silicon chip surface. The thinner or missing sections of the beads correspond to the regions facing the fluid exit opening. Pair (A-E) depict the same bead at a stage close to the equilibrating point. Pairs (B-F), (C-G) and (D-H) are beads at approximately the same assay stage. Note the elongated target-void pocket. Pair (D-H) shows an extreme case where a heightened flow rate emphasizes the effect of the flow anatomy even though the target distribution apparently looks uniform from the plane parallel to the silicon chip surface standpoint of view.

The images 'top view' (plane parallel to the silicon chip surface) shows a fluorescence ring corresponding to the region with immobilized fluorophore labeled target. The circular symmetry of the ring suggests a non-discriminated movement direction of the fluid towards the bead. The symmetry is lost though if a different plane is considered such as one perpendicular to the chip surface.

The deformity discernible in a HA bead can be explained by considering the drop in the hydrodynamic pressure across the bead as it occurs in a chromatographic column. The fluid pressure at the top opening of the well (and the bead) is higher than at the exiting aperture. Most of the fluid is diverted around its external spherical surface. The incoming fluid applies pressure directly over the top portion of the bead promoting a thin diffusion layer (DL). As the fluid exits there is a hydrodynamic drag of the fluid away from the lower region of the bead developing a thicker DL, Figure 3.4. Because of the flow direction the beads are compressed against the wells. At the four bead-well contact points the soft agarose gel experiences a minute flattening. As a result, the small flattened regions are not directly accessible to the mobile phase and the fluid enters the HA beads only by diffusion around the flattened contours.

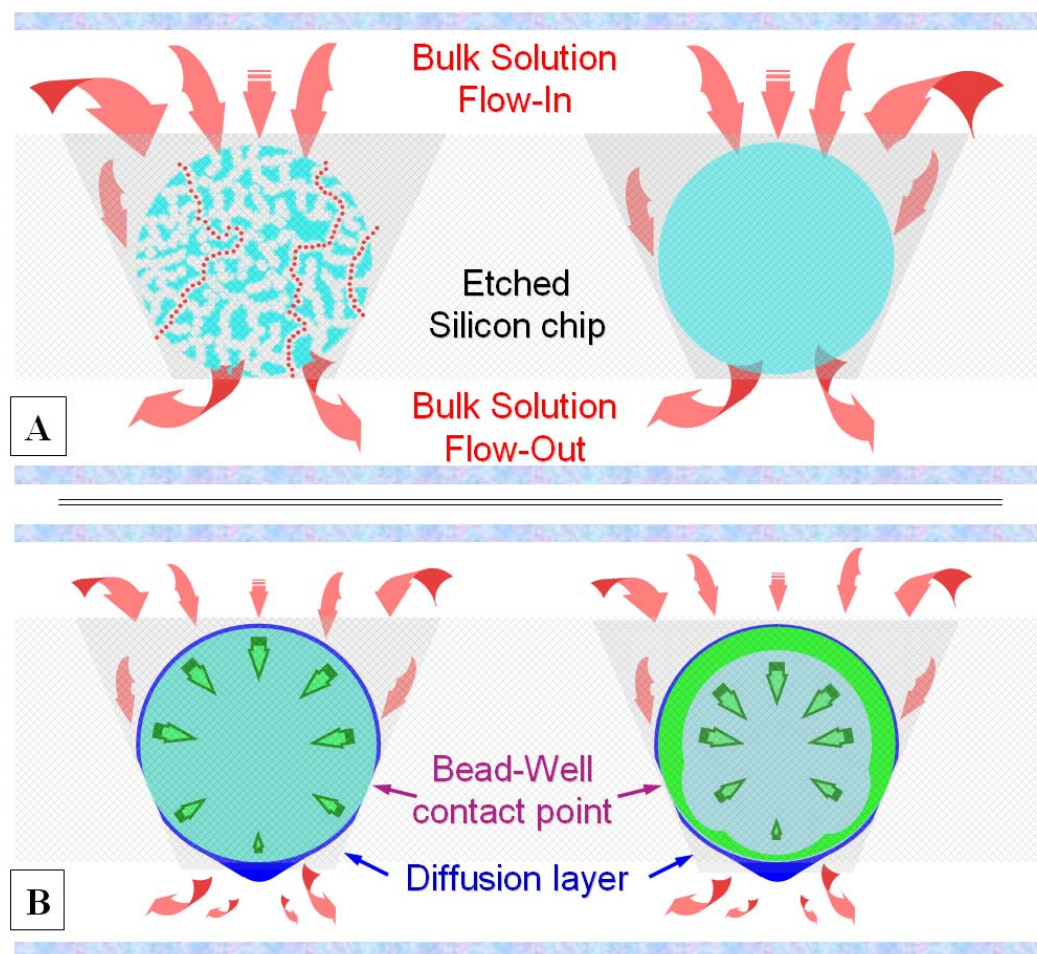


Figure 3.4. (A) Schematic of HA and SA bead in a silicon chip wafer confined between transparent polymer/glass covers. Arrows show the direction of fluid flow. Fluid bypasses beads through the sides of the well. In addition, SA bead at the left, allows fluid ‘flow through’ helping in the delivery of target to the bottom portion of the bead and to the bead-well contact points. (B) Green arrows show the relative diffusion rate inside the bead due to the differential pressure exerted by the fluid from top to bottom of the well. The diffusion layer is exaggerated in the illustration. The effect of a non-uniform diffusion rate in the homogeneous bead promotes the formation of a thicker fluorescence layer on the top portion of the bead.

In contrast, convective flow from the bulk solution is brought inside and across a SA bead providing a fluid delivery ‘leveling’ effect. The facilitated flow-through large channels reduces the drop in pressure. The HA regions and the DL

thickness where diffusion occur is downsized and impoverished target feeding at the lower hemisphere of the bead is not evident. In certain experimental settings were a combination of relatively low fluid flow rate and non efficient eradication of air bubbles from the analysis chamber work together to enhance the ‘pulsing’ effect of the characteristic peristaltic pump fluid delivery action. The HA beads are not constantly held tightly in position and have some intermittent freedom to rotate. The random change in position favors a more even distribution of fluid to the bead. The presence of air bubbles in unpredictable positions though is most of the times detrimental.

3.3.1 Fluorescence Signal Response Rate Comparison

The direct capture of fluorophore tagged-analyte is used here to compare directly the rate of diffusion on HA and SA beads. The superpores allow for a rapid and efficient irrigation of an agarose 3-dimensional matrix. This is supported by the disparity on the amount of signal collected at any point in time of an oligonucleotide or protein assay as depicted on Figures 3.5 and 3.6. The difference on the signal accumulated on SA and HA beads are undeniably significant. The saturation of reactive sites on SA beads occurs within 10 min for DNA capture and about 43 min for labeled-CRP immobilization. In contrast the HA beads required about 4 h for the small DNA molecule and 8 h for the larger CRP protein to reach its correspondent equilibrium points. At expense of longer exposure time it is indisputable that the larger amount of available reactive sites in homogeneous beads eventually provides a stronger fluorescence response than the superporous counterpart.

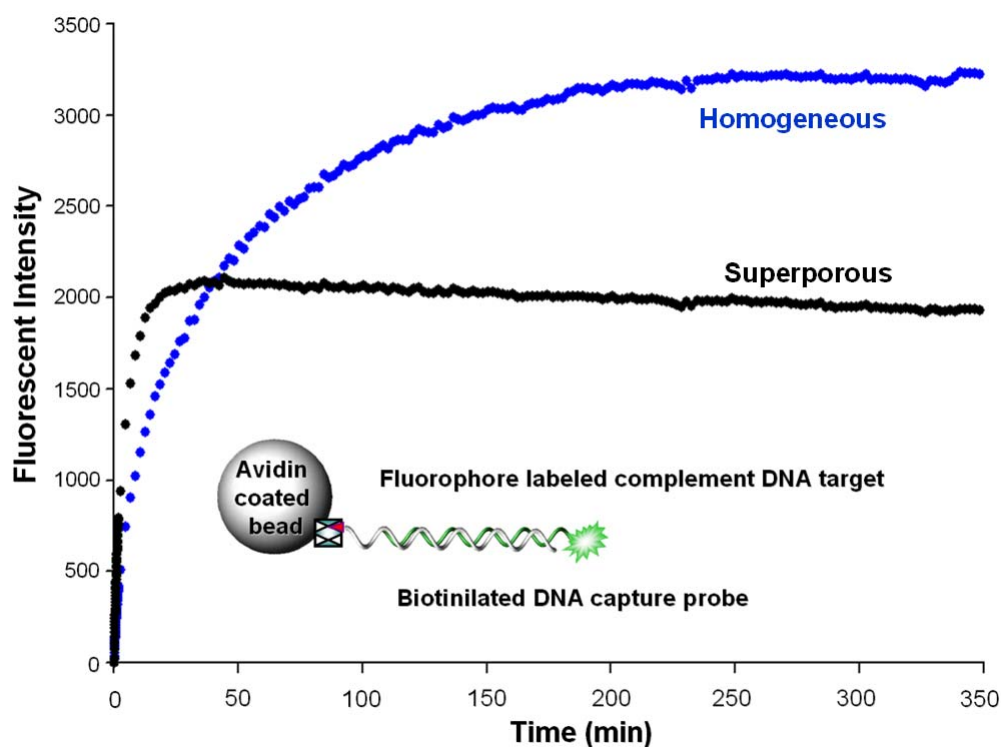


Figure 3.5: Development of fluorescence intensity signal as a function of time during the capture of fluorophore labeled DNA. Data collected with epifluorescent microscope coupled to CCD camera. Schematic of capture is included. The bead is coated with avidin. The biotin-DNA capture strand is immobilized on the bead. The target is a complement of the capture strand. Complement DNA sequence is conjugated to FAM6 dye. (Data provided by Mehnaaz Ali)

Note that at 6 min and 15 min of assay progress for DNA and CRP detection respectively more than 90% of the maximum measured intensity signal on the superporous bead is accounted for due to the improved mobile phase mass transfer. It is in particular this boost in speed at which a strong measurable signal is attained in superporous beads that makes it a highly desirable attribute to be included in fast response multianalyte detection systems.

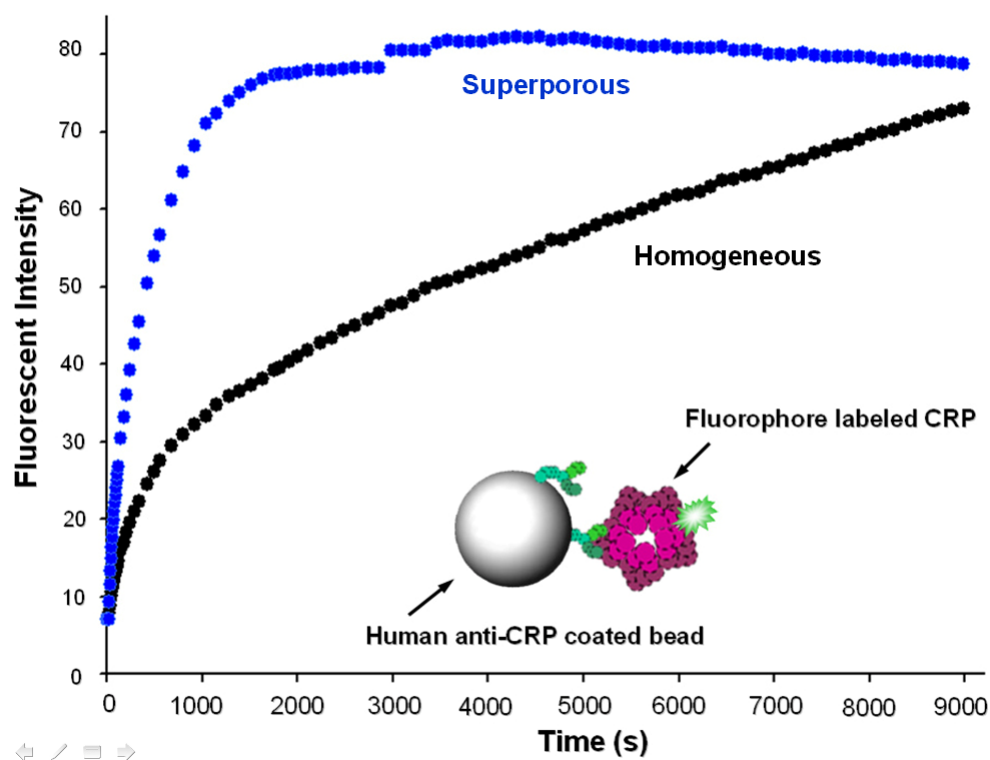


Figure 3.6. CRP capture data collected from the medial-cross section of beads using confocal microscopy. Schematic of capture is shown. Human anti-CRP is immobilized on beads. CRP is labeled with Alexa Fluor-488. After 50 min of assay labeled CRP aggregates are formed and accumulate on the pores and surface of the beads increasing the intensity of the signal (at about 3000 s in the diagram) after the equilibrating point

The consummation of assays on a reduced amount of time favors experimentation with molecules of unstable nature in the experimental conditions. Proteins are found to experience aggregation and denaturation attributed to shearing stress when flowed using a peristaltic pump.¹²⁴ The biological activity of CRP has not been measured during the assay progression and denaturation of the protein may have not happened. On the other hand aggregation of CRP was noticeable after 50 min of continuous pumping. The prolonged time assay required for the HA beads to present an equivalent fluorescence signal to the superporous analogue is

tarnished by the accumulation of CRP clusters. The immediately perceptible effect is undesired fluorescence signal from fluorophore labeled CRP clumps on the surface of the beads. SA additionally admits protein clumps to enter the beads body through the large flow through pores and be therefore trapped inside. Not visually noticeable though are the smaller aggregated protein particles that are physically arrested in the homogeneous agarose regions of both types of agarose beads. Coupled with unwanted fluorescence signal, the obstruction of pores attenuates the diffusion speed process thus lengthening even more the assay. The accumulation of CRP aggregates in SA beads at an advanced stage of the assay accounts for an observed slow progressive escalation of fluorescence intensity signal 10 min after the signal equilibration has been reached.

Protein denaturation are also more likely to occur at room temperature than at 4 °C and in an environment different than physiological conditions.¹²⁵ Low temperatures to be kept during the assay incurs in a more costly device to be designed and affects the size and maintenance requirement of a practical portable device.

3.3.2 CRP Dose Response Test.

HA beads were shown to perform efficiently on CRP dose response assays.^{1, 7} The superporous counterpart was tested and poses competitiveness on the capture of a set amount of CRP existent in the mobile phase. Here the ‘sandwich’ style assays were carried out in a closed loop environment to recirculate antigen and detecting antibody solutions for a period of 5 min. Here CRP is captured by the affinity ligand in the bead followed by a washing process with PBS. In a second

step the detection is accomplished by sending the tagged anti-CRP antibody. After a final rinse with PBS fluorescence data was collected with a 4X objective at exposure times between 0.169 and 1 s. Concentration of CRP ranged between 0.1 and 40000 ng/mL. Data collected is shown in Figure 3.7.

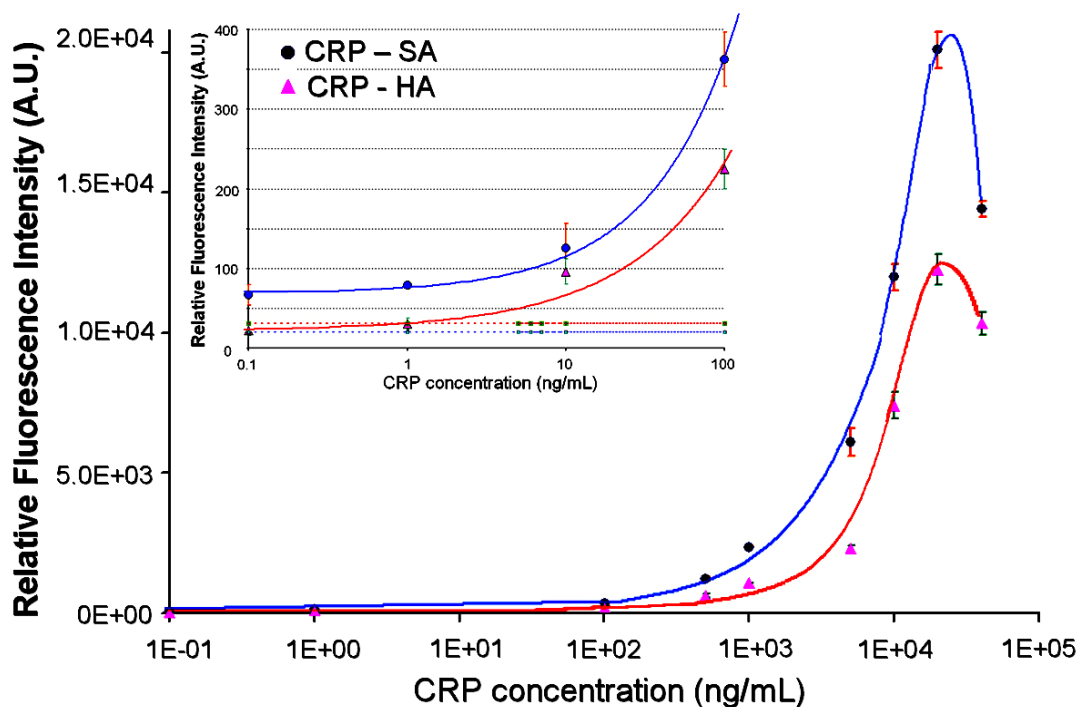


Figure 3.7. CRP dose response test in a “sandwich” immunoassay format. The small embedded graphic is a close up for low CRP concentration 0.1 to 100 ng/mL. SA beads compete for the available amount of CRP due to a larger surface area immediately available through facilitated mobile phase flow.

At low availability of CRP in the mobile phase a larger amount of protein resulted immobilized in SA beads. It is though not manifested as a dramatic intensity signal gain because of the small amount of protein to be shared by all of the beads in the array. As the concentration of CRP is augmented the breach in the

developed signal between both types of beads is still not mind blowing but the intensity disparity is undoubtedly more pronounced.

The elimination of any non-bounded active molecule from the mobile phase is also accomplished in an accelerated fashion. The time required for the washing steps can be reduced for SA beads since the washing process is faster and more thorough than in the HA counterpart. The labeled anti-CRP solution obviously fluoresces and illuminates the beads and its neighborhood. As the labeled antibody is washed away, the inherent transparency of the beads consents effortless contemplation of the bottom opening of the well. The dilution progress of the labeled anti-CRP past the bottom exit aperture can be followed at higher exposure times and therefore more evident in low target concentration capture. In wells where HA beads are resting it is frequently found to be slow and can take up more than 1 min even at high flow rates. In contrast, below SA beads the labeled antibodies are swept away within 2 to 5 s. Consequently the collected signal is cleaner and the dissociation of immobilized analyte is also minimized. This turns out to be more important when the concentration of analyte to be detected is low.

3.3.3 Diffusion Rate Comparison.

A closer examination of the diffusion process was performed with confocal microscopy. The focus plane was set to scan the medial slice of the beads as shown in Figure 3.8. Excited with an Ar^+ laser the intensity of the accumulated fluorescence signal provided a bright ring showing on one end the external perimeter of the beads. The other end of the ring is a moving fluorescence front.

This moving boundary allowed for the measurement of the traversed distance of the captured biomolecule as a function of time.

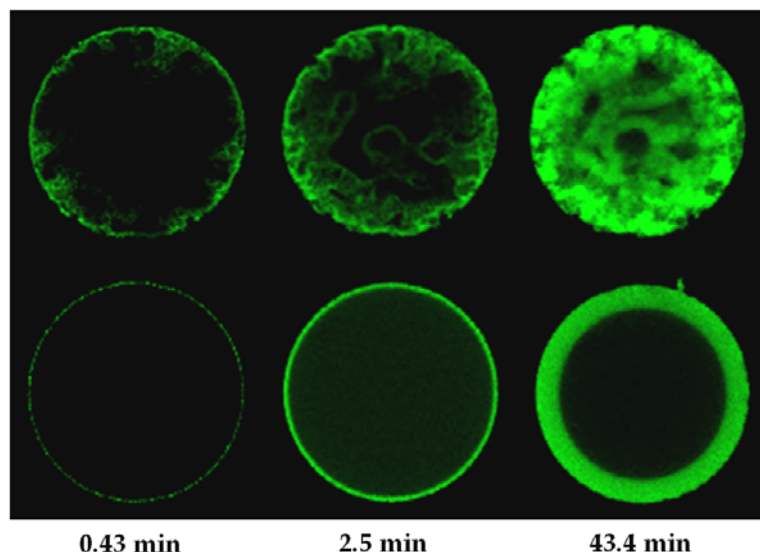


Figure 3.8. Confocal micrographs showing the medial-cross section of SA and HA beads during labeled CRP capture. Penetration is shown at different lapses of time. At 43 min the saturation of reactive sites in SA is achieved. The moving fluorescence front is sharply defined in HA beads owing to the immediate association of protein to capturing ligand as the protein diffuses into the bead.

In both DNA and CRP transport into the confines of the beads the center of the SA bead is reached within 10 min of assay. Data collected from the 10 initial minutes of exposure to the analyte allows for the determination of the diffusion coefficient from the slope as shown in Figure 3.9. The radial diffusion shows a linear behavior at short analyte exposure time which is in concordance with linear Fick's second law prediction.¹²⁶

$$D \propto L^2 / t \quad (1)$$

Where D is the diffusion coefficient, L is the distance traversed by the diffusing analyte, and t is the time spent to cover distance L . A factor of 30 and 50

times increase in the mass transport velocity is seen for a small DNA and a bigger CRP molecule respectively. The SA beads exercise a competitive appropriation of the labeled coupling agents because of the reduced resistance to mobile phase mass transfer. It is obvious that the decay of the coupling agent concentration occurs progressively as the assay progresses. The labeled targets DNA and CRP concentrations were set in large excess to guarantee the depletion of the agarose reactive sites. As the CRP assay was left to progress the equilibrating fluorescence signal point was reached at typically 43 min for SA beads as mentioned before. This result was consistent even when the initial concentration of labeled CRP was changed from 0.1 to 0.07 μM . In contrast HA beads required lapse time for the equilibrating point was 8 and 11 h for a 0.1 and 0.07 μM labeled-CRP solution. Thus the SA beads response to the transport and therefore to the capture of analytes is in this assay is not dependent on the initial concentration of analyte.

Visualization of the transport phenomena in the beads is better noted employing existing mass transfer mechanism models for rapid electrochemical reactions at electrode surfaces. The call for rapid reactions is required in order to secure mass transfer events as the rate determining step in electrochemical and biomolecule capture processes. As opposed to an electrode, the active surface of the bead in capturing events is of a 'dynamic' nature. The association-dissociation equilibrium favors remarkably the formation of the ligand-target complex ($K_d \ll 1$, e.g. $K_d = 2.39 \times 10^{-8} \text{ M}$ for the oligonucleotide interaction). Therefore, the docking positions are annihilated progressively as target biomolecules are sequentially captured.

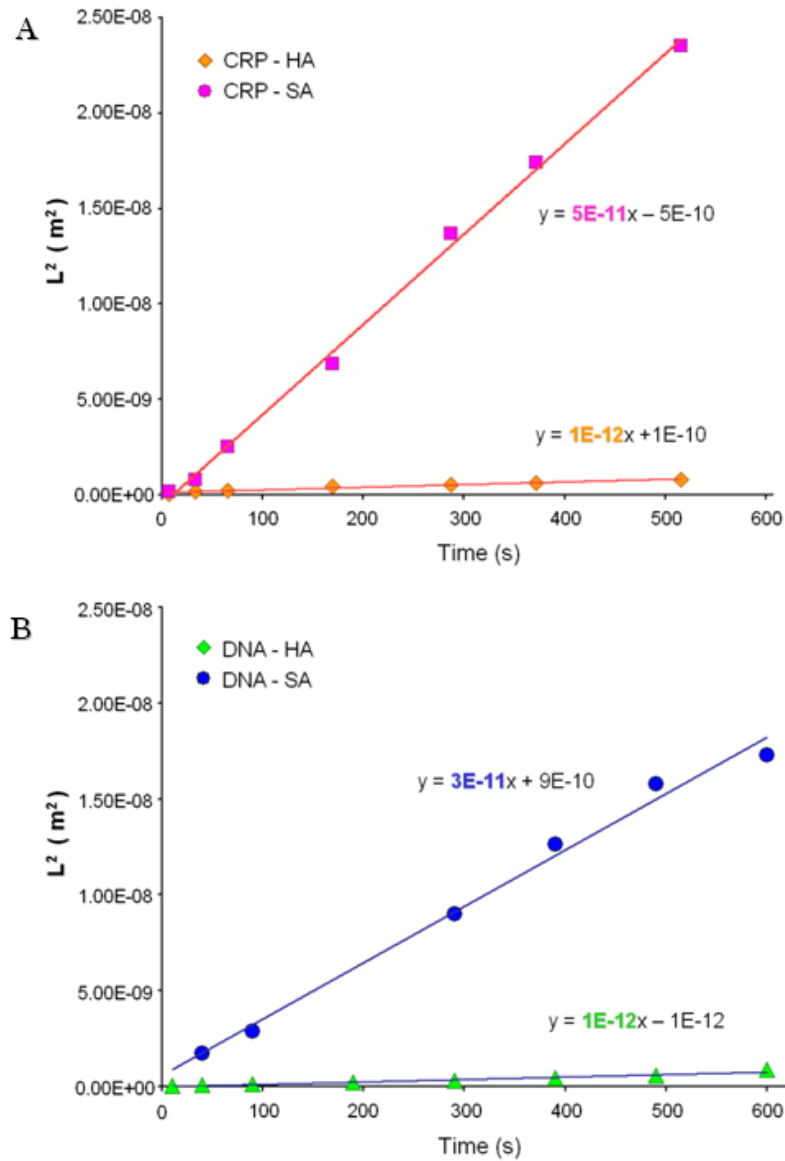


Figure 3.9. Diffusion coefficient estimation for SA and HA beads. Data collected from the initial 10 minutes of assay for both (A) CRP and (B) DNA capture. In both cases the slope is more pronounced for SA beads. For DNA assay the diffusion coefficient is 30 times faster than for HA beads. For CRP assay the factor is 50. (DNA assay data provided by Mehnaaz Ali)

The probability of a target moving past a docking site is greatly diminished by a sterically hindered environment of the agarose matrix loaded with capturing ligand. As a result, the target is sequestered efficiently from the solution as the target-front advances into the bead (correspondingly the capturing ligand-front (CLF) retreats towards the center of the particle), Figure 3.10.

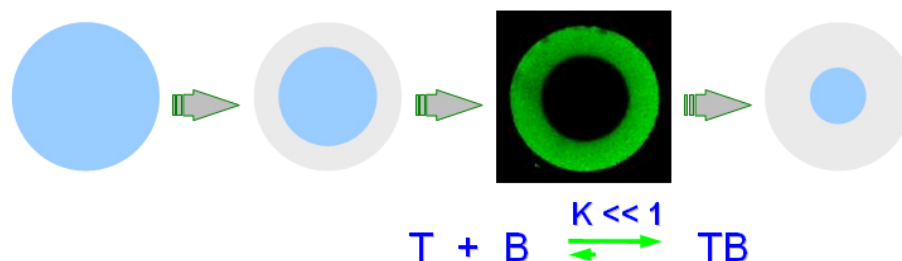


Figure 3.10. Schematic representation of dynamic active surfaces in the bead. The diagram includes a confocal micrograph showing the sharp front of the fluorescence ring due to immediate immobilization of target as it encounters a docking site. The retreating capturing ligand front (CLF) also here referred as the advancing target-front is the ‘interface’ between the fluorescence region and the non-reacted internal portion of the bead. A high affinity interaction draws the equilibrium towards the binding event ($K \ll 1$).

Rapid reaction episodes deprive the immediate vicinity of electrode-solution and CLF-solution interfaces from the reactive solutes. The disappearance of reactive species originates a stagnant diffusion layer (DL) where the movement of solutes is governed by a concentration gradient. The mathematical model that operates over the mass transfer to an electrode (Je), given by the Nernst-Plank equation accommodates three terms from which migration is not included in our target sequestration arrangement.¹²⁷

$$Je = \text{diffusion} + \text{migration} + \text{convection} \quad (2)$$

$$Jb(x) = -D \cdot \frac{\partial C(x)}{\partial x} + C(x) \cdot v(x) \quad (3)$$

Therefore, the one dimensional mass transfer to a bead (Jb) at a distance x from the CLF-solution interface is restricted to diffusion and convection terms shown in equation 3, where D is the diffusion coefficient ($\text{cm}^2 \cdot \text{s}^{-1}$), $Jb(x)$ is the mass flux ($\text{mol} \cdot \text{s}^{-1} \cdot \text{cm}^{-2}$), $\partial C(x)/\partial x$ is the gradient concentration of the target biomolecule ($\text{mol} \cdot \text{cm}^{-4}$), and v is the velocity of a solution volume element ($\text{cm} \cdot \text{s}^{-1}$). In the absence of migration and at steady state (reaction rate equal to rate of mass transfer) the mass transfer to an electrode is also reduced to diffusion and convection terms. In both of our systems, convection is not dominant at the DL and the velocity of a solution volume element can be approximated to zero, $v(x) = 0$. The approximation provides a proportional relationship between the velocity mass transport and the gradient concentration of the reactive solute.¹²⁸

$$-D \cdot \frac{\partial C(x)}{\partial x} = Jb(x) \quad (4)$$

$$k_C (C_{BS} - C_{DL}) = -D \cdot \frac{\partial C(x)}{\partial x} \quad \text{at } x = 0 \quad (5)$$

$$C_{DL} = 0 \quad \text{at } x = 0 \quad (6)$$

Here, C_{BS} is the concentration of the reactive solute in the bulk solution, C_{DL} is the concentration at the diffusion layer and k_C is the convective mass transfer coefficient. At the surface, $x = 0$, the concentration of reactive species is zero. As a

result, the variation in the target concentration profile at the DL is analogous to the electroactive species concentration decay at the electrode surface region as illustrated in Figure 3.11. The DL thickness in both schemes can be minimized provided there is efficient convective transport expedited by mechanical gadgets such as stirring or pumping.

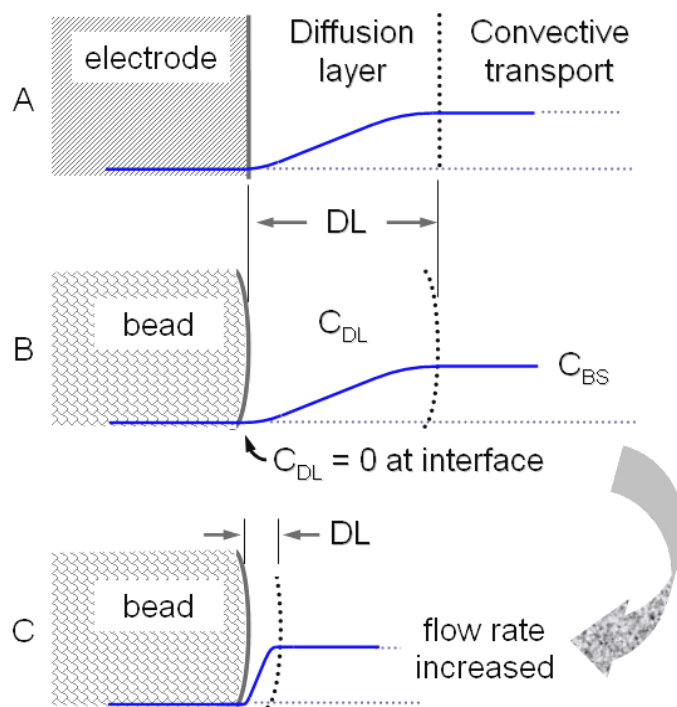


Figure 3.11. Concentration depletion profiles of the target biomolecule and electroactive species at the diffusion layer. Diffusive and convective transport regions are shown. Convective transport maintains the bulk solution concentration constant. C_{BS} and C_{DL} are the concentrations of reactive species at the bulk solution and at the diffusion layer respectively. The decay of the concentration reaches zero as we approach the electrode/bead-solution interface. The diffusion layer thickness δ can be minimized in the bead arrangement as depicted going from (B) to (C) by increased flow rate provided by the peristaltic pump.

The geometrical features of electrodes acting upon the speed of an electrochemical reaction are also present in the beads. A planar electrode is

comparable to a HA bead at the surface-solution interface. In contrast, a SA bead falls closer to a hanging drop electrode, Figure 3.12. Since the diffusion to a planar surface can be treated as linear, the DLs will have a planar contour parallel to the electrode surface. Hence, the surfaces parallel to the electrode remain constant despite the thickness of the DL.

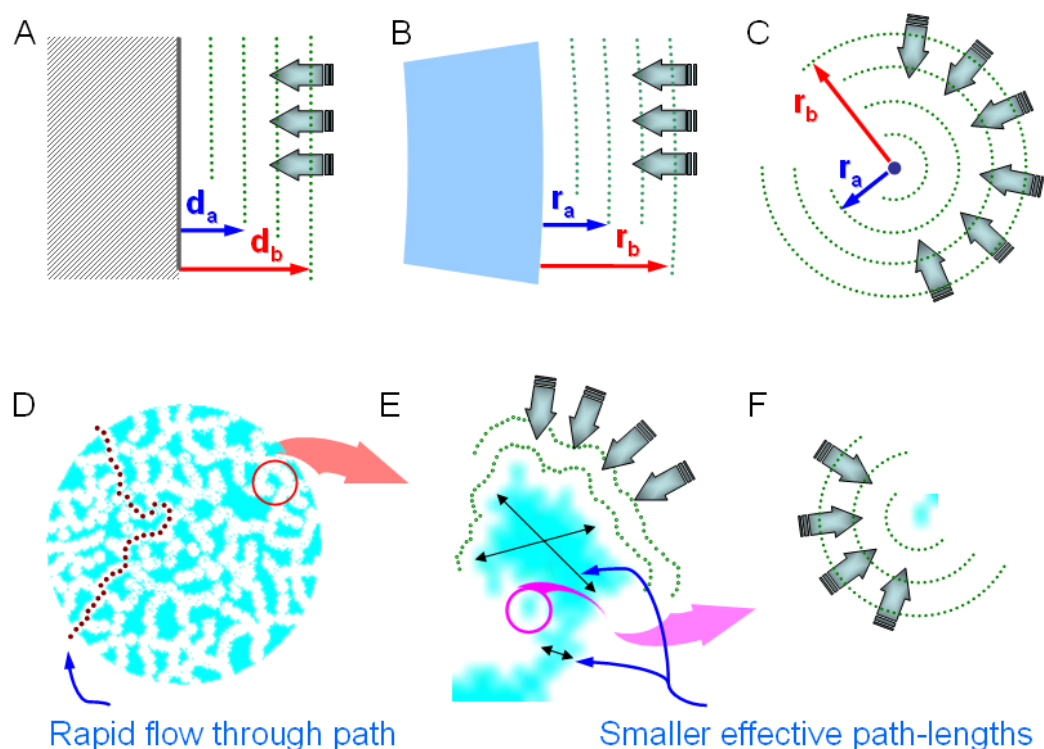


Figure 3.12. Depiction of planar and spherical geometries showing DL envelopes stretching into the bulk solution. (A) linear diffusion to a planar electrode, (B) 'linear' diffusion to a homogeneous agarose bead, (C) radial diffusion to a hanging drop electrode, (D) superporous agarose beads illustrating the large flow through pores where 'convective' transport aids in the mobile phase mass transfer, one of the possible paths is delineated by the dotted line, (E) diffusion to a magnified section of the SA bead showing smaller effective diffusion path lengths indicated by the double ended arrows, and (F) further magnification of some regions on the SA bead resembling a spherical hanging drop electrode.

On the other hand, the diffusion to a drop electrode is radial and the DL shapes spherical and concentric. With increasing radii of the concentric surfaces so does the area available for diffusion. The mass transport thus is heftier towards smaller dimension electrodes as well as towards the small HA regions of a SA bead surrounded by flow through pores. Moreover, the smaller size of the homogeneous regions equates smaller effective path lengths with mass transfer governed by diffusion. For very small dimension electrodes Chen S. et al reported that an enhanced mass transport rate can overcome the speed at which the electroactive species are reacted at the surface. In addition to a heightened mass flux, the depletion layer is also found to be thinner with decreasing size of electrode.¹²⁹ In terms of an ideal very small gel volume the mass transport speed may approximate the target-ligand association rate.

The reduced mobility inside an agarose matrix is certainly indicative of resistance to the transit of solutes from the solution into the bead at the solution-bead interface. The electrochemical counterpart is found when membranes are inserted between solution and electrode such as in electrochemical membrane biosensors.¹³⁰ When the resistance becomes important there is a sudden drop in the concentration profile, Figure. 3.13.

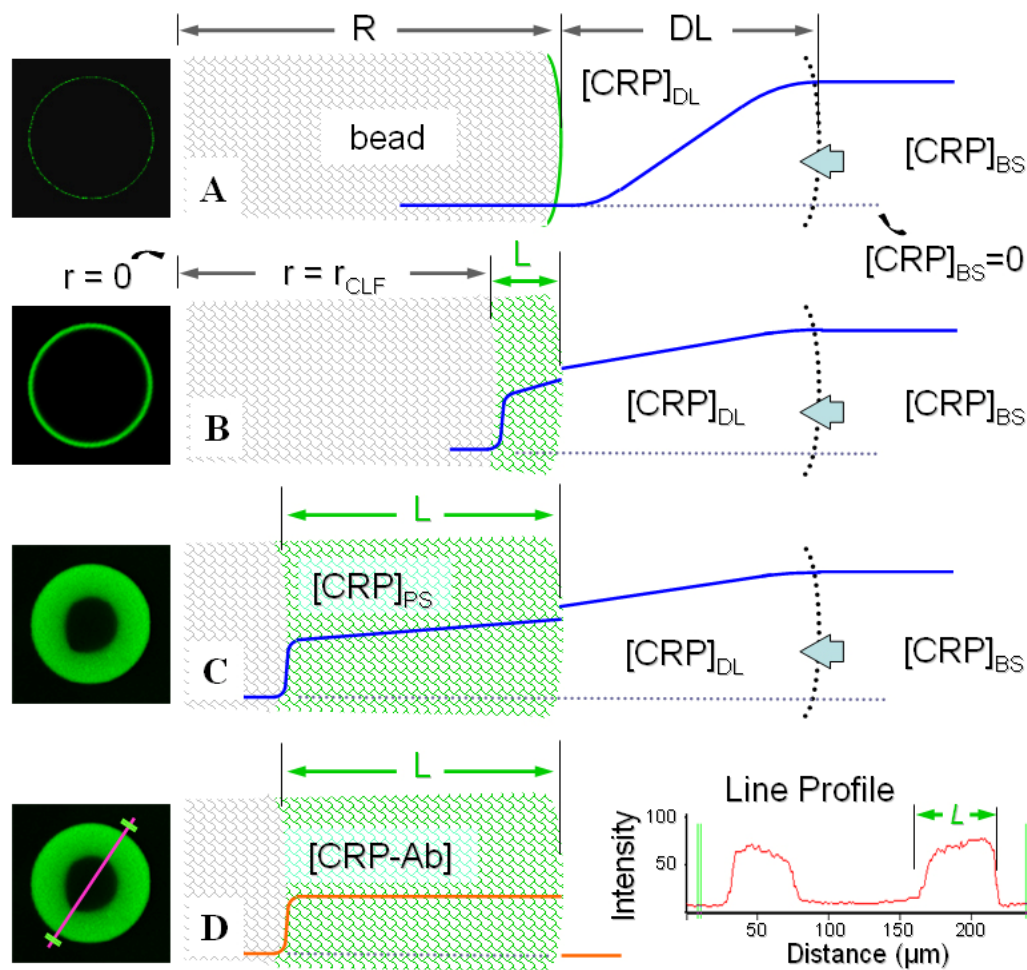


Figure 3.13. Illustration of concentration profiles at the diffusion layer, DL, for the direct immobilization of fluorophore labeled CRP. A linear concentration gradient is assumed. Here $[CRP]$ denotes concentration of labeled CRP, subscript BS indicates bulk solution region, DL the depletion layer at the interface between bead and solution region, PS solution at the polymer region. The depth of penetration L occurs at a distance $r = r_{CLF}$ from the center of the bead of radius R . The confocal pictures are representative penetration stages suggesting (A) immobilization of CRP at the bead-solution interface, (B) penetration transition at the bead-solution interface and (C) inside the bead. The evolution of the fluorescence front is shown in green from A to C. At the fluorescence front, the rapid capture of labeled CRP causes $[CRP]$ to fall sharply to zero. Resistance to mass transport in agarose generates a drop in the concentration profile at the solution-agarose region transition shown in (B) and (C). The concentration profile of labeled CRP conjugated to antibody, $[CRP-Ab]$, and the intensity line profile of the confocal micrograph bead medial slice are depicted in (D).

A simple 1-dimensional Fick's diffusion model may suffice for small target penetration depth when compared to the radius of the spherical bead environment. It is though more appropriate to include the spherical symmetry in the diffusion equation to account for the change in surface area through which target approaches the center of the bead:

$$\vec{j} = D \cdot \frac{\partial C}{\partial r} \cdot \hat{r} \quad (7)$$

For small depth penetration the amount of target entering a surface equal to $4\pi \cdot r^2$ will be constant, where r represents the distance of the spherical surface from the center of the bead or radius R . Within this small region the surface flux j is related to the target current i , at a distance r from the center of the bead as follows:

$$i(r) = 4\pi \cdot r^2 \cdot j(r) \quad (8)$$

If r is somewhere close to the surface, within this differential penetration, the integration of Equation 7 provides the concentration at a position r from the center of the bead as a function of the surface flux j_R , distance R and the target concentration at the bulk solution, C_{BS} :

$$j(r) = j_R \cdot \frac{R^2}{r^2} \quad (9)$$

$$C(r) = C_{BS} + \frac{j_R \cdot R}{D} \cdot \left(1 - \frac{R}{r}\right) \quad (10)$$

The reactants are consumed at the CLF-solution interface at a rate, k_{CLF} , which depends on the flux of target and the target concentration at $r = r_{CLF}$.

$$j_{CLF} = k_{CLF} \cdot C_{CLF} = j_R \frac{R^2}{r_{CLF}^2} \quad (11)$$

$$j_{CLF} = \frac{C_{BS} \cdot D}{\frac{D}{k_{CLF}} - \frac{r_{CLF}^2}{R} + r_{CLF}} \quad (12)$$

The flux at the CLF-solution interface, Equation 12, proceeds from combining Equations 10 and 11. The penetration L is $R - r_{CLF}$, and if n is the number of reaction sites per unit volume:

$$\frac{\partial L}{\partial t} = \frac{j(r_{CLF})}{n} = \frac{D \cdot C_{BS} / n}{\frac{D}{k_{CLF}} - \frac{L^2}{R} + L} \quad (13)$$

$$-\frac{1}{3R} \cdot L^3 + \frac{1}{2} \cdot L^2 + \frac{D}{k_{CLF}} \cdot L - \frac{D \cdot C_{BS}}{n} \cdot t = 0 \quad (14)$$

Integrating with initial conditions $L=0$ at $t=0$ the reaction depth is obtained as a function of time, Equation 14. The radial diffusion relationship is certainly more complex than the linear proportionality expressed in Equation 1. For a small penetration ($L \ll R$) the third order dependence in Equation 14 can be approximated to zero bringing the result closer to a quadratic proportionality. In SA localized homogeneous gel regions surrounded by convective flow the depreciation of the cubic term in Equation 14 may constitute a good approximation model. More detailed mathematical modeling of diffusion into spherical environments from constant concentration reservoirs can be found in the literature which is generally applicable to diffusion with symmetric spherical surface flux.¹³¹ Characterization of the beads microenvironment is necessary to model the variation in hydrodynamic pressure on the beads from top to bottom in the well in order to include a pressure-dependent DL variable at the external surface of mainly HA beads.

3.4 SUMMARY AND CONCLUSIONS

The diffusion in agarose beads is dependent on the size of the porosity as it is with any other porous material. The pore size can be increased by using a less dense agarose gel which can be achieved if the gel is prepared from a low agarose concentration solution. Despite the concentration of the original solution the diffusion into beads of HA type is limited to a radial displacement in order to take advantage of the whole available reactive sites of the beads body. Thus the inclusion of large flow pores allows for a proper irrigation of the agarose network as the surface of agarose in close contact to the solution is largely increased. Once the superpores are filled the normal diffusion process occurs into the HA regions. The advantages of including the SA beads into our chip based multianalyte detection system is essentially the cascading effect due to an enhanced mobile phase transport in a short span of time. This is appreciated on the high loading capacity in a short frame of time as the entire volume of a SA beads is readily accessible. Larger pores allow for fast distribution of larger biomolecules inside the beads since the steric hindrance between analytes in the mobile phase and between analytes and the solid skeleton of the gel is reduced. Mass transport governed by diffusion processes are minimized owing to the reduction in thickness of the depletion zone and due to the smaller effective path length associated to smaller homogeneous gel regions. Mass flux is enhanced to the smaller homogeneous gel domains through a radial diffusion pathway. More effective partitioning of analytes between solid and mobile phase as the solution is momentarily confined within the beads pores due to turbulent hydrodynamics in the tortuous paths to be traversed

before exiting the beads body. Rapid and thorough elimination of unwanted analytes from the bead domains during the wash processes. Lower applied pressure requirements on the delivery of solutions. As the interaction of the beads capturing capacity and the targets in the mobile phase is essentially of an association-dissociation equilibrium process, the reduced time of washing with any other solution containing the target biomolecule will effectively diminish the loss of target biomolecule of interest. Reduced assay times that minimize the loss of effective biological activity due to denaturation, aggregation or precipitation. Overall, rapid and more reliable results from each assay which, as addressed before, represents an upgrade to the chip based multianalyte detection system.

Chapter 4: Multifunctional and Multicompartment Beads for Sensor Applications

4.1 INTRODUCTION

In this chapter, new methods are developed so as to create a series of interesting multifunctional composite systems that have potential to serve as novel sensing ensembles. The chapter is organized in the following manner. First, a short introduction is provided for this general area. This is followed by an experimental section whereby the various important synthetic strategies are documented. Then a results section describes a series of compartments and multifunctional sensor ensembles. Here the physical characteristics and general methods for assembly are described. In the final section of the chapter, selected promising systems are utilized in sensor studies involving protein and DNA analysis.

Agarose is a versatile media into which particles of nearly any shape or material may be embedded-in. With some imagination and dedication it is possible to create multifunctional particles within the confines of the 3-dimensional gel network. The engulfing media may be shaped conveniently into a sphere by implementing emulsification of an agarose solution with the particles dispersed inside.

The size of spherical particles relative to the coating agarose thickness dictates the type of the resulting composite beaded material. The diameter of the beaded composite elements may contain a single core comparable in size located at the center of the embedding media, may include a multitude of small microspheres

dispersed randomly in the beaded gel or may be a more elaborated combination of centered core with ‘randomly’ dispersed smaller beads. Figures 4.1 and 4.2 illustrate the basic homogeneous and superporous agarose microsphere structures discussed previously. The illustrations also depict a few conceptual composite bead systems where either homogeneous or superporous agarose gel physically locks smaller microspheres inside. Superporous gel coating is pretended to bring convective mobile flow into the composite beads to speed up the delivery of target analyte.

Most of the microsphere particle ensembles depicted in Figures 4.1 and 4.2 and others shown later serve as adaptations of systems that have been explored previously in the literature, but for different applications in such areas. For instance, microcapsules may be used for controlled release of drugs in biotechnological applications, functionalized encapsulated magnetic particles facilitate separation and purification processes in immunoassays by using a magnetic field to draw away the microspheres from a complex mixture, and quantum dots are multilayer core-shell microspheres used in sensing applications as a labeling agent.¹³²

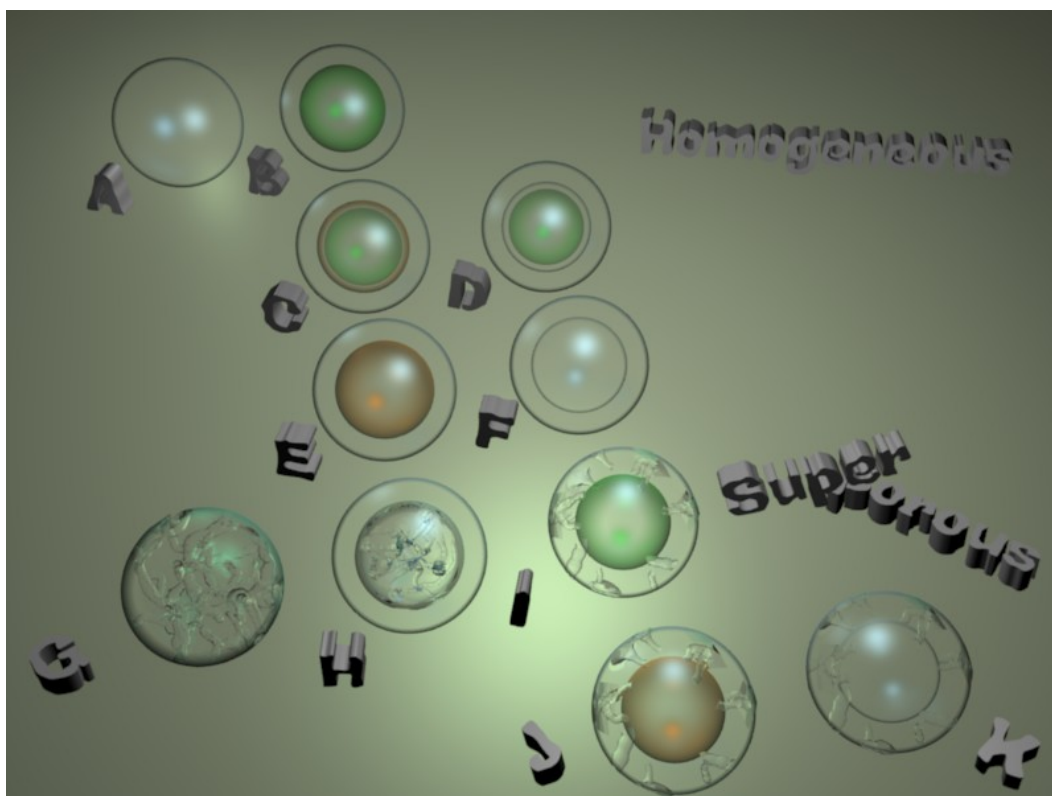


Figure 4.1. Microsphere Design Concept I. Composites microspheres are here categorized into beaded particles containing only homogeneous type regions, and a combination of homogeneous and superporous based zones. Homogeneous type composites illustrated include (A) a classic homogeneous beads, (B) basic core-shell beads, (C) multi-layer core-shell type bead, (D) multi-layer core-shell with intermediate soluble layer, (E) basic core-shell with a soluble core and (F) hollow homogenous bead. Superporous-homogeneous composite depict (G) a basic superporous bead, (H) superporous core with a homogeneous shell, (I) homogeneous core with a superporous coating, (J) soluble core with a superporous coating and (K) superporous hollow bead.

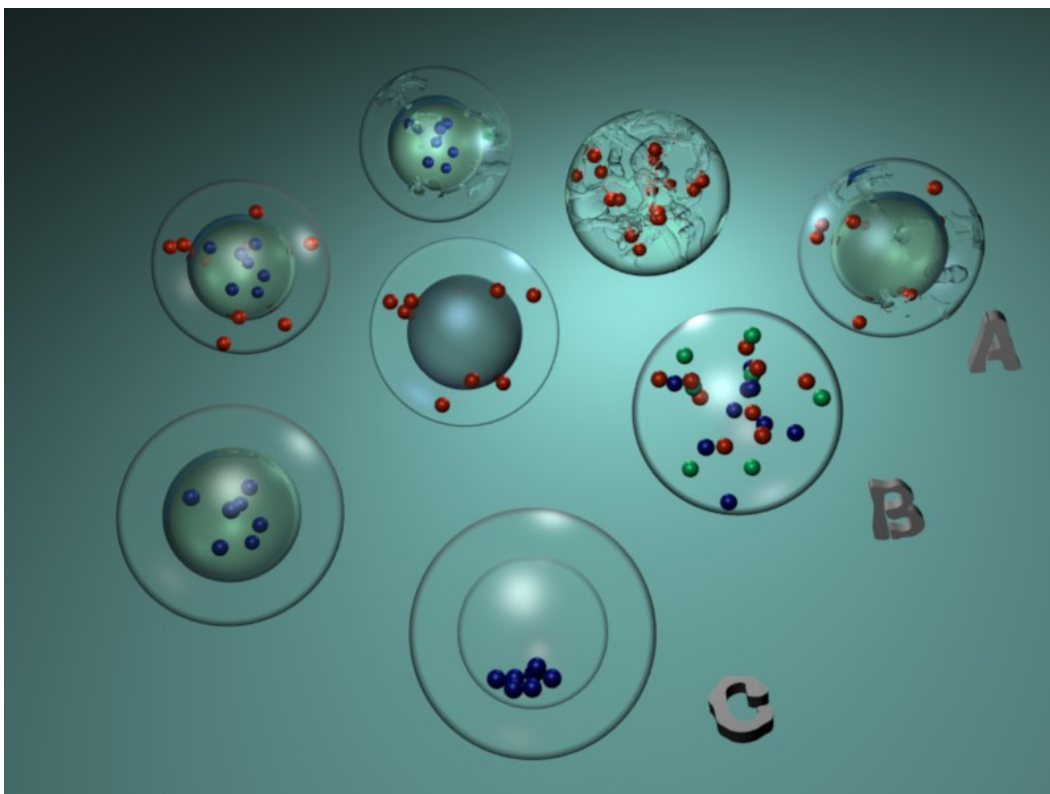


Figure 4.2. Microsphere Design Concept II. Composite beads contain small agarose derivatized beads. Diverse capturing ligands may be immobilized on the embedded beads and enable multiplexing capabilities within a single agarose bead. (A) Superporous and (B and C) homogeneous moiety used as the embedding media. Beads of different sizes may be included. On (B), from right to left, sets of small beads may be dispersed within the gel as a random mixture, small beads may be fixed as satellites around a big centered core, or small beads may be isolated in a core region and layers with a different set of small beads build sequentially upon the existing one. In (C) small beads may be supported initially on soluble polymer and the resulting core solubilized after releasing the beads inside.

Polymer particles and hybrid particles composed of a polymer and inorganic compounds are important in biomedical applications and therefore it is desired a biocompatible product. However, it is not common to find agarose as the preferred material in the elaboration of composite beads. In this chapter, agarose is used to build composite beads with defined isolated functionalized regions. The isolated ‘islands’ in any of the configurations depicted in Figures 4.1 or 4.2 can be modified to contain a different chemical functionality. A diverse chemical nature in a single bead is consequently comparable to having several sets of beads with different chemistries packed together conveniently in one single element. The resulting composite bead is, therefore, rendered with multianalyte detection capability and may be used for sensing applications.

The advantage of agarose composites here described over latexes relies on the innate porosity of agarose gels which confers a facilitated rapid access to the internal volume of the gel. Latexes and other materials such as glass may be included to form hybrid microspheres, or excluded from the composite microspheres and solely agarose be used to define the compartmentalized reactive regions in the final beaded product.

The interest on SNPs studies targets testing of common disease markers and their incorporation into a portable analytical device as an alternative and complementary tool to the developing immunoassays. The previous results on the porous sensing elements of the chip-based platform allowed for rapid high sequence detection efficiency on three dimensional gel structures with high binding capacity and superior mobile phase mass transport when compared to planar DNA

micro-arrays.¹³³ In an attempt to contribute to the analysis of oligonucleotides it is reasonable to inquire into alternative routes to augment the multiplexing capabilities of the chip-based MAD system. Here compartmentalization in a single bead may play an important role. In a typical ordered array, the sensing elements are identified by its position, a feature to be conserved. Here discrete isolated volumes of gel are used to demonstrate multiple analyte detection capabilities in a single bead-based array sensing element. The combination of color in the sensing elements and position in the array may prove effective and expand the number of analytes to be probed.

The demands of fast assays in analytical sciences applied to environments such as proteomics, drug development screening and evaluation of diseases spurs towards added capabilities in performing multiple assays simultaneously to probe a single sample test with the least possible specimen modification. Potential reduction in material cost, sample volume requirement and assay time are just a few of the benefits that multiple analyte testing capabilities provide.

Before the imminent completion of the human genome sequence the identification of single nucleotide polymorphisms (SNPs), as a link to proclivity to common diseases including myocardial infarction, asthma, ovarian and breast cancer, enforced the impending high throughput SNP genotyping platforms to appear.¹³⁴⁻¹³⁸ The abundance in the variations found on at least two base pairs at the same location in the genomic sequence regions (about 1 on every 1000 nucleotide positions) from person to person calls for extensive screening of genetic disease markers. The identification of disease markers are frequently determined with two

groups of patients frequently referred as disease and control groups from which large scale association studies are performed if the genome-wide approach is used. Alternatively, the candidate genome approach targets specific parts of the genome thought of being connected to the disease based on previous biological studies.¹³⁹ Understanding of the molecular basis associated to a disease and the events triggering the expression of a complex trait, usually governed by a large number of genes, are expected to help on the design of prevention and treatment procedures. The response to medications in complex disorders is also found susceptible to mutations in the genetic information. Medication shown to have adverse or no effect at all on a large group of individuals may benefit therapeutically to individuals with a certain genetic profile.^{140, 141}

Many scenarios are used in SNP analysis and they all compromise amplification of target sequences. Some approaches are followed by analysis of DNA sequences by hybridization probes with perfectly matching and mismatched variants of target sequences.^{142, 143} Detection of oligonucleotide single mismatches was implemented within the group's interests in an effort to extend the diversity of analytes in the chip-based MAD platform.

4.2 EXPERIMENTAL

4.2.1 Methods and Instrumentation

Emulsification was procured with an overhead stirrer IKA RW20 DzM.n acquired from (IKA Works Inc.; Wilmington, NC). The chip-based MAD system was described beforehand. The optical interface included a compound microscope (Olympus America Inc.; Melville, NY) equipped for epifluorescent imaging with a 100 W Hg lamp, 4x and 5x objectives, interchangeable filters including FITC, Texas Red, Pacific Blue dual band FITC-Texas Red and triple band FITC-Texas Red-Pacific Blue excitation cube filters (Chroma Technology Corp.; Brattleboro, VT) and a 12-bit charge-coupled device (CCD) color camera (DVC Company, Austin, TX). Data was processed using Image Pro Plus 4.5 software (Media Cybernetics; Carlsbad, CA). Fluid delivery to the analysis chamber was carried out with peristaltic pumps from FIA labs (Bellevue, WA) and controlled with FIA lab software. Confocal Laser Scanning (CLS) images were obtained with a Leica SP2 AOBS Confocal Microscope (Exton, PA). Standardized metallic screens were purchased from W.S. Tyler (Mentor, OH) and Newark Wire Cloth Company (Clifton, NJ).

4.2.2 Reagents

Triton X-100, carboxyl and amine polystyrene bead suspensions (6 and 10 μm diameter) and glass beads (150-210 μm diameter) were purchased from Polysciences, Inc. (Warrington, PA). Neutravidin biotin binding protein was purchased from Pierce Biotechnology (Rockford, IL). Amine functionalized crosslinked polystyrene polyethylene glycol graft copolymer (Tentagel resin; ~ 130

µm dry diameter and 230 µm wet diameter) were purchased from Novabiochem Corporation (San Diego, CA). Sodium tetraborate, boric acid, 3-glycidoxypopyl trimethoxysilane, perfluoromethyldecalin, divinylbenzene, sodium hydroxide, acacia powder, trichloromethane, sorbitan monooleate, toluene lauroyl peroxide and 1-Ethyl-3-(3-dimethylaminopropyl) carbodiimide were purchased from Sigma-Aldrich (St. Louis, MO). Styrene monomer and methyl cellulose were purchased from ACROS organics were purchased from Sigma-Aldrich. The DNA 18 bp capture sequences and their complements (Figure 4.1) were acquired from Integrated DNA Technologies, Inc. (Coralville, IA). Four molecular beacon sequences and their complements (Table 4.2) were also acquired from Integrated DNA Technologies. The molecular hairpin structures are complementary to target sequences from HIV-1 gag gene (two of them) and specific to the 16S rRNA region of *Bacillus anthracis* and *Bacillus subtilis*.

4.2.3 Core-Shell Beads

The preparation of agarose beads into agarose was performed as follows: 1 mL glyoxal activated 150-180 µm agarose beads resuspended in 2 mL water was added to 6 mL 5% agarose solution stabilized at 60 °C and mixed for 3 min. A suspending solution prepared by diluting 5 mL Span 85 to 100 mL with hexanes was equilibrated to 60 °C and stirred at 1100 rpm. The agarose mixture was added to the stirring solution and after 1 min the mixture was allowed to cool to room temperature. The product was washed with water, size sorted with standardized screens and the beads resuspended in PBS buffer.

Microspheres other than agarose are coated in a similar fashion. Experimental conditions for polystyrene and glass beads are summarized in Table 2.5. Pre-treatment of polystyrene beads before the coating was performed to facilitate imaging and discrimination of regions within the bead composites. The particles do not require previous modification to be coated. Polystyrene beads with diameter size between 200 and 300 μm were died with Coumarin 30 through a polymer solvent swelling stimulation process. 25 mg polystyrene beads were soaked in 2 mL of a 50/50 methanol/chloroform mixture. 16 mg Coumarin 30 was added and mixing proceeded for 40 min followed by copious rinsing with water.

	ps thick coat	ps thin coat	glass
Bead size to be coated	200-300	200-300	150-210
No. beads per water volume	60 mg/mL	60 mg/mL	1 mL dry
Agarose concentration	2.50%	1.50%	5%
Agarose solution volume	10 mL	10 mL	10 mL
Span 85	20 mL	20 mL	0
Suspending solution solvent	hexanes	hexanes	fluorinated oil
Suspending solution volume	100 mL	100 mL	25 mL
Mixture stabilization T	55-60 °C	55-60 °C	50 °C
Stirring speed	1600 rpm	1600 rpm	1500 rpm

Table 4.1. Coating experimental conditions used for glass and polystyrene in the production of core-shell hybrid beads. The thickness of the coating for polystyrene may be regulated, in the table above by changing the concentration of the coating agarose solution.

4.2.4 Raspberry-Type Beads

The coupling of carboxyl to amine functionalized beads proceeded with a water soluble carbodiimide. Reagents used are used in excess. Amine functionalized Tentagel beads were previously rehydrated in water overnight. Glass beads required surfaces modification. Glass beads were initially cleaned with piranha solution followed by rinse with HCl 1 M, water, acetone and air dried. To 0.5 mL of glass beads in 4 mL toluene, 1 mL of 3-aminopropyltriethoxysilane was added and shaken overnight and washed with acetone and dried under nitrogen. Coupling buffer was prepared with 1250 μ L Boric Acid, 362.5 μ L tetraborate and 250 μ L NaOH 1M. Carboxylated polystyrene beads suspension was either 6 or 10 μ m bead diameter size and of 2.6% solid contents. Aminated glass or Tentagel resin beads (40 to 50) in 1 mL coupling buffer, 100 μ L of carboxylated polystyrene beads suspension and 25 mg carbodiimide in a 2 mL eppendorf tube were mixed and rotated for 3 h followed by rinse with water.

4.2.5 Macroporous Polystyrene Beads

The suspending solution made with 3 g acacia powder dissolved in 75 mL water was stabilized to 65°C and stirred at 150 rpm. 50 mL styrene monomer was cleaned by extracting the stabilizing agent 3 times with 10 mL NaOH 1 M followed by drying through activated alumina column. The crosslinker was subjected to the same cleaning procedure. The high internal phase emulsion (HIPE) contained 0.1397 g lauroyl peroxide in 1 mL toluene, 0.01 g methyl cellulose previously dissolved in 1 mL trichloromethane, 1.5 mL sorbitan monooleate, 3.75 mL styrene and 0.25 mL divinylbenzene. The HIPE was prepared by adding to 75 mL water

the above internal phase and the mixture stirred at 1400 rpm for 5 min. The resulting HIPE was added to a 200 rpm stirred suspending solution made of 3 g acacia previously dissolved in 75 mL water and stabilized at 65 °C. Stirring continued for 3 min and readjusted to 150 rpm. After 6 h at 150 rpm and 65 °C stirring was stopped, the product was washed with water and ethanol and the 63-75 µm fraction collected with the corresponding sieves.

Protein adsorption on beads was performed by adding sheep anti-CRP conjugated to Alexa Fluor 488 to 100 µL settled 63-75 µm polystyrene beads and shaking for 22 h followed by rinse with phosphate buffer pH 7.4. The beads were then observed under an epifluorescence microscope.

4.2.6 Homogeneous Agarose Beads: 20-32 µm

A 2% agarose solution was prepared with 1 g agarose in 50 mL water. The solution was stabilized at 60 °C and stirred at 1800 rpm. A suspending solution at 60 °C consisting on 15 mL sorbitan triolate diluted to 150 mL in hexanes was added to the stirred agarose solution. Stirring proceeded at 57 °C for 1 min and the reactor was left to cool to 49 °C and in a water bath at room temperature to 26 °C. The product was collected in a metallic sieves, washed with water and the fraction with diameter size between 20 and 45 µm was collected, washed with a 50% ethanolic solution followed by water.

4.2.7 Avidin Functionalization of Agarose Beads

Agarose beads were coated with avidin to perform the capture of biotin conjugated oligonucleotide in the chip-based MAD system. For that purpose, agarose beads of 2% concentration were glyoxal activated previous to the coating

process following procedure described in section 2.3.1.1.5. Custom made agarose bead diameter sizes used here include fractions 20-32 μm and 150-180 μm . Aviding was also coupled in a similar fashion to commercial 250-280 μm homogeneous 6% ABT glyoxal activated agarose beads. Neutravidin protein was reconstituted with nanopure water to a concentration of 10 mg/mL. To 0.5 mL of settled beads, 330 μL of Neutravidin solution, 60 μL NaCNBH₃ 0.44 M and carbonate buffer pH 9.6 was added to complete 1500 μL total volume. Triton X-100 was also added to produce a 1% surfactant solution. The mixture was rotated overnight in a 2 mL eppendorf tube then washed 3 times with phosphate buffer pH 7.4. To the beads resuspended in 500 μL phosphate buffer, 1 mL Trizma buffer 50 mM pH 7.15 and 60 μL NaCNBH₃ 0.44 M was added and reacted for 1 h. Afterwards beads were washed with phosphate buffer.

4.2.8 DNA Functionalization of 20-32 μm Agarose Beads

The 18-mer DNA oligonucleotides were previously reconstituted in TE buffer (10 mM Tris-HCl, PH 8.0, 1 mM EDTA).¹³³ To 25 μL of settled beads in water 100 μL 50 μM of an oligonucleotide was added and reacted overnight followed by rinsing with nanopure water. The oligonucleotide modified beads were stored at 4 °C. Three different sets of small beads coated with the 18-mer DNA-capturing ligands were prepared.

The molecular beacons were reconstituted in nanopure water. 1 μM virus and 10 μM bacterium molecular beacon solutions were prepared. To 50 μL aliquots of settled beads 75 μL molecular beacon solution was added and reacted overnight followed by rinsing with nanopure water. Four different sets of small beads with

immobilized molecular beacon-capturing ligands were prepared with the different virus and bacterium sequences.

4.2.9 Agarose Beads with 20-32 μm Functionalized Agarose Inclusions

To prepare composite beads with only one single set of DNA-coated small beads, a 3.7 % agarose solution was prepared with 2.22 mg agarose in 600 μL water in a 2 mL eppendorf tube and equilibrated to 42 $^{\circ}\text{C}$. A 50 μL modified 20-45 μm settled beads was resuspended in 100 μL water. The suspension of beads was stabilized 2 min at 42 $^{\circ}\text{C}$, then added to the agarose solution and mixed for 3 min at 42 $^{\circ}\text{C}$. The mixture was added to a 40 $^{\circ}\text{C}$ 800 rpm stirred suspending solution prepared with 3 mL Span 85 diluted to 50 mL in hexanes. After 1 min the solution was left to cool to 25 $^{\circ}\text{C}$ with continuous stirring. Stirring was stopped and the product was washed with water and sieved. The fraction 250-280 μm was collected, washed with PBS buffer and stored at 4 $^{\circ}\text{C}$.

To include the three sets of modified 20-45 μm beads in the composite microspheres, ~ 12.5 μL of each bead type were mixed and diluted with water to 50 μL . The coating procedure was as described above.

The bacterium and virus sequences were paired respectively. The preparation was similar as described above but an equal volume of avidin coated small beads was added to each of the paired sequences mixtures to complete a final volume of 150 μL of mixed small beads. The resulting composite beads were stored in nanopure water at 4 $^{\circ}\text{C}$.

Additionally avidin-coated small beads were coated with agarose and used to test the capturing viability of the protein after the emulsification processing and later as control beads.

4.2.10 Sensor Application: Multiple Analyte Detection in Composite Beads Assay

Composite beads consisting on small agarose microspheres dispersed in agarose gel were tested here for multiple analyte detection, namely, sets of oligonucleotides with one or two base pair mismatches between sequences in a single oligonucleotide set.

Hybridization buffer contained 20 mM Tris-HCl and 300 mM MgCl₂ with pH adjusted to 7.8. High stringency washing buffers were diluted 5 times from a concentrated stock solution with pH 7.8 containing 5 M NaCl, 1 M Tris buffer pH 7.6 and 0.5 M EDTA pH 8.0.

18-mer oligonucleotides: Composite beads containing one single set of small beads coated with a different DNA capturing ligand (DNAcap~R, DNAcap~G and DNAcap~B) and composite beads containing small avidin coated microspheres were used to form a 3 x 4 array in the chip. The composite beads were exposed 10 min to 500 µL of 0.1 µM target solutions delivered sequentially in a close looped circuit at 1.6 mL/min. Between targets washing buffer was delivered for 45 s. Exposure time was set to 1 s for beads containing single sets and 5 s exposure for beads containing three sets.

For molecular beacons detection 500 µL of 0.25 µM target solutions were delivered for 20 min in a closed loop with 30 s wash. Exposure times for composite beads capture ranged between 0.15 s and 3.5 s.

4.3 RESULTS AND DISCUSSION

4.3.1 Agarose in Agarose Core-Shell Beads

One of the first multifunctional compartments to be explored here is agarose in agarose core-shell systems. Agarose beads coated with agarose procure concentric agarose regions to be systematically modified with different chemical moieties. The regions are made of the same material to which, theoretically, the same porosity may be given granting the concentration of agarose used to build the layers is the same. Adopting a different concentration, on the other hand, warrants partial control on the regulation of the diffusion rate through the different regions. Thus, the diffusion rate may be more restricted at regions closer to the center of the bead with a high density gel and adding successively lower density gel mantles. Conversely, tethered mobility at the surface of the bead with a thin blanket of compact agarose and may be use it to moderate discharge of reagents inside the bead. The latter may be applied to modulate the entrance of compounds for multi-step reactions into the core microreactor and of feeding to live particle such as embedded bacteria.

The dissimilarity in gel density between core and shell facilitates the distinction between simple and composite homogeneous beads when observed under bright field mode of a compound microscope. Alternatively, a capturing ligand such as a oligonucleotide probe was immobilized on the core of the composite beads. Following the delivery of a complementary DNA sequence tagged with a fluorophore, the core is shown to be the only region of the composite

bead to participate in the capture of the oligonucleotide, Figure 4.3. The capture of the fluorophore labeled DNA is described in more detail below.

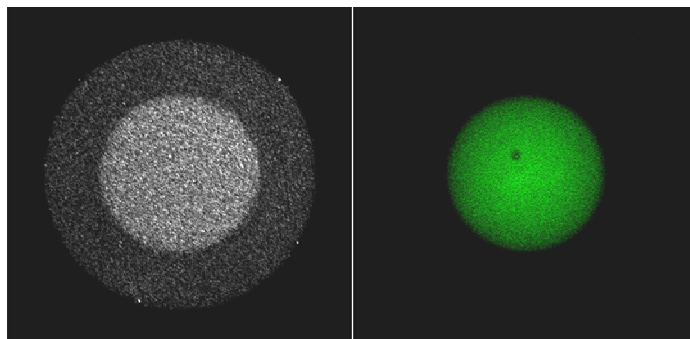


Figure 4.3. Confocal laser micrographs illustrating the capture of oligonucleotide labeled with FAM6. The core of the composite bead is coated with a 50 bp DNA probe with target complementary sequence. At the left, the confocal image is in transmission mode and both core and shell can be identified. Right picture show the fluorescence at 488 nm excitation indicating the specific capture at the core.

Agarose solution for coating is used here in excess to coat the composite core shell beads. As a result a mixture of composite and plain homogenous beads, described previously in Chapter 2, is obtained. The density of core and shell are very similar and the separation of the core-shell composites from the homogeneous beads in the final product is lengthy if they are of about the same size. It is therefore, really convenient to utilize low excess of agarose solution to minimize the amount of undesired beads. An automated high-throughput particle analysis/sorting instrument may be used to clean up the product adjusting the settings to eliminate the plain homogeneous agarose beads.

The agarose-agarose 290 μm diameter core-shell beads utilized in this section contain a 2% glyoxal activated 150 μm diameter core embedded in a 5% non-activated agarose 67-70 μm thickness shell. Avidin protein was coupled to the

core of the composite beads and also to commercial ABT glyoxal activated 6% conventional homogeneous agarose beads of similar size (~290 μm diameter). The avidin-coated gels were exposed to a solution of biotinylated 50 bp oligonucleotide (5'→3': AAAGCCTTCATCACTCACGCCGCGTTGCTCCGTCAGACTTTCGTCCATT-biotin). Both bead types were placed on a microchip and following the delivery of 500 μL 10 μM fluorophore-labeled complement target solution (5'→3': AATGGACGAAAGTCTGACGCAGCAACGCCGCGTGAGTGATGAAGGCTTT-FAM6) at 1.5 mL/min flow rate, the penetration of the DNA was monitored as a function of time, Figure 4.4.

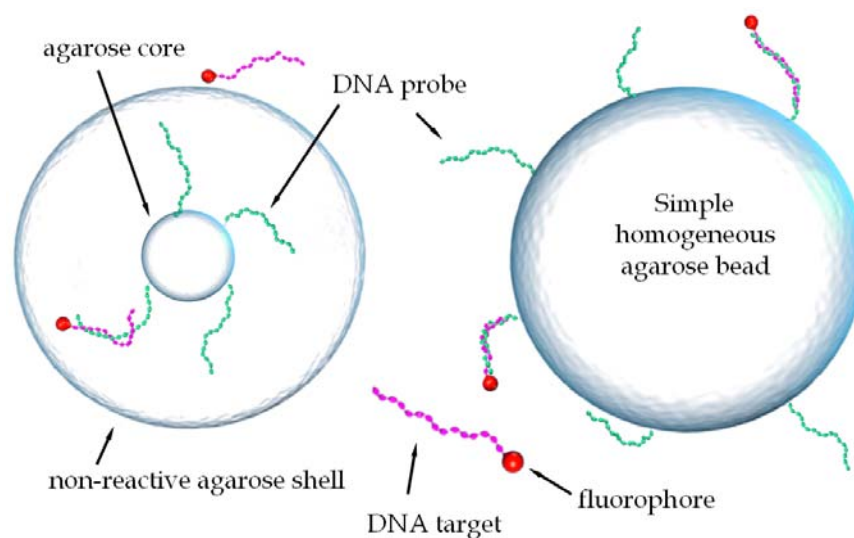


Figure 4.4. Capture of fluorophore labeled oligonucleotide (DNA target) by complementary DNA sequence (DNA probe) immobilized on the core of an agarose-agarose core-shell ensemble and on a conventional homogeneous agarose bead. (Left) The capture of the target in the core-shell beads is delayed momentarily until the target reaches the core by diffusion through a non-reactive agarose shell. (Right) In contrast, the conventional agarose beads react immediately with the target and free target diffuses progressively into the interior of the bead as the available binding sites are gradually consumed.

It is expected that the shell will delay the development of fluorescence signal on the core of composite beads, delay not to be observed on the conventional homogeneous beads. After fluorescence signal equilibration on both beads, rinse with a 300 mM MgCl₂ solution was followed by water. The measured fluorescence density signal was determined by drawing an area of interest (AOI) as a circle defined by the perimeter of the bead. During the microchip assay, the 5% agarose shell delays the development of fluorescence signal in the core which is appreciated after ~2 min. The signal equilibration in the core-shell bead occurs after 30 min, Figure 4.5. In contrast, 6%-CHA beads of similar size and shape require about 1 h for fluorescence count equilibration.

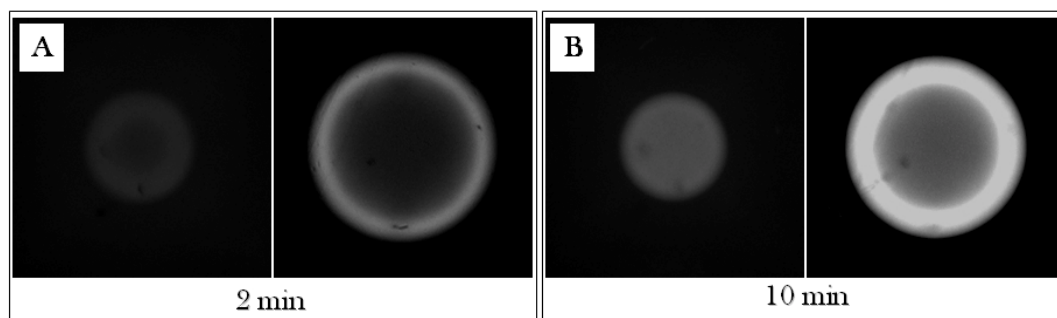


Figure 4.5. Capture of 50 bp oligonucleotide (5'→3': AATGGACGAAAGTCTGACGCA GCAACGCCGCGTGAGTGATGAAGGCTTT-FAM6). The fluorescence of composite core-shell and conventional 6% homogeneous beads is depicted for (A) 2 min and (B) 10 min assay. At 10 min assay the core has been all pervaded by the oligonucleotide. Equilibration of signal in core-shell beads occur after 30 min (data not shown).

Interestingly, the mobility of the target through an inert agarose shell of agarose in the composite bead is substantially faster when compared to the apparent mobility in a reactive agarose matrix in conventional homogeneous beads. Within 2 min of assay, the analyte moves through 70 μm of non-reactive shell in the composite bead. On the other hand, about 30 min is required to traverse the same

distance when there is a capturing probe. The arrest of the oligonucleotide by avidin depletes the solution from the DNA to be captured and, therefore, the analyte is replenished continuously as it has been discussed previously in Chapter 3. The depletion of analyte accounts in part for the apparent slower penetration speed into the interior of the reactive bead. The equilibration of signal at the conventional homogeneous beads occurs when the analyte pervades the remaining non-reacted interior corresponding to a sphere of about 150 μm in diameter. This non-reacted sphere in the conventional agar bead is equivalent in size to the core of the composite microsphere. In addition to a continuous depletion of target at the moving fluorescent front, an electrostatic barrier is built upon the continuous accumulation of DNA in the matrix. The free incoming DNA target from the solution will experience a repulsive force strong enough to slow down significantly the diffusion of analyte into the interior of the bead.

Although the porosity and the number of available reactive sites is not exactly the same in both types of beads compared here, previous DNA and antigen detection assays have shown that the crosslinked commercial 6% agarose beads and 2% conventional homogeneous agarose home made beads are comparable with respect to the mobility of small molecules such as the 50 bp oligonucleotide used in this assay (data not shown). Assuming that the distribution of capturing ligand is homogeneous throughout the agarose matrix, as suggested by confocal images, Figure 4.3, the total mean fluorescence intensity measured in the 6% conventional homogeneous beads is only 60% more than the fluorescence obtained in the core-shell microspheres, both measured at their corresponding equilibrating points.

Theoretically, once the reactive sites are ‘totally’ consumed, the fluorescence intensity in excess on the conventional homogeneous beads should be close to 75% since the shell on the composite beads is not reactive and the core is basically a smaller conventional homogeneous agarose bead. The 15% difference between the expected and the theoretical value of the signal intensity indicates that the density of capturing ligand in the core of the composite beads is larger to the density of reactive sites in the plain beads. Thus, in terms of ligand density, the penetration into the core of core-shell beads should be slower than the 6% beads were a less dense electrostatic barrier is built. The slightly larger pores in the 2% core, on the other hand, compensates for the excess in electrostatic repulsion bringing the diffusion speeds on both beads to a similar value. The actual contribution of each factor is more complex since the composite bead also has a 5% shell barrier. It is though, somewhat coincidental that the amount of time required to take over a 150 μm diameter bead volume corresponding to both the composite and the plain beads is about the same, that is, 30 min.

The penetration of the target analyte through the external agarose layer may be accelerated if the coating is made of lower agarose concentration, adding a thinner layer or including superpores. The shell also serves as a protecting shield against physical damage during handling with mechanical devices. Additionally, the core may be fabricated with a higher gel concentration to increase the density of reactive sites.

In short length assays, the internal volume of a homogeneous bead is normally not used because of delayed diffusion to the interior of the bead. The core

may be intentionally crippled with a ligand inert to the target and the shell used instead as the sequestering media. For instance, a glycidol activated core was reacted with excess of a short mono-aminomethylated compound such as propylamine previous to encapsulation with agarose. The encapsulating shell was then chemically modified using the same glycidol activation chemistry. The methyl termination added to the core, in this example, is necessary to transform the core into a region not available for protein immobilization or capture. Therefore, a smaller amount of capturing ligand may be immobilized solely on the shell as opposed to the whole bead volume. Alternatively, both regions may be used to capture a different target which requires careful activation and immobilization of capturing ligands to avoid undesired overlapping of zones.

The immobilization of the capturing ligand and of oligonucleotides followed by agarose coating is possible without significant loss of activity on both the protein and the oligonucleotide. The experimental coating temperature, set between 50 and 60 °C on the core-shell beads used in this section can be reduced to 40 °C. This ligand immobilization approach is described later in section 4.3.9.

4.3.2 Polystyrene in Agarose Core-Shell Beads

Instead of agarose, polystyrene can be used as a core. The result is a hybrid-material ensemble with an agarose shell that can be activated for sensing applications. Unlike homogeneous agarose, homogeneous polystyrene has a substantially denser matrix with pore size typically smaller than 10 nm, thus, the diffusion into polystyrene is hindered when compared to the polysaccharide. Here again, the shell may be used as the reactive region for short assay applications

where the latex cores may also participate in sensing applications by the addition of affinity ligands through covalent ligand immobilization or physical adsorption. Additionally, the highly dense matrix of crosslinked beaded latexes, such as polystyrene or polystyrene-polyethylene glycol graft copolymer, is an attribute exploited to physically arrest dyes in the internal volume of the latex microspheres. The addition of dyes allows for the colorimetric encoding of beads that facilitate multiplex analyte assays on analytical platforms such as the one offered by Luminex Corporation previously described in Chapter 1.

During the coating of polystyrene beads with agarose, at a fixed stirring speed and in excess of surfactant, the viscosity of the agarose solution dictates the thickness of the coating. The lower the agarose concentration the easier the agarose is displaced from the latex bead surface and the thinner the coating is, Figure 4.6. Conversely, more concentrate agarose solutions will lead to thicker coating, but too viscous solutions also tend to hold more than one latex bead together and to deliver non-centered latex beads. In Figure 4.6-C, a dye (Coumarin-30) was physically entrapped in the latex beads previous to the addition of an agarose shell which facilitates the identification of beads with proper excitation source.

An excess of surfactant can be used to stabilize the excess of agarose solution and to control the final size of the composite beads. The amount of surfactant and also the stirring speed aids in tweaking the thickness of the layer. The excess of agarose solution may produce beads similar in size to the composite beads, but the separation of particles is quite straightforward. The weight of the latex-agar hybrids is large enough to accelerate its precipitation when the mixture is

suspended in water. The plain agarose beads tend to form a layer on top of the hybrid particles easing its isolation.

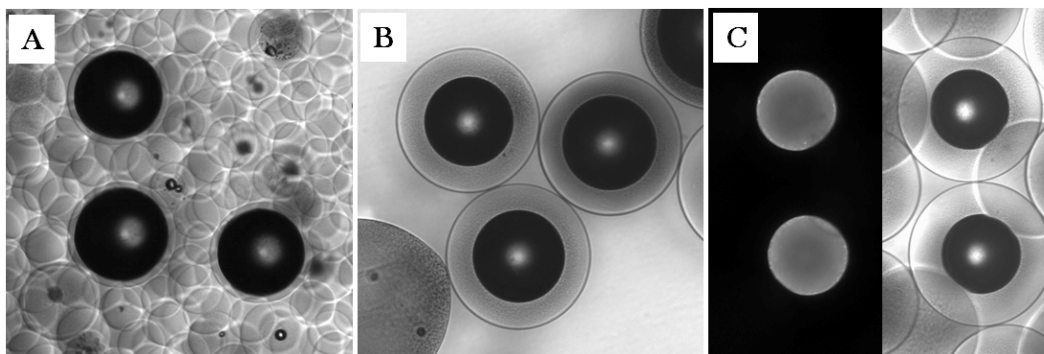


Figure 4.6. Bright field images of polystyrene beads coated with agarose. (A) Agarose solution 1.5% provides a thinner coating. The background in the image shows the excess in agarose solution used. (B) Agarose solution 2.5% leads to a thicker coating. (C) Bright field image of latex-agar composites and corresponding beads excited with mercury lamp to show the fluorescence of Coumarin-30 dye utilizing pacific blue filter.

Latex beads are heavier than agarose beads of similar size. As a result, the stirring speed needs to be increased for such materials or a denser suspending media used to maintain the stabilized composite droplets suspended. The latex-agarose solution mixture is broken down during stirring. Following the transition of agarose to a gel state the final product does not necessarily contain centered latex microspheres with a coating uniform in thickness. To obtain centered latex in the composite bead is frequently found easier if the thickness of the coating is not larger than the radius of the latex. A combination of stirring speed and viscosity of the agarose solution is found to affect the positioning of the latex bead. A more viscous agarose solution is obtained with either a higher agarose concentration solutions or a lower stabilized temperature of the agarose solution. It is also possible to change the viscosity of agarose solution with the ionic strength of the

solvent since the viscosity is a function of the polymeric agarose chains interaction. A more viscous solution usually requires higher stirring speeds to strip off excess of coating agarose solution. Excessive stirring speed, on the other, hand pulls and deforms the agarose layer still attached to the latex which in extreme conditions is finally lost and plain naked latex is recovered, Figure 4.7. In fact, an extremely thin skin of agarose is more likely to be the outcome.

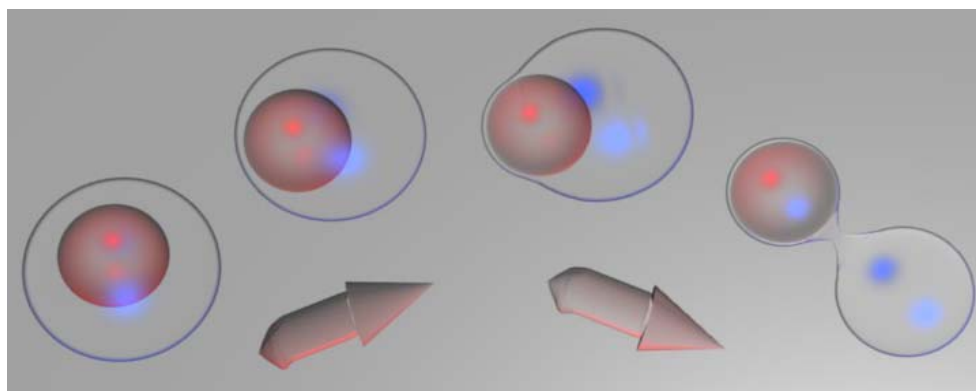


Figure 4.7. Extreme stirring speed during the coating of microspheres. Agarose solution is shown to be stripped away from the latex bead before gelation occurs. Any intermediate stage on excessive stirring speed leads to non-centered cores in the final composite bead.

In situations where the latex is not centered and a thick coating is wanted, it is necessary to allow repositioning of the latex within the surrounding agarose solution. To allow proper localization of the core, time must be given with mixture temperature above the gelling point while adjusting stirring speed to avoid the deformation. If the stirring speed on the other hand is too low at the beginning, broken suspended particles are big even in excess of surfactant and the inclusion of more than one bead in random position held together by agarose is found in the final product.

4.3.3 Glass in Agarose Core-Shell Beads

Glass beads sold commercially are used for many applications including catalysis and chromatography, and are found with a wide range of diameters. Glass beads composed of borosilicate can be rendered porous if heated at elevated temperatures followed by dissolution in acid. The hydrophilic surface characteristic is imparted by hydroxyl groups available for chemical activation akin to agarose gels. In this section, we explore the use of glass beads as an element to multicompartment system that serve as reactive particles for sensing applications.

Glass beads are intended here to perform as a supporting material for agarose. The inactive solid non-porous core participates as dead volume and the agarose coating may be glyoxal activated. For rapid reactions the volume that is actually used corresponds to the shell in this case composed of reactive agarose. Glass lacking of auto-fluorescence and being transparent to light does not interfere with the signal generated on agarose in an assay.

Glass beads are more dense and heavy than agarose, latexes and common suspending solutions. Solvents such as tetrabromoethane or perfluoromethyldecalin are highly dense with tetrabromoethane being relatively toxic. The vapor pressure for both solutions is comparable to tetrachloroethane and heated to temperatures between 50 and 60°C rapidly depletes the suspending solution from solvent. With solvents such as n-heptane the density is too low to maintain the glass beds suspended and they accumulate in the bottom of the reactor. Faster stirring can lift them off the bottom of the reaction vessel, but the shearing stress strips off the agarose coating. Every once in a while a really thin film of agarose is found on the

surface, but slight touch with tweezers was enough to damage the thin skin. Solvents such as glycerin were briefly tried with similar adverse results although is more promising than regular liquid hydrocarbons. Perfluoromethyldecalin assisted with better suspending conditions and centered coated glass beads were obtained. The addition of agarose and the consequent stirred mixture fragmentation in the fluorinated oil demonstrated to be an endothermic process. The temperature dropped from 50°C to 27°C in less than 1 min forcing a fast transition of agarose into the gel. Glass microspheres are more difficult to center in the final beaded product and many fluorinated oil droplets are more likely to form part of the agarose coating, Figure 4.8. Extraction of the oil droplets is complicated because of its high surface tension and poor miscibility with non fluorinated liquids. The agarose layer of the core shell beads in Figure 4.8 felt relatively frail when manipulated with tweezers probably due to the large content of oil droplets as well as the fast gelation process.

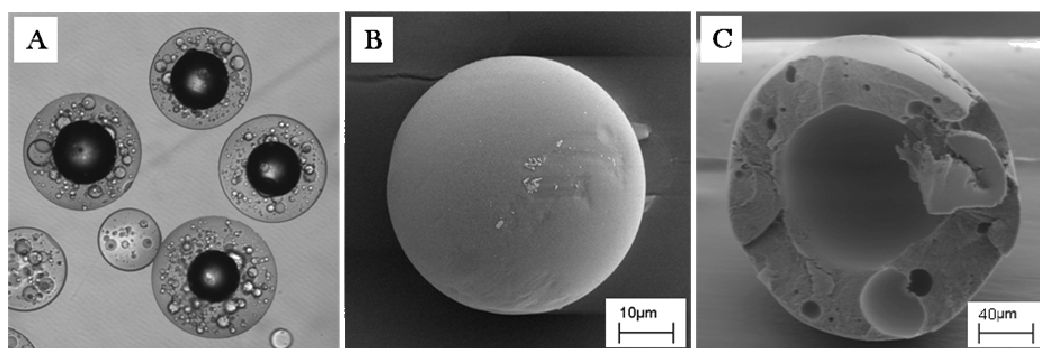


Figure 4.8. (A) Brightfield image of glass bead coated with agarose. Perfluorinated liquid embedded in agarose as small droplets. Glass bead is not necessarily centered. (B) SEM image of external surface of the glass coated bead. (C) An agarose bead was fragmented before CPD. The glass bead is lost during drying and empty big cavity is left. The small cavities were occupied by the fluorinated oil most likely lost on CPD.

Embedding of smaller glass beads is easier, but a concentric layer is not obtained when the thickness of the layer is much larger than the glass microsphere diameter. Instead, more than one small glass bead is frequently found fixed in the beaded gel.

4.3.4 Raspberry Coating Like

Instead of core-shell composite beads to generate concentric zones of polymer, beads of smaller dimension in size may be used to form a ‘raspberry-like’ structure. In theory, more the one layer of small coating beads may be built on top of the already deposited, Figure 4.9. In practice, however, it is necessary to provide strong bonding between the small beads to hold together as a single construct

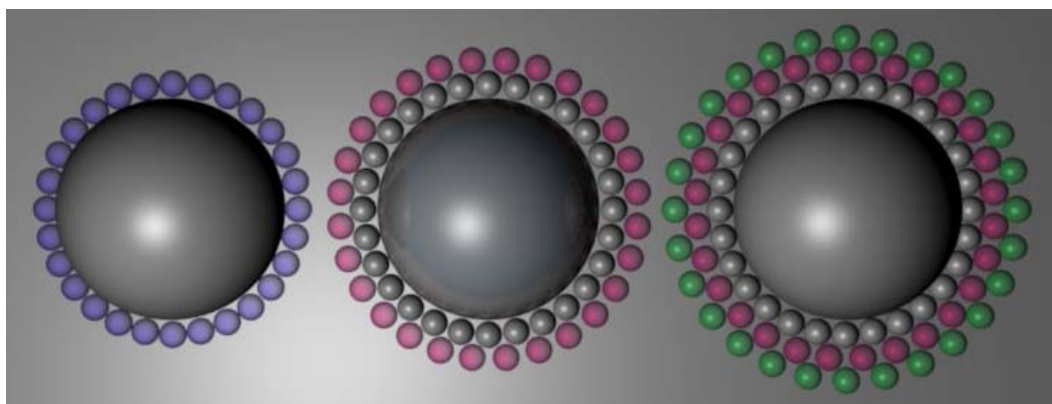


Figure 4.9. Concept coating of core bead with smaller microspheres to form a raspberry-like composite bead. The successive addition of layer should theoretically provide a highly porous shell.

The progressive building of small beads on top of the other should in principle provide a ‘superporous’ ensemble surrounding a homogeneous core. The small beads may be the same or varied in size enabling control of cavity dimensions in the superporous shell.

The attachment of 6 μm carboxyl-polystyrene beads to the surface of glass beads resulted in a better surface coverage when compared to coating of polystyrene-polyethyleneglycol copolymer beads (Tentagel), Figure 4.10. Empty patches are seen on the cores where small beads are missing. The 6 μm carboxyl-polystyrene coating beads had a narrower size distribution of particles than the 10 μm coating particles. The coverage of Tentagel resins with 6 or 10 μm beads did not show significant difference.

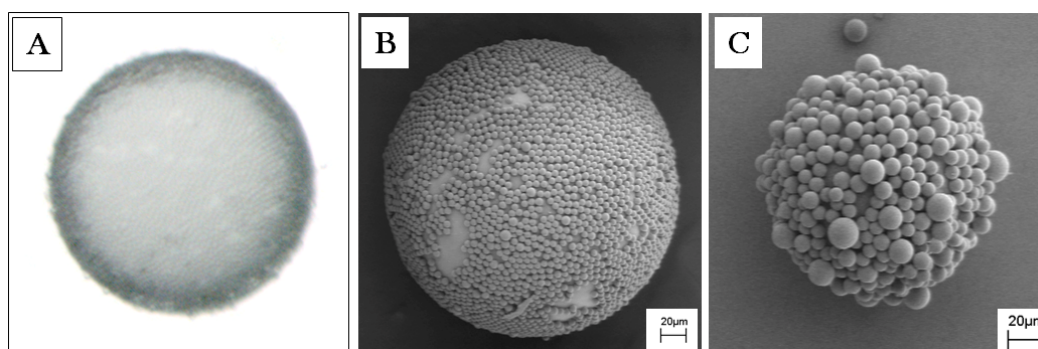


Figure 4.10. (A) Brightfield image of a 210-250 μm glass bead coated with small 6 μm carboxylated polystyrene beads. Some empty areas on the core surface can be seen. The coated ps/peg cores look similar except that the empty areas are larger. (B) SEM micrograph of the coated glass bead. There is no reduction of the core size due to CPD. The SEM picture shows pretty much the degree of coverage accomplished with the small beads. (C) SEM image of Tentagel resin core coated with 10 μm carboxyl-ps beads. The latex ps/peg cores shrink to about one third of its original sizes leading to an apparently high density of small beads per area unit.

The drying of glass beads does not affect its size unlike the Tentagel resin cores. The small coating beads are held tight enough to survive CPD in both glass and resin cores although the shrinkage of Tentagel resin puts coating beads too close to each other that some are lost during the drying, thus, they appear to have a better and denser coverage of the surface, Figure 4.10-C.

The attempt to add a second layer promotes the loss of beads from the glass surfaces. On the other hand, on Tentagel resin cores the empty areas found on the first layer are usually filled up, and localized small regions do show a second layer.

The building of the layers was not revisited due to the easy loss of coating beads when manipulated with mechanical devices. The assemblies shown in the illustration may be protected from mechanical damage by adding a thin layer of agarose gel similar to the core-shell composite beads. These high surface beads are expected to show rapid response times and high responses when applied to sensing applications.

4.3.5 Macroporous Polystyrene Beads

Other polymers are also found to be prepared with large pores or cavities in the matrix to provide high internal accessible reactive surface area. The resulting macroporous particles may possess either hydrophilic or hydrophobic surfaces and they proceed frequently by suspending a HIPE. Hydrophilic and hydrophobic monomers such as vinylacrylamides, vinylpyrrolidones, acrylates and styrene are found to return porous material with cavities as large as 50 μm , particle diameter up to 3000 μm and void volume as high as 90%.^{109, 110}

Polystyrene and other latexes composition are materials extensively used in bead based immunoassays including those run in MAD systems. The material is described as versatile because of the somewhat mature manufacture and post-manufacture existent development in the area. On the beaded constitution, though, latexes are found to be prepared as a homogeneous dense material resulting in slow mobile mass transport into the polymeric matrix. Despite the restrained mobility,

many immunoassays are devoted to the exploit the surface of smaller particles (usually not larger than 8 μm) which actually fits quite well their analytical instruments as described in Chapter 1. Because of the small diffusion path length linked to the small dimensions to be traversed by any analyte part of the internal volume is also involved on the affinity separation processes. The chip-based MAD system is also open to the use of polystyrene beads and several attempts were made here to prepare macroporous polystyrene beads similar to superporous agarose beads.

The particles obtained under the conditions described above engender crosslinked microspheres with a macroporous internal structure as suggested by SEM micrographs, Figure 4.11. Most of the particles are coated with a layer of the latex in the exterior, most likely due to monomer diffusion from neighboring small stabilized unreacted monomer droplets. The formation of the sphere external dense skin isolates the internal pores making them practically unusable for fast fluid flow through. Here macroporous polystyrene beads of 75 μm diameter size were exposed to a solution of Alexa Fluor 488 labeled anti-CRP antibody. The confocal images in Figure 4.11-E and 4.11-F illustrate non-consistent adsorption of the labeled protein from bead to bead. The brightest beads apparently allowed easy penetration of the protein to be immobilized on the internal network since a few beads show an intense fluorescence signal inside delineating a macroporous structure. The coating inside is but, not enough to coat the whole bead. Figures 4.11-A and 4.11-B show beads with an open structure which does not occur as frequent as the beads with a skin in the final product represented by Figures 4.11-C

and 4.11-D. It appears the skin is formed only on the surface leaving a highly porous interior untouched.

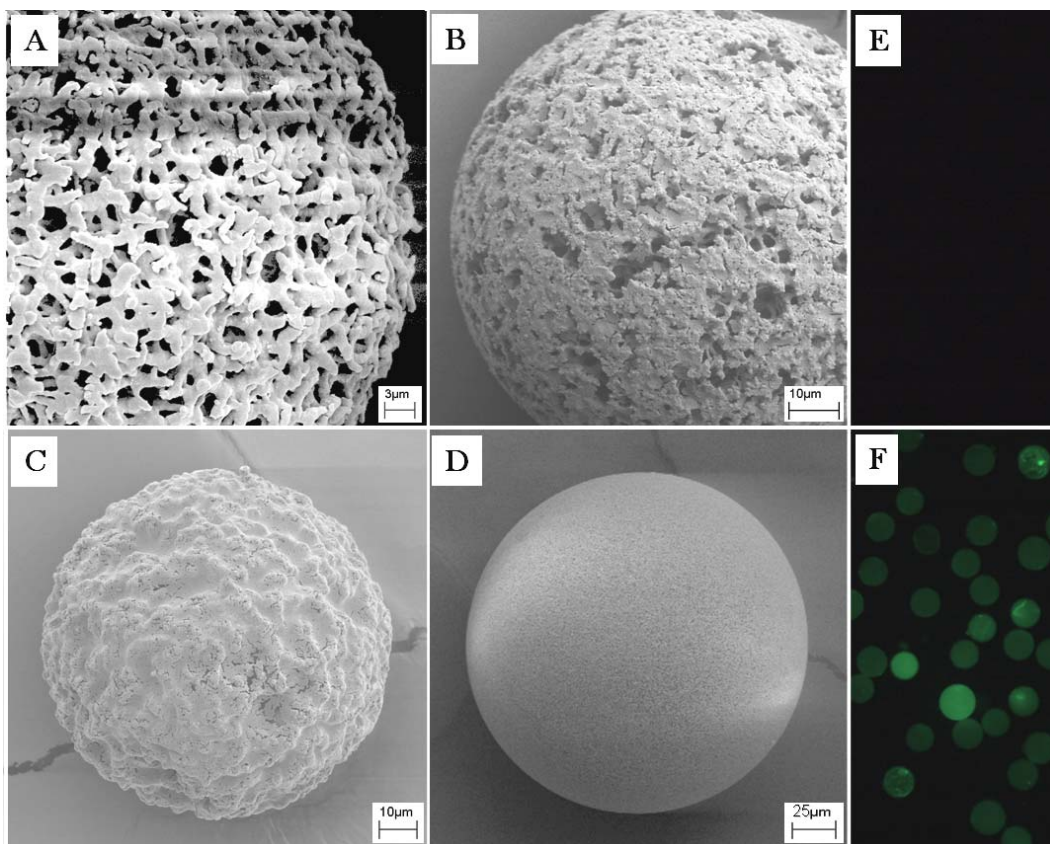


Figure 4.11. (A to D) SEM images illustrating the development of a skin on top of macroporous polystyrene beads to render finally a relatively smooth surface. (E) Green fluorescence of macroporous polystyrene beads at 2 ms exposure. (F) Green fluorescence of sheep anti-CRP protein labeled with Alexa Fluor 488 adsorbed on the surface of the macroporous polystyrene beads at 2 ms exposure. Note the irregular reactivity from bead to bead. The brightest beads are linked to open structure shown in image (A).

The formation of 3-dimensional dendritic-like networks, some with a fully developed skin, evidence local variations on polymerization speed in the suspending solution. The above polystyrene particle images correspond to 63-75 μm diameter size fraction after 6 h of polymerization. Larger beads were mostly

amorphous particles or aggregates. Longer reaction time periods did not contribute to the increase in size with an open structure. Instead the growth involves thickening of the skin. Below 6 h particles were too small to be of practical use. The building of the skin also appears in the preparation of superporous agarose beads and more studies are needed to find the experimental conditions to reduce its formation and to obtain larger particles. Specific ended chemical terminations may be added to the macroporous beads by adding substituted monomer to plain styrene.

4.3.6 Beads in Concentric Layers

The compartmentalization of preactivated agarose gel within a bead is not limited to core-shell or raspberry-like composite beads. A combination of different bead sizes within agarose gel is possible and easily performed by following the same procedure described before for core-shell beads. A relatively larger agarose sphere may be included as a central core and smaller microspheres may surround the core resembling small satellites. Also, a centered composite core with small beads inside and surrounding satellites is obtained by successive emulsification of agarose solutions containing the composite core and the satellites to be coated, Figure 4.12. The illustrations above only show one layer built around the core. The addition of layers may include one or more sets of particles per layer which can be added progressively. The incorporation of another layer may include small beads with compartmentalized agarose regions in different levels may help on the identification of a set of small beads by its position relative to the center of the composite microsphere. These beads are expected to find utility in a variety of

sensing applications in areas such as genetic testing, analysis of simple and complex sugars as well as for cholesterol testing.

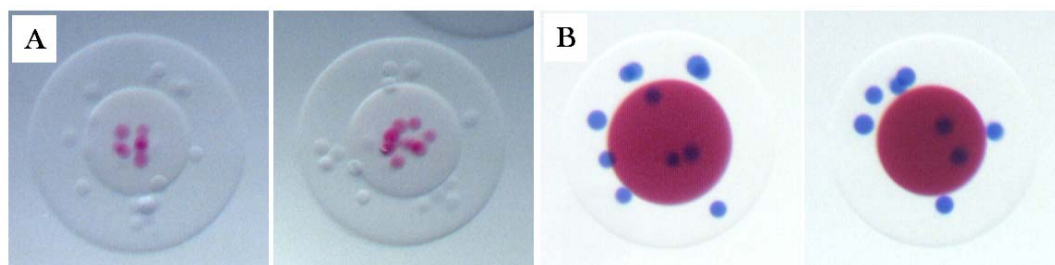


Figure 4.12. Blending of agarose moieties into composite beads with: (A) a composite core surrounded by small beaded satellites, (B) a simple homogeneous core with satellites. The red portions are glyoxal beads stained with Schiff's reagent. The blue satellites in (B) are avidin coated beads stained with Coomassie Blue. The satellites in (A) are not stained.

4.3.7 Agarose Beads with 20-32 μm Randomly Dispersed Functionalized Agarose Inclusions

A series of small spherical agarose particles added to an agarose solution followed by emulsification of the mixture provide small beads dispersed inside a larger microsphere. A characteristic feature to small bead sizes 20-32 μm when compared to 250-280 μm during the capture of analytes is the localization of the available target analyte in the sample test into a small volume. The localization of affinity ligands into a small region centers target capture to specific isolated reactive islands intensifying fluorescence signal as opposed to diluting the fluorescence response in a large matrix. Unlike small color encoded beads used in other platforms where the reactive volume immediately available correspond to the surface, the agarose beads uses all of its 3-dimensional volume with faster diffusion events.

The wells in the bead-based array sensor analysis chamber are currently not designed to accommodate 20-32 μm microspheres. Therefore, suspending the small microspheres in beaded gel of the same nature brings in a composite bead that is in harmony with the chip dimensions requirements. The small agarose inclusions are also content in the familiar neighborhood made also of 'agarose'.

A remarkable attribute of the multiple analyte system, in continuous evolution at the McDevitt laboratory, is the flexibility in the design as it is described in Chapter 1. The analytical platform is able to accommodate membrane filters with a few modifications in the geometry of the analysis chamber to fit properly a membrane instead of a silicon chip. The polymeric membranes, such as nitrocellulose, are highly porous and typical pore diameter sizes used are smaller than 5 μm . The membrane-based variation of the MAD system has been used as a 'cell processing unit', where efficient separation and count of T lymphocytes from serum samples to evaluate HIV infected individuals.⁹ Within this membrane format, it is possible to envision small sized agarose beads as compartmentalized sensing elements where, they are either supported solely by the membrane or immobilized on a thin layer of agarose to form an "agarose pad" ensemble.

Utilizing a concentrated suspension of 20-32 μm diameter agarose beads may be coated with a relatively small volume of agarose solution to prepare composite beads with a large amount of small agarose spherical compartments 'closely packed', Figure 4.13. Sets of 20-32 μm beads may be chemically derivatized separately to produce different population of beads. In theory, a larger mixture of different populations of small beads should lead to a higher probability

of finding small beads from each set inside a composite ensemble. In practice, it is true if the degree of aggregation of small particles belonging to the same set of beads is flimsy or completely avoided. The aggregation of small beads of the same population may grow enough to displace beads from other sets. As a result during fluorescence sensor applications the random pick-and-load of composite beads in the chip may lead to wrong result assessment (false negatives) if small microspheres from a specific population were excluded during the coating with agarose.

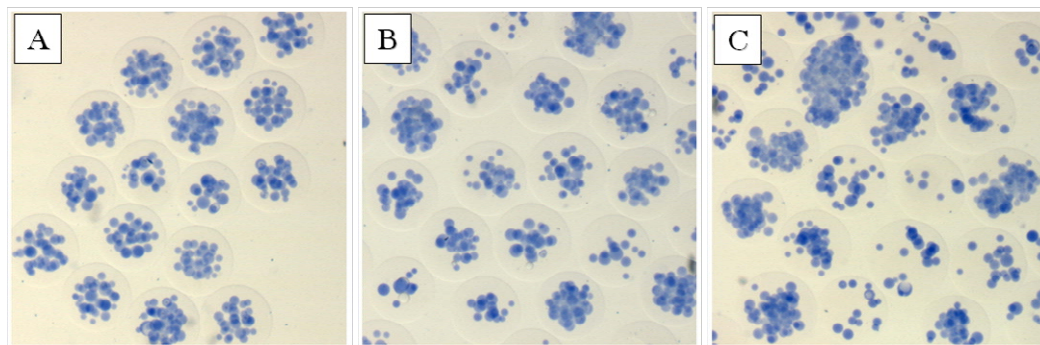


Figure 4.13. Dispersion of small avidin beads previous to coating with agarose. The protein avidin immobilized on the beads was stained with Coomassie Blue. (A) 2 min sonication of avidin suspended beads, (B) 2 min sonication of avidin coated beads suspension in 1% Triton X-100, (C) suspended beads in 1% Triton X-100.

The aggregation of small microspheres may appear after the immobilization of a protein such as avidin. The relatively small size of the beads, 20-32 μm compared to 250-280 μm , favors the agglutination of small particles especially when the beads are not suspended properly in the avidin containing solution. Avidin can perform the function of a crosslinking agent between small beads and, in circumstances where aggregation is excessive, the agglutinates must be removed

or re-dispersed. Removal of aggregates is straightforward since they are relatively heavier and precipitate faster than singled particles, but removal or aggregates can reduce drastically the amount of usable protein-coated minibeads. When instead re-dispersion is attempted with sonication, the disintegration of the aggregates may not be thorough. Figure 4.13 depicts the effect of small microsphere aggregation on the resulting composite beads. With aggregates growing in size the population of beads obtained is highly irregular with respect to inclusion contents. A small volume ratio of beads-to-be-coated to coating-agarose-solution provides better results in both aspects: the separation of small particles inside the gel and the inclusion of particles from the many bead populations to be added.

4.3.8 Protein Viability Test after Agarose Coating

Up to this juncture, much of the discussion has been directed to the development of new multi-component polymer and polymer-glass composite assemblies. Next, the suitability of selected systems to service sensor applications on the analysis of oligonucleotide systems is described.

Previous to the immobilization of any oligonucleotide on small beads to be coated, the viability of protein avidin was tested in a chip-based assay on the capture of a fluorophore labeled biotinilated target. Previously in Section 4.3.1, glyoxal activated core was coated with agarose followed by covalent coupling of avidin to the core and immobilization of a biotinilated DNA probe. Here the protein is immobilized on 20-32 μm beads followed by coating with agarose gel to produce the microspherical ensemble. The detection process of the nucleotide is represented schematically in Figure 4.14.

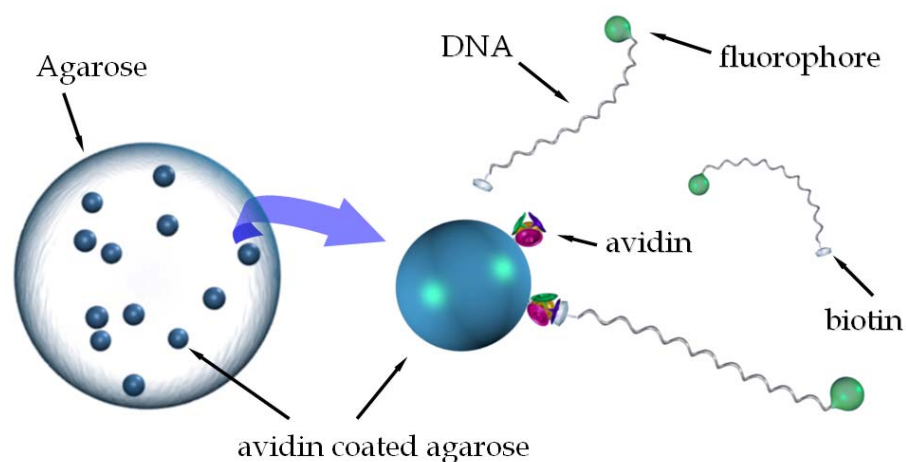


Figure 4.14. Agarose in agarose bead showing spherical agarose compartments embedded in agarose. The compartments are coated with avidin capturing ligand. One of the compartments is magnified showing the capture of biotinylated fluorophore labeled oligonucleotide. Free avidin ligand contains four biotin binding sites. Not all of the binding sites in avidin are available after it is immobilized on the agarose matrix.

The agarose solution used was stabilized at a low temperature, 40 °C, to accommodate for biomolecules that are more susceptible to damage at higher temperatures. The temperature may be reduced even more if low melting temperature agarose with gelling temperature between 24 and 28 °C is used.

After the emulsion procedure the beads were washed and wet sieved with distilled water followed by exchange of the solvent with nanopure water or an appropriate buffer free of undesired impurities. The conditions here used for the cleaning of the composite beads are not optimal and the immobilized biomolecules may be subjected to reduced reactivity or contamination. Nevertheless, the resulting product obtained has proven to perform satisfactorily for the assays to be described.

Composite beads with avidin-microspheres were loaded in a 3 x 4 chip and placed in the chip-based MAD analysis system. A solution containing a biotinylated

oligonucleotide labeled with Texas Red was delivered and immobilized by avidin on the small beads. Confocal micrographs on the embedded small beads show the full penetration of the oligonucleotide inside the small beads which is achieved under 10 min exposure to the target, Figure 4.15.

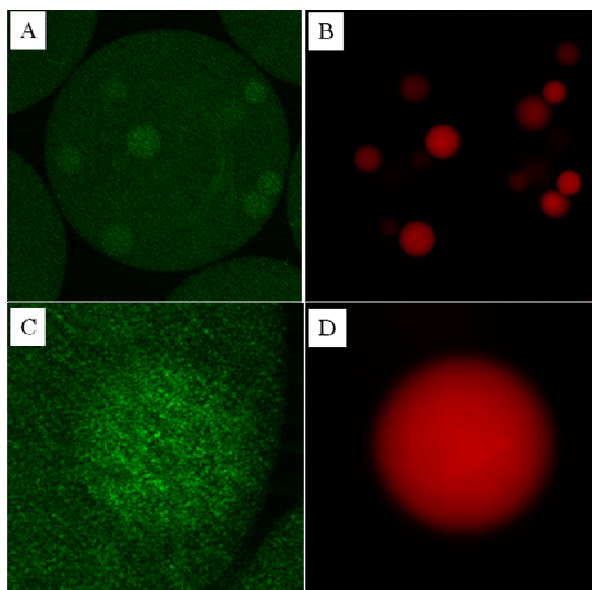


Figure 4.15. Confocal micrographs showing small beads inclusions in beaded agarose gel. (A) and (C) autofluorescence of agarose, (B) fluorescence of immobilized Texas Red labeled oligonucleotide, (D) complete penetration of oligonucleotide on small bead.

4.3.9 Multiple Analyte Detection Assay on Multifunctional and Multicompartment Agarose Beads

In this section, the suitability of the agarose in agarose composite systems for DNA detection is explored. The beaded ensembles used in this section consist on reactive 20-32 μm diameter spherical agarose compartments embedded in non-reactive agarose. The agarose minibeads embedded within agarose were chosen for sensor applications as they had the following characteristics: (i) good mechanical

properties, (ii) high surface area, (iii) reduced sample and reagent consumption, (iv) they exhibited low background levels, i.e. minimized problems with non-specific binding, (v) and provided some unique features for multiplex analyte detection not previously afforded with prior generations of sensing spheres used in the McDevitt laboratory.

Here, three different closely related oligonucleotide sequences, Table 4.2, are utilized as capturing ligands targeting their own complementary DNA sequences. The different biotinylated-DNA sequences were immobilized on 20-32 μm diameter avidin-coated agarose to produce three different populations of beads prior to the preparation of the agarose in agarose composite beads. For DNA sensing to be competitive, it is necessary that the system allow for selective sensing of single nucleotide polymorphism with probe length on the order of 18 to 25 base pairs. To demonstrate the oligonucleotide discrimination capability of the composite systems, five groups of composite beads were prepared. Three of these groups contained only one type of capturing ligand immobilized on the reactive compartments. One group of composite beads, without DNA, served as control beads. The last group contained all three compartment types of capturing ligand in a single composite bead unit. The DNA target strands conjugated to Texas Red, Oregon Green 488x and Pacific Blue and their respective complements DNA-capturing ligands (DNAcap) immobilized on the compartments is summarized on Table 4.2. The capture of the DNA targets is illustrated in Figure 4.16.

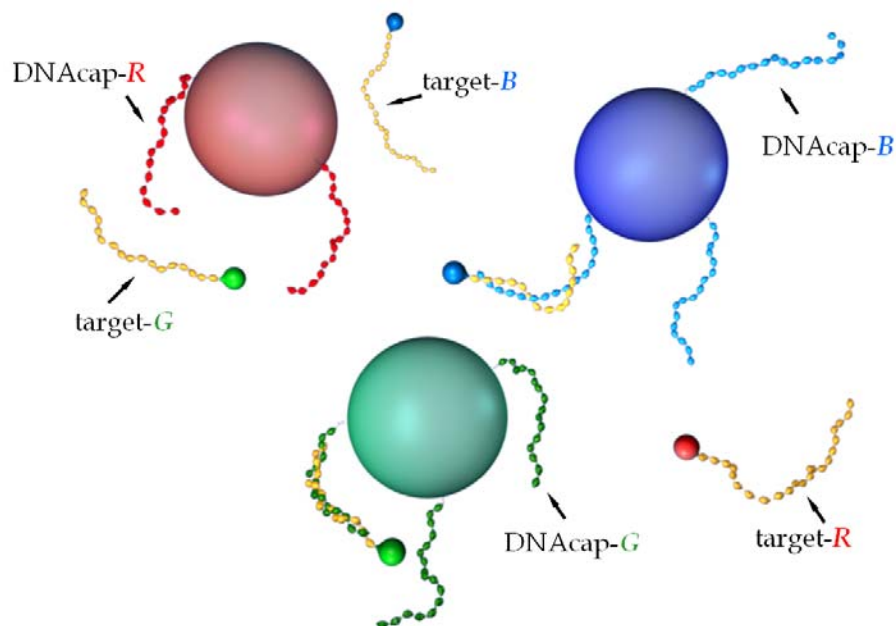


Figure 4.16. Hybridization of DNA target by complementary oligonucleotide sequence immobilized on agarose beads. The schematic shows three sets of 20-32 μm agarose beads coated with DNA capturing ligand DNAcap-R, DNAcap-G and DNAcap-B. The complementary sequence targets are labeled with fluorophores Texas Red, Oregon Green and Pacific Blue, target-R, target-G and target-B respectively.

DNA-capturing ligand	DNAcap
biotin~ATA CCA <u>CCT</u> TAT T <u>G</u> A ATT	DNAcap- <i>R</i>
biotin~ATA CCA <u>G</u> CT TAT T <u>C</u> A ATT	DNAcap- <i>G</i>
biotin~ATA CCA <u>CCT</u> TAT T <u>C</u> A ATT	DNAcap- <i>B</i>
DNA-target	Target
<i>TxR</i> ~AAT T <u>C</u> A ATA AG <u>G</u> TGG TAT	Target- <i>R</i>
<i>OrG</i> ~AAT T <u>G</u> A ATA AG <u>C</u> TGG TAT	Target- <i>G</i>
<i>PcB</i> ~AAT T <u>G</u> A ATA AG <u>G</u> TGG TAT	Target- <i>B</i>

Table 4.2. Sequences used in the array. The biotinylated strands were conjugated to avidin coated 20-32 μm diameter agarose beads prior to the preparation of composite agarose in agarose beads. The 5' ends of the strands are modified with biotin and fluorophores Texas Red (*TxR*), Oregon Green (*OrG*) and Pacific Blue (*PcB*).

In Table 4.2, it is possible to identify two base-pair and one base-pair mismatch of DNACap-R relative to target-G and target-B respectively. Also, there is a single base-pair mismatch between DNACap-G and target-B. Likewise, DNACap-B shows one base-pair mismatch relative to target-G and target-R.

Oligonucleotide discrimination capabilities on 250-280 μm homogeneous agarose beads was previously demonstrated in the bead chip-based MAD system.⁵ A similar study performed in the chip-based system utilizing the five groups of composite beads described above. A 500 μL 0.3 μM sample volume of each DNA target was delivered sequentially. Each target sample was recirculated for 10 min at 1.6 mL/min flow rate at room temperature with a short rinse with high stringency buffer between target samples to eliminate previous unbound target and non-complementary oligonucleotide interactions. The developed fluorescence signal, after the end or the rinse sequences, is illustrated in Figure 4.17 for hybrid beads on the individual capture of target-G, followed by target-R and lastly by target-B. In addition, the composite beads with all three sets of DNACap beads can be observed with a long band-pass filter after the 3 targets were delivered. It is clearly appreciated the compartmentalized capture and differentiation of the closely related DNA strands on a single composite unit sensing element. The development of fluorescent signal was indeed fast and clearly appreciated within 3 min at 1 s exposure. The accumulation of target in a small element volume produces localized intense fluorescent signal on the hybrid beads as opposed to being distributed on a large surface area of a plain conventional homogenous agarose bead described in Chapter 2.

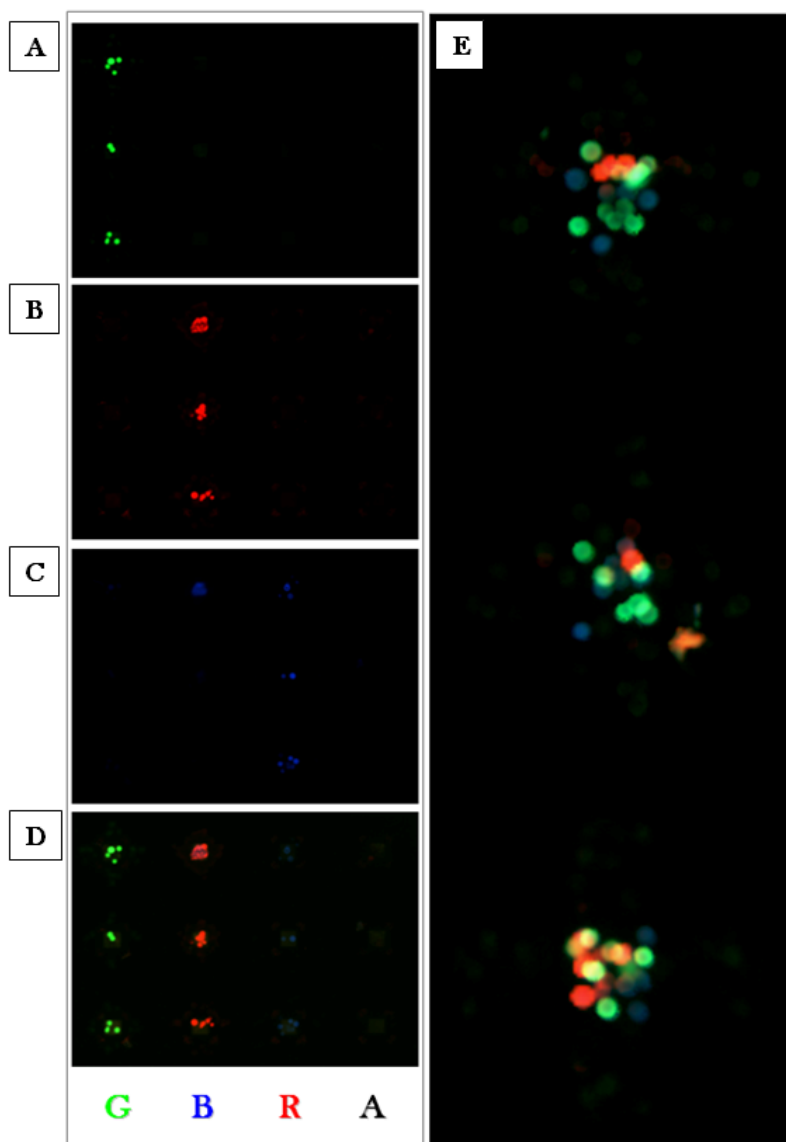


Figure 4.17. Representative illustration of multiple analyte capture and detection on multicompartiment beads. Capture and detection of targets follow the sequence (A) target-**G**, (B) target-**R** and (C) target-**B**. Composite avidin-coated beads were included as a control in the microchip. (D) Following the targets a short rinse with high stringency washing buffer was performed and a triple band excitation filter cube set is used to capture the images. (E) Fluorescence response of composite beads containing all three sets of DNACap after delivery of targets followed by rinse with high stringency buffer. Exposure times set to 1 s from (A) to (D), and 5 s for (E).

The selectivity capabilities of the multicompartment sensing elements is explored following the progressive rinsing after each target using high stringency buffer. The relative fluorescence intensity versus time of the compartmentalized capture sequences exposed to the targets is depicted in Figure 4.18. The following analysis was on three random beads each containing one of the three capture oligonucleotides from Table 4.2. Upon introduction of the target-R, signal of ~300 counts is obtained at the complementary capture DNACap-R beads after 5 min of assay. The signal grows to ~1000 counts after 10 min of assay. During this time period, signal at the other two other capture beads, DNACap-G and DNACap-B, is noted a 13% level relative to the perfect match in the complementary beads. Following a rinse for 1 min at 1.5 mL/min flow rate, the signal reduces to ~2% of the complementary beads. The signal ratio of the complement hybridization to the non-specific mismatch binding shows a selectivity factor of ~60 for the perfect complement relative to the single base pair mismatch (DNACap-B) and a ~40 ratio for the dual base pair mismatch (DNACap-G). Following the delivery of target-G, the signal count for the perfect match DNACap-G is ~95 and ~270 after 5 and 10 min assay respectively. A 19% intensity level relative to the perfect match is noted for the two other capture beads DNACap-R and DNACap-B during this time period. The rinse brings down the mismatch signals to ~1% of the complementary beads. Here, a discrimination ratio for the perfect complement is ~190 for a single mismatch (DNACap-B) and ~90 for the two base pair mismatch (DNACap-R).

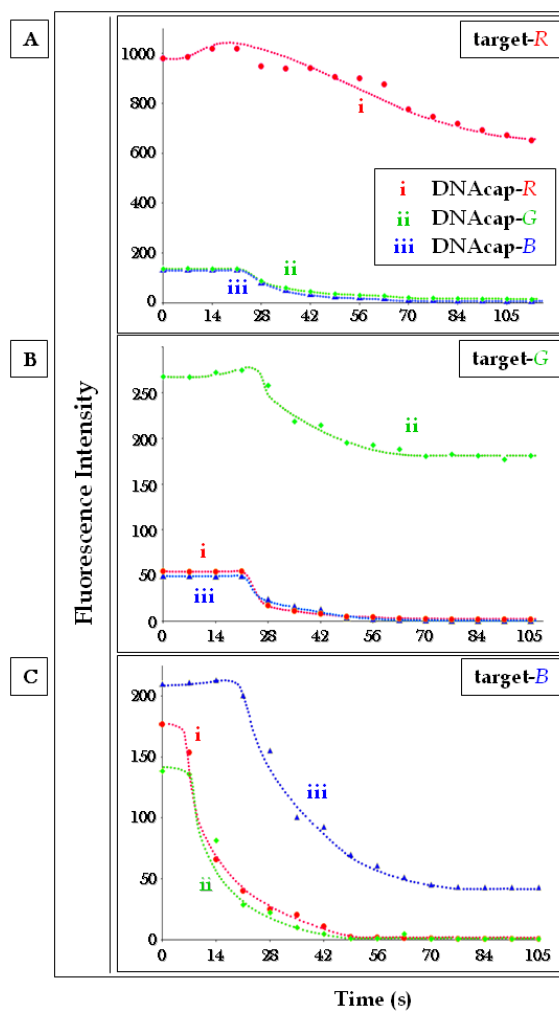


Figure 4.18. (A) Fluorescence signal intensity curves recorded as a function of time during buffer rinse of target-R with all three DNA-capture sequences: (i) hybridization to the complement DNAcap-R, (ii) discrimination from the G:G and C:C two base pair mismatch sequence DNAcap-G, and (iii) discrimination from the G:G one base pair mismatch sequence DNAcap-B. (B) Fluorescence intensity curves recorded as a function of time during buffer rinse following the reaction of target-G with all three DNA-capture sequences: (i) discrimination from the G:G and C:C two base pair mismatch sequence DNAcap-R, (ii) hybridization to the complement DNAcap-G, and (iii) discrimination from the G:G one base pair mismatch sequence DNAcap-B. (C) Signal intensity curves as a function of time during buffer rinse following the reaction of target-B with all three DNA-capture sequences: (i) discrimination from the less stable G:G one base pair mismatch sequence DNAcap-R, (ii) discrimination from the highly stable G:G one base pair mismatch sequence DNAcap-G, and (iii) hybridization to the complement DNAcap-B. High stringency buffer rinses carried out at a flow rate of 1.5 mL/min.

In a similar fashion, following the delivery of target-B complementary to DNACap-B after 10 min assay the count for the perfect complement is ~230. The DNACap-R and DNACap-G mismatches are at 70% and 60% level respectively from the perfect capturing match. After the rinse the count levels of the mismatches drop to ~1% of the signal in the complementary bead. The measured discrimination ratio for the perfect complement relative to a single base pair mismatch is ~65 for both DNACap-G and DNACap-R.

The analysis of this data shows a rapid and effective elimination of non-complementary interactions within the microreactors. The rinse process, ~1 min at 1.5 mL/min, brings non-specific fluorescence signal down to a level where positive identification of the target analyte is unmistakable. Hybridization time length for each nucleotide were explored in a range between 10 and 20 min, although above 10 min the intensity signal did not improve significantly under the experimental conditions used here. The discrimination of DNA by the three target capture beads follow the stability of the DNA duplex formed, which in turn can be associated to a melting temperature (T_m). For instance, during the detection of target-G, the hybridization to its complement DNACap-G is more stable than the complex formed with the mismatched sequence capture beads. In this particular case the calculated T_m for the perfect match target-G/DNACap-G is 69.5 °C, for one base pair mismatch sequence DNACap-B is 57.3 °C, and two base pair mismatch sequence DNACap-R is 48.1 °C.

The results obtained here are consistent with prior DNA discrimination studies performed at the McDevitt laboratory. In those studies, conventional homogeneous agarose beads were used.⁵ Thus, the larger 250-280 μm diameter size of conventional beads provides a larger target immobilization capacity as opposed to a few compartmentalized 20-32 μm diameter minibeads embedded in non-reactive agarose matrix. The volume of a single 32 μm diameter bead is equivalent to $\sim 0.15\%$ of a 280 μm diameter spherical particle. Ten 20-32 μm diameter beads, is therefore, only about 1.5% of a 280 μm diameter bead. The larger volume of a 280 μm diameter bead will provide a substantially larger amount of capturing sites which under excess of target generates a far more intense fluorescence response. As a result, conventional beads in the microchip array system report single nucleotide discrimination indexes in the 10,000-50,000 range within a 3.2 min rinse cycle at 1.5 mL/min.¹³³ For the hybrid beads used in this section, in contrast, the ratio of signal between the perfect match and single base pair mismatch varied from 10 to 400 after 1.2 min rinse cycle at 1.5 mL/min. A selectivity factor ranging from 35 to 150 is though, more frequently the measured selectivity value. Although the discrimination index values are considerably smaller than conventional beads, the selectivity factor values measured utilizing the minibeads system are comparable to the reported values in the majority of prior DNA detection methodologies.¹⁴⁴⁻¹⁴⁶

Many bead-based MAD systems such as the ones described in Chapter 1 include small microspheres as sensing elements in their platforms. The sensing microspheres are typically 3-10 μm latex beads with a dense polymeric matrix not suitable for fast mobile phase mass transport. Target immobilization is basically

restricted to the external surface of the bead. Their effectiveness in sensing applications though, is the ability to localize target in a small volume element resulting in dense significant fluorescence signal relative to the background noise that facilitates its detection. Here, the same approach is used to accumulate signal in the minibeads small volume. An imminent advantage of utilizing agarose over latex as a matrix, besides a lower background signal in agarose media, is the intrinsic high porosity of the gel. Therefore, the internal volume of the spherical gel is available for target immobilization in addition to its external surface.

It was noted previously, in core-shell beaded ensembles, that a 50 base pair oligonucleotide can diffuse through $\sim 70\ \mu\text{m}$ 5% agarose gel of a non-activated bead under 3 min at $\sim 1.5\ \text{mL/min}$ flow rate. The minibeads system used in this study is coated with a lower agarose concentration, $\sim 3.5\%$. Here for the minibeads system, it is observed a delay of less than 1 min for short sequence oligonucleotides as it is observed in Figure 4.18 during the rinse sequences. Thus, the embedding media does not really represent a constraint to the target capture process.

A remarkable feature of conventional agarose beads in the microarray system, is the ability to provide a highly refined oligonucleotide discrimination capacity to link single nucleotide mismatch variations to their respective melting temperatures.⁵ As previously noted above, during the rinse session of target-B, the displacement of non-specific binding between target-B and the non-matching beads is possible due to the low stability of the formed complexes. From the two possible DNA duplexes formed with target-B, depicted in Figure 4.19, the most thermally stable single nucleotide mismatch G:G occurs with DNAcap-G with a calculated

T_m value of 69.5 °C for the hybridization. The G:G mismatch flanking base pairs are A:T and G:C. The same G:G mismatch is also present when hybridized to DNAcap-R, but the calculated T_m value of 69.2 °C is lower because of the nearest neighboring base pairs, both of them A:T associations. Because of the more stable base pair association G:T relative to A:T, the rate of dissociation of target-B from DNAcap-G should be slower than that from DNAcap-R. It is observed, though, a comparable speed of target-B dissociation from both of the mismatching capture beads during the rinse sequence.



Figure 4.19. Hybridization of capture beads with target-B. The capture beads are labeled with R, G and B and represent DNAcap-R, DNAcap-G and DNAcap-B respectively. The perfect complement is present in DNAcap-B beads, and the mismatch occurs with DNAcap-R and DNAcap-G beads. The nearest neighbor base pairs to the mismatch occurring with DNAcap-R are two A:T associations. On the other hand the flanking base pairs associated to the mismatch with DNAcap-G are A:T and G:C. The most stable neighbor base pair G:C relative to A:T assigns a higher melting temperature to the complex formed with DNAcap-G.

Further analysis was performed on the fluorescence signal count measured on single beaded ensembles corresponding to the population of beads shown in Figure 4.17-E. In this case, each single ensemble contained all three DNAcap-R, DNAcap-G and DNAcap-B capture compartments within. The ensembles were

exposed as described previously to target-R, target-G and target-B in sequence with rinses in between. The fluorescence signal was measured after each rinse using color selective filters. A coefficient of variance ranging from 20 to 25% ($n=10$) was observed for the three capture beads in their respective color channels. In addition the variation of signal in the DNA capture compartments was monitored as the rinse of target-R was performed. In Figure 4.20, fluorescence versus time is depicted for the DNACap-R and DNACap-G compartments during the rinse of target-R. Only three curves are shown on each diagram, each representing one multicompartment ensemble. The curves for the perfect hybridization show similar signal decrease profiles.

As the rinse progress, the signal counts corresponding to the discrimination from mismatch DNACap-G for the same three ensembles drop to a similar residual fluorescence level. The signal drop count in the three individual ensemble beads for the perfect hybridization follow parallel curves, even though, the initial signal count is different for each them. The direct proportionality of the signal counts observed in the DNACap-R compartments suggest the same relative proportional contents of DNA capture ligand complementary to target-R, but not necessarily the same amount of minibeads. This proportionality is consistently followed by the relative amount of non-specific signal in DNACap-G before the rinse. Therefore, by narrowing the number of compartments of one class in population of beaded ensembles it is expected to reduce the fluorescence signal count CV between ensemble units.

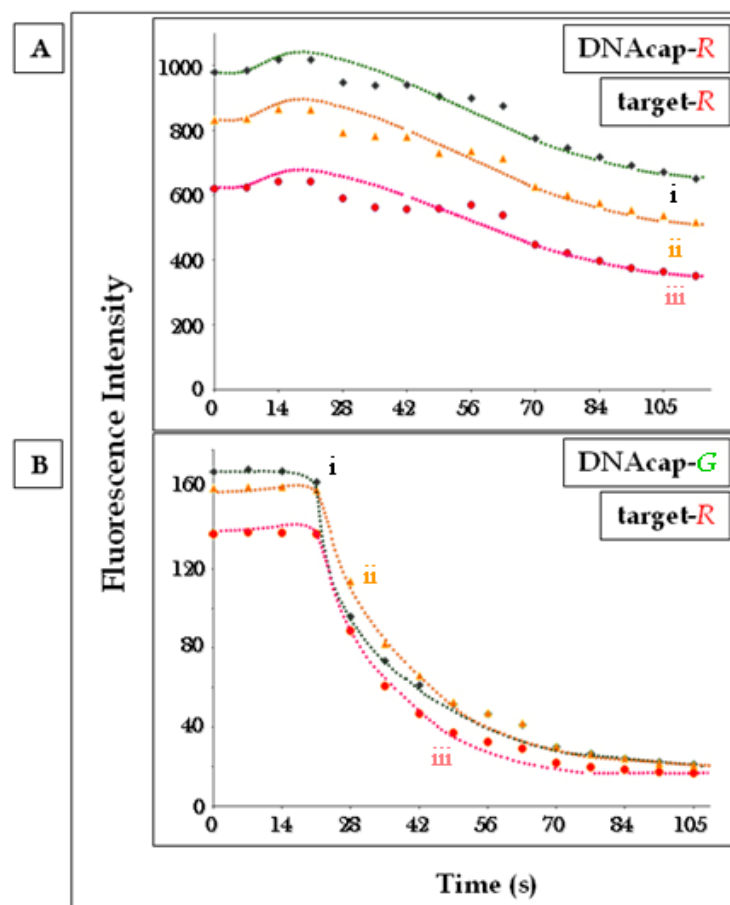


Figure 4.20. Fluorescence signal intensity curves recorded as a function of time during buffer rinse of target-R for three beaded ensemble units. Each beaded ensemble unit, represented by curves i, ii and iii contains all three capture compartments within: DNAcap-R, DNAcap-G and DNAcap-B. Only hybridization to DNAcap-R and discrimination from DNAcap-G is represented. (A) Hybridization to the complement DNAcap-R. After hybridization the signal count level is different for all three ensembles because of the different amount of compartments with DNAcap-R. Note the similar pattern of the signal count decrease in all three ensembles. (B) Discrimination from the G:G and C:C two base pair mismatch from the sequence DNAcap-G. Here again due to the different amount of DNAcap-G compartments in the three ensembles, the signal count associated to non-specific association of target-R is also different for the three ensembles. Despite the different amount of target-R/DNAcap-G complexes formed, the high stringency buffer brings all the fluorescence of non-specific association down to a similar residual level.

As a second example of the utility of these hybrid reactors for DNA detection, a multiplexing assay was also performed with biologically relevant consensus sequences relative to HIV-1, *Bacillus anthracis* and *Bacillus subtilis*. For this case, four molecular beacons (MB) were designed to contain the studied bacterium and viral strands. The MBs were immobilized directly on the small beads to serve as capturing ligands, Figure 4.21. The MBs and their complementary target sequences are summarized in Table 4.3.

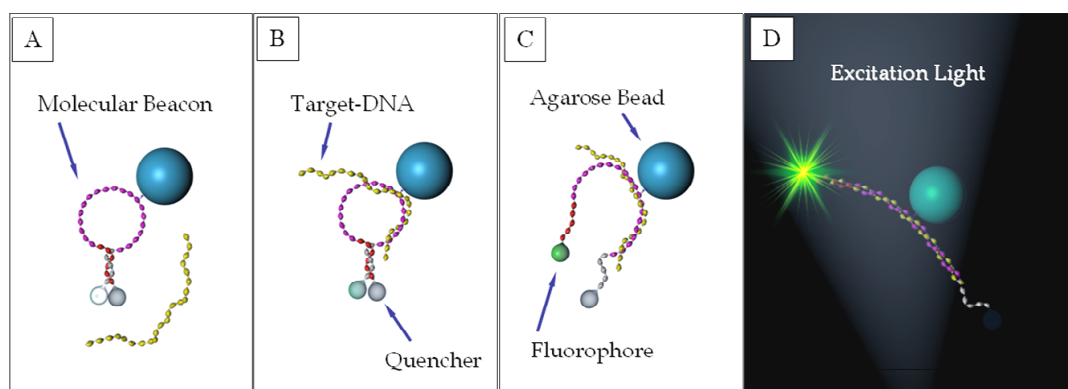


Figure 4.21. (A) A DNA molecular beacon showing the hairpin loop-stem structure. When the self-complementary stem sequence regions are associated (hybridized) the fluorophore and the quencher are in close contact. In this configuration, fluorescence is quenched when the molecular beacon is excited with appropriate light wavelength. From (B) to (D), following the delivery of complementary DNA target, hybridization occurs and gradually the hairpin is opened drawing apart the fluorophore and quencher. (D) Strong fluorescence is obtained after the fluorophore and quencher are drawn apart.

Utilizing 20-32 μm diameter agarose beads previously coated with avidin, four sets of MB immobilized were prepared using MB1, MB2, MB3 and MB4 in Table 4.3. Plain avidin-coated agarose minibeads were used in combination with the four MB-bead sets to prepare two populations of MB-composite beads: virus MB1/MB2 and bacteria MB3/MB4 beads (avidin/MB1/MB2 and avidin/MB3/MB4 respectively). Here MB1 and MB4 contain a green channel fluorophore while MB2

and MB3 are linked to red emission fluorophore. Composite agarose-in-agarose 250-280 μm diameter microspheres were collected for microchip sensing assays.

Molecular Beacon (MB) and Complement Target (T) Sequences	
HIV-1 gag gene	
MB1: 5' FAM6 / <u>CGGATGCGCTTGATG</u> /ibiodT/CCCCCACTGTGTT <u>GCATCCG</u> /BHQ 3'	
T1: 5' – AACACAGTGGGGGACATCAAGC – 3'	
MB2: 5' TxRed / <u>CGGATGCGGGTATTACT</u> /iBiodT/CTGGGCTGAAAGGCATCCG/BHQ 3'	
T2: 5' – CTTTCAGCCCAGAAGTAATACCC – 3'	
Bacillus Anthracis	
MB3: 5' TxRed / <u>CGATGCG</u> AAGATTCCCTAC/ibiodT/GCTGCCTCCCGTAC <u>CGCATCG</u> /BHQ 3'	
T3: 5' - TACGGGAGGCAGCAGTAGGGAATCTTC – 3'	
Bacillus Subtilis	
MB4: 5' FAM6 / <u>GCCTGCG</u> AAGCCACCTT/ibiodT/TATGTTTGA <u>CGCAGGC</u> /BHQ 3'	
T4: 5' – TTTTCAAACATAAAAAGGTGGCTT <u>CGCAGGC</u> – 3'	

Table 4.3. Molecular beacon stem-loop structures and target complement sequences for *Bacillus anthracis*, *Bacillus subtilis* and HIV-1 *gag* gene. The underlined and italicized characters correspond to the complementary hairpin stem regions.

In a virus detection assay the MB1/MB2 beads were loaded on a microchip followed by the sequential delivery of 500 μL 0.25 μM target solutions, T1 and T2, at 1.6 mL/min flow rate with high stringency buffer rinse after each target was recirculated for 20 min, Figure 4.21. The sensing of bacteria was similarly performed with their respective complement targets T3 and T4. The composite beads depicted in Figure 4.21 were prepared with a larger amount of beads-to-be-

coated (a factor of 3 to 4) in the same volume of coating-agarose-solution used in the hybrid microspheres shown in Figure 4.16. It is observed a relatively poor dispersion of small beads similar to Figure 4.13-B. The addition of plain avidin-beads to either MB1/MB2 or MB3/MB4 composite beads was initially intended as a diluting aid of the MB-beads mixture. Instead, the avidin-beads displaced MB-beads from being included in the composites microspheres, thus, in some hybrid beads in Figure 4.22 a low content of MB-beads is observed.

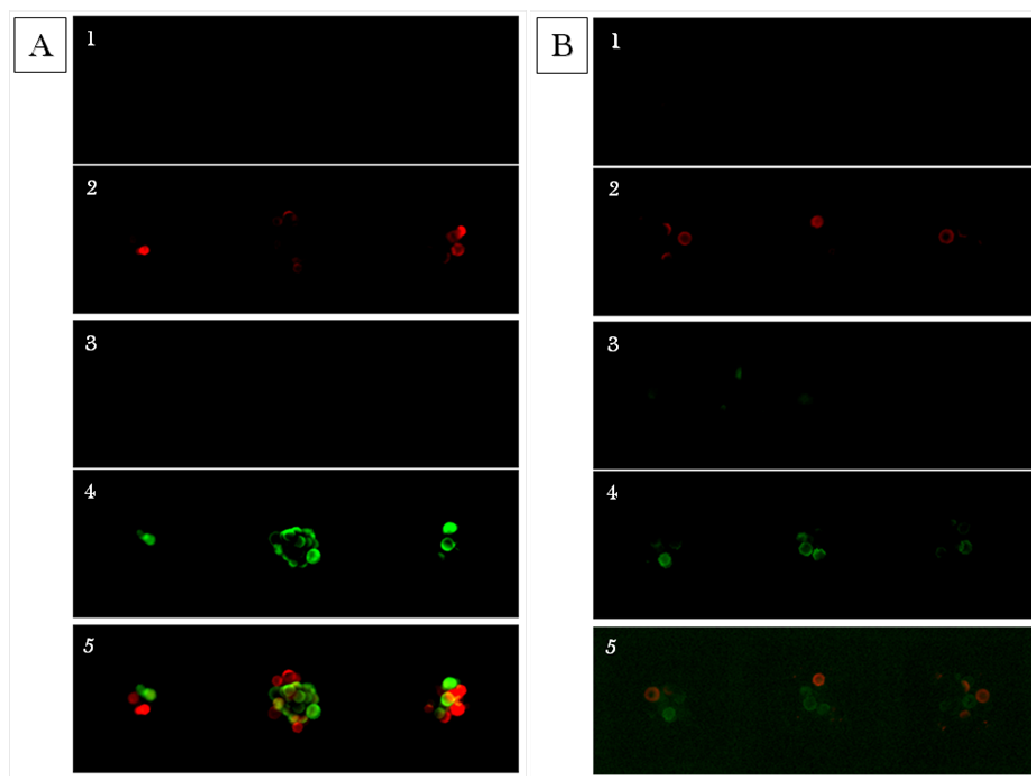


Figure 4.22. Detection of (A) *Bacillus anthracis* in red and *Bacillus subtilis* in green strands by molecular beacons with complementary sequences, (B) HIV-1 gag gene sequences. Images 1 and 3 are pictures before the target complements were delivered. Exposure (A) TxR 0.15 s, FITC 0.45 s, Dual band excitation TxR & FITC 1 s, (B) TxR 0.75 s, FITC 2 s, Dual band excitation TxR & FITC 2.5 s.

Although a relatively uniform amount of embedded beads may be obtained with a high bead-to-agarose solution volume ratio similar to Figure 4.13-A, strong fluorescent responses tend to illuminate adjacent beads. The emitted light may be strong enough to suggest non-specific association and, overlapping of colors is frequent during direct discrimination with a multiple band excitation filter. It is found to be easier to discriminate the different bead populations when the beads are more readily dispersed, which in turn, is linked to smaller bead-to-agarose solution volume ratios.

It is interesting to note in Figure 4.22 that, even though, the amount of compartments of one particular ligand class is highly restricted in number (1 to 3), the accumulation of signal in these isolated compartments is strong. Such strong measurable signal localized in a small volume element suggests that a relatively high concentration of compartments is not necessary in a single beaded ensemble. Instead, a careful selection of a highly stable hybridization DNA pair, design of optimized ligand immobilization protocols and proper preservation of ligand-immobilized ensembles may be used to refine the sensing capabilities.

The further demonstrate the multiplexing capabilities offered by the composite beads, an array containing both viral and microbial composite beads was assembled. Hybrid beads containing only 20-32 μm avidin coated beads were also prepared and included as control beads to monitor for non-specific background signal. Following the sequential delivery of all four complement targets with high stringency buffer wash between each target sequence, the identification of each target strand was made possible, Figure 4.23.

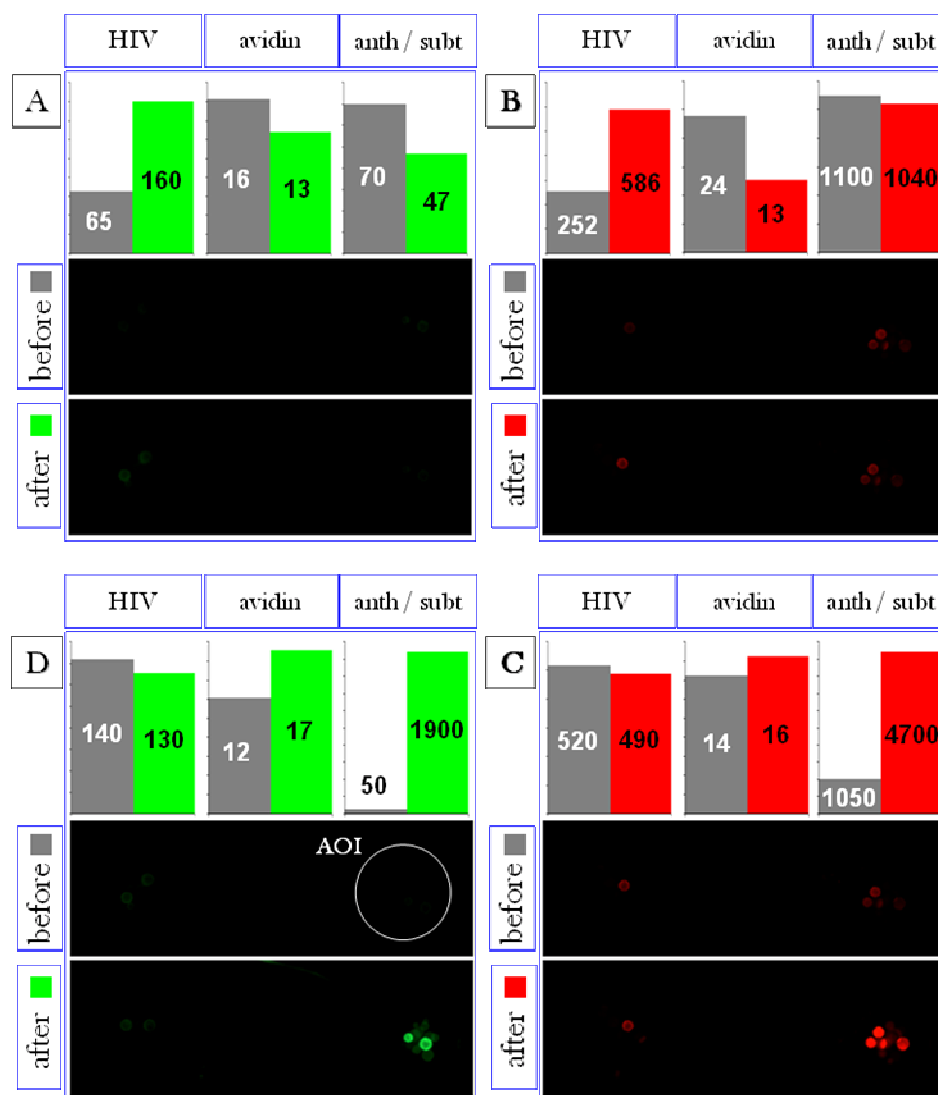


Figure 4.23. Development of fluorescence on the capture of bacteria and virus DNA targets by their complement sequences immobilized on beads. The intensity on the fluorescence signal is indicated by the number contained in the bars before (in gray) and after (green or red) the respective target was delivered. Sequential delivery of virus targets followed by bacteria targets is indicated from (A) to (D). Washing with high stringency buffer was performed between targets. The exposure on both green and red channel was set to 3.5 s. At 3.5 s exposure there initial fluorescence signal on the bacteria molecular beacons is not zero, but the increase on fluorescence intensity is pronounced confirming the capture of the respective DNA complements. Control beads containing avidin were included. The area of interest (AOI) for fluorescence measurement include the area defined by the hybrid beads.

The intensity in fluorescence signal was measured before and after the delivery of each target. The area of interest (AOI) for the fluorescence measurement was a circle delineating the perimeter of the hybrid beads. The exposure setting were set to 3.5 s for both green and red channels although the bacterial MBs show a noticeable background signal before the corresponding targets were delivered to the bead ensembles. Nevertheless, the bacterial MBs initial signal decreased during buffer washing steps. The exposure to the high stringency buffer promoted to some degree the association of the bacterial MB hairpin stems that were open in the absence of the complementary bacterial sequences.

In an additional assay, the development of signal intensity as a function of time was further explored during the delivery of the same complement targets to a microchip with both virus and bacteria hybrid beads, Figure 4.24. Upon the introduction of target T1 complementary to MB1, green fluorescence accumulates on the HIV hybrid beads, and a decrease in the green fluorescence of non-complement MB4 in bacteria hybrid beads is observed. The drop in intensity is indicative of MB4 stem region hybridization to form the hairpin structure. In the presence of T1, hybridization to non-complement MB4 is not significant even though there is initial MB4 beacon open. A similar behavior was observed in the red fluorescence channel for MB2 and MB3 during the delivery of T2 complementary to MB2.

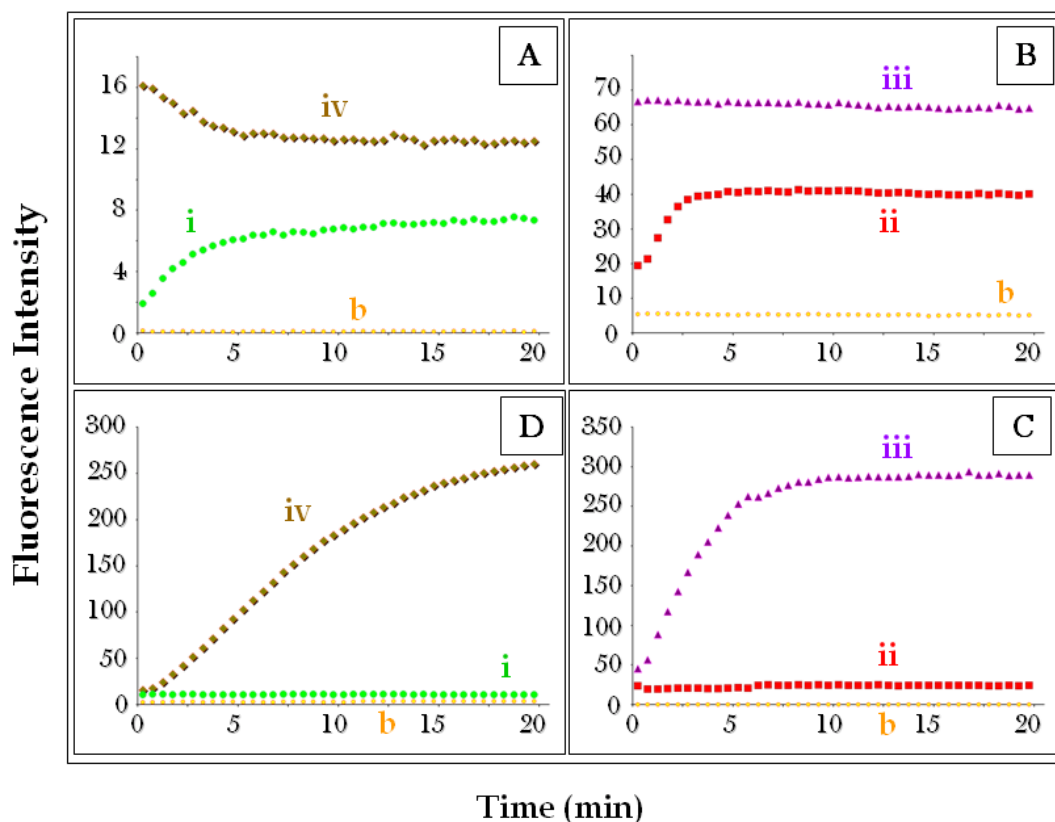


Figure 4.24. Fluorescence signal development during the hybridization of virus and bacterial targets to its corresponding molecular beacons. Fluorescence converted to 2.5 s exposure time. (A) Fluorescence signal development in green channel upon introduction of HIV sequence target T1: (i) hybridization to complementary sequence in beacon MB1, and (iv) discrimination from *Bacillus subtilis* MB4. The decrease in signal as a function of time is due to the association of stems in MB4. (B) Signal intensity during delivery of HIV sequence target T2: (ii) hybridization to complement beacon MB2, and (iii) discrimination from *Bacillus anthracis* MB3. There is also a reduction in fluorescence similar to MB3, not noticeable in the scale used. (C) Fluorescence development following delivery of target T3: (iii) hybridization to complement MB3, and (ii) discrimination from MB2. The signal in MB2 remains practically constant. (D) Signal intensity following the delivery of target T4: (iv) hybridization to complement MB4, and (i) discrimination from beacon MB1. A 15 to 20% reduction in the fluorescence of HIV MB1 and MB2 is observed at the end of the assay.

After buffer rinsing, green and red fluorescence for hybridizations increased in a factor of 4 and 2 relative to the initial signal HIV T1-MB1 and T2-MB2 respectively. Although a relatively small change in the signal was obtained, the gain is significant with respect to the background noise. Following the delivery of bacterial targets T3 and T4, a gain factor of 8 and 17 was measured for red and green fluorescence relative to the initial signal for T3-MB3 and T4-MB4 oligonucleotide associations respectively. In all four instances, when no matching target was delivered, it is noticed a loss of fluorescence during prolonged rinses. The drop in fluorescence is substantial in the T1-MB1/T2-MB2 hybrid beads because of the relatively weak signal obtained after the hybridization to their respective perfect oligonucleotide matches.

The fluorescence signal increase for the bacterial composite beads is considerably larger than the observed on the viral counterpart. The more intense signal obtained here is likely due to a number of causes including the design of the bacterial MB. The bacterial MBs target binding region includes the loop and part of the stem, Figure 4.25. During the bacterial target delivery, the target will hybridize to the loop up to the complementary fraction on the stem. Therefore, there is expected to be a competition for the shared stem fraction between the stem complement sequence, at the other end of the beacon, and the target. Once the target has bound to the shared stem fraction, it is less likely the hairpin structure will form again since part of the stem is occupied. On the other hand, the viral MBs hairpin structures contain a loop corresponding to the target binding region, and the self-complementary stems are dedicated only to the formation of the hairpin

structure. The stem regions tend to associate if they are free to interact. Incomplete hybridization or partial denaturation of the target-MB complex favors the tendency of stem regions to associate to form a stable hairpin structure.¹⁴⁸ As a result, the shared-stem bacteria MBs form more stable duplexes with their complement targets when compared to the conventional virus MBs. The lower stability of virus target-MB interaction contributes to the reduction of intensity signal after progressive rinse with bacterial solutions and washing buffer.¹³³

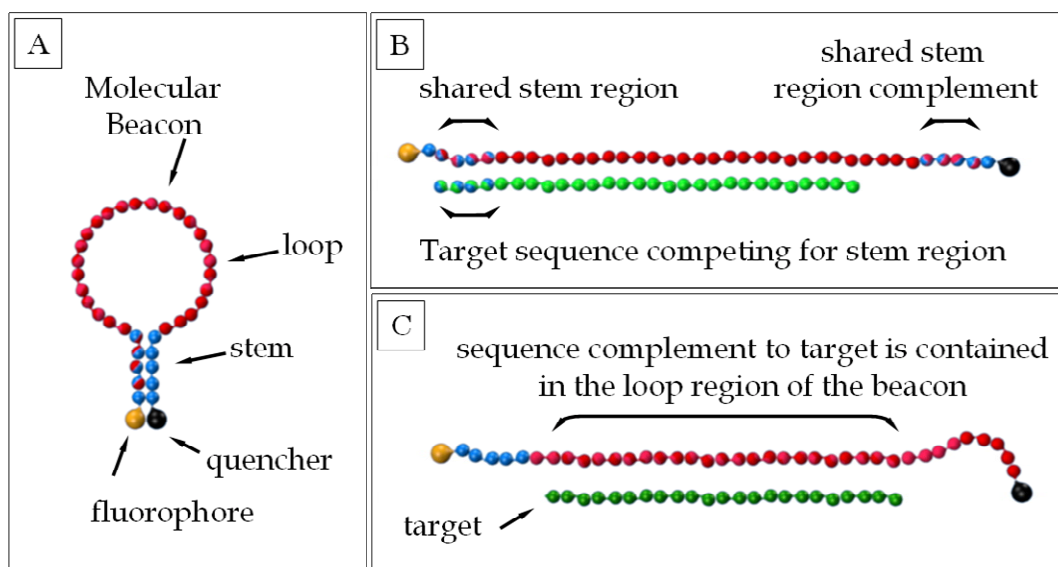


Figure 4.25. (A) DNA molecular beacon. (B) Stem in molecular beacon contains a region complementary to the target oligonucleotide. During hybridization the oligonucleotide competes against the shared stem region complement sequence. (C) The target complementary sequence is contained in the loop region of the hairpin molecular beacon. Both sides of the stem are free to hybridize. The bacterial DNA sequences were designed to contain a region complementary to the part of the stem of its respective molecular beacon.

The prospect of compartmentalized regions within a beaded element unit to assist on the detection of single nucleotide polymorphisms share similar features found in the conventional homogeneous beads. Both bead systems are able to

discriminate single point mutations of nucleic acids. The conventional beads offer larger capturing capacity due to its size and binding capacity relative to the minicompartments. In contrast, the minibead system accumulates in a small volume-element the captured analyte and hence the fluorescence signal. This in turn, translates into intense localized signal facilitating its detection. In addition, the development of fluorescence occurs rapidly since the non-reactive embedding media displays little interference towards the transfer of small sized analytes. Due to insufficient control in the number of compartments of one specific ligand class, quantification of signal as an aid to evaluate dose dependent analyte responses is still restrained. In the qualitative arena, on the other hand, the multicompartment ensemble is capable of sensing oligonucleotide solutions as low as 0.1 μM . It is certainly necessary to explore the detection limit of the ensembles and fine-tune the experimental conditions for the new system within the microarray platform.

An unusual observation associated with the multicompartment ensembles is that more than one separation event can be performed in a single beaded ensemble demonstrating a higher multiple analyte detection functionality level relative to the conventional beads. For the analysis of a mixture of analytes, here tested for three different DNA sequences, in the conventional beaded system three positions in the microarray are occupied. One multicompartment ensemble, on the other hand, takes over only one position in the microchip. It is this multiple analyte detection proficiency, within a single ensemble, the contrasting feature that sets it apart from the conventional systems.

4.4 SUMMARY

In this chapter, a number of novel bead reactor ensembles were created and characterized. Included here were the following major categories: core-shell beads, raspberry microspheres, macroporous polystyrene particles, and compartmentalized agarose microreactors in agarose microspheres. The systems afford additional functionality for integrated bead-based sensing applications that has not been available previously. While many new structures were created, based on physical properties, tolerance to non-specific binding and easy of fabrication, the microsphere incorporated into macrobeads based on agarose building blocks were used in DNA and protein detection applications. Those systems allowed for the rapid, sensitive and selective detection of proteins and oligonucleotides. The ability to detect three different analytes within a single bead ensemble allows for the expansion of the detection power and analytical capabilities of the bead based sensor system. Further, a number of interesting application areas might be envisioned for future work that may employ these multifunctional, multicompartment systems. These new application areas fall outside the scope of this dissertation work. Included here are clustering of antigens on single beads that may be associated with different diseases. For example, HIV diagnosis could be done more accurately if glycoproteins GP-120, GP-41 and GP-160 are detected simultaneously on the same bead using different colors.¹⁴⁹ Similarly, for hepatitis, hepatitis B surface antigen, hepatitis B core antigen and hepatitis B antibodies all can be detected simultaneously. For analysis of simple and complex sugars, various coupled enzymes can be envisioned to be included in color coded compartments.

Finally, cholesterol analysis using multiple, coupled enzymes could be imagined for purpose of completing lipid profile analysis.

References

- (1) Christodoulides, N.; Tran, M.; Floriano, P. N.; Rodriguez, M.; Goodey, A.; Ali, M.; Neikirk, D.; McDevitt, J. T. *Analytical Chemistry* **2002**, *74*, 3030-3036.
- (2) Curey, T. E.; Goodey, A.; Tsao, A.; Lavigne, J.; Sohn, Y.; McDevitt, J. T.; Anslyn, E. V.; Neikirk, D.; Shear, J. B. *Analytical Biochemistry* **2001**, *293*, 178-184.
- (3) Goodey, A.; Lavigne, J. J.; Savoy, S. M.; Rodriguez, M. D.; Curey, T.; Tsao, A.; Simmons, G.; Wright, J.; Yoo, S.-J.; Sohn, Y.; Anslyn, E. V.; Shear, J. B.; Neikirk, D. P.; McDevitt, J. T. *Journal of the American Chemical Society* **2001**, *123*, 2559-2570.
- (4) Lavigne, J. J.; Savoy, S.; Clevenger, M. B.; Ritchie, J. E.; McDoniel, B.; Yoo, S.-J.; Anslyn, E. V.; McDevitt, J. T.; Shear, J. B.; Neikirk, D. *Journal of the American Chemical Society* **1998**, *120*, 6429-6430.
- (5) Ali, M. F.; Kirby, R.; Goodey, A. P.; Rodriguez, M. D.; Ellington, A. D.; Neikirk, D. P.; McDevitt, J. T. *Analytical Chemistry* **2003**, *75*, 4732-4739.
- (6) McCleskey, S. C.; Floriano, P. N.; Wiskur, S. L.; Anslyn, E. V.; McDevitt, J. T. *Tetrahedron* **2003**, *59*, 10089-10092.
- (7) Christodoulides, N.; Mohanty, S.; Miller, C. S.; Langub, M. C.; Floriano, P. N.; Dharshan, P.; Ali, M. F.; Bernard, B.; Romanovicz, D.; Anslyn, E.; Fox, P. C.; McDevitt, J. T. *Lab on a Chip* **2005**, *5*, 261-269.
- (8) Rodriguez William, R.; Christodoulides, N.; Floriano Pierre, N.; Graham, S.; Mohanty, S.; Dixon, M.; Hsiang, M.; Peter, T.; Zavahir, S.; Thior, I.; Romanovicz, D.; Bernard, B.; Goodey Adrian, P.; Walker Bruce, D.; McDevitt John, T. *PLoS Med FIELD Full Journal Title: PLoS medicine* **2005**, *2*, e182.
- (9) Christodoulides, N.; Floriano, P. N.; Acosta, S. A.; Ballard, K. L. M.; Weigum, S. E.; Mohanty, S.; Dharshan, P.; Romanovicz, D.; McDevitt, J. T. *Clinical Chemistry (Washington, DC, United States)* **2005**, *51*, 2391-2395.
- (10) Floriano, P. N.; Christodoulides, N.; Romanovicz, D.; Bernard, B.; Simmons, G. W.; Cavell, M.; McDevitt, J. T. *Biosensors & Bioelectronics* **2005**, *20*, 2079-2088.
- (11) Goodey, A. P.; McDevitt, J. T. *Journal of the American Chemical Society* **2003**, *125*, 2870-2871.
- (12) Wiskur, S. L.; Floriano, P. N.; Anslyn, E. V.; McDevitt, J. T. *Angewandte Chemie, International Edition* **2003**, *42*, 2070-2072.

- (13) Morais, I. P. A.; Toth, I. V.; Rangel, A. O. S. S. *Spectroscopy Letters* **2006**, 39, 547-579.
- (14) Bangs, L. B. *Pure and Applied Chemistry* **1996**, 68, 1873-1879.
- (15) Molina-Bolivar, J. A.; Galisteo-Gonzalez, F. *Surfactant Science Series* **2004**, 116, 54-101.
- (16) Benecky, M. J.; Post, D. R.; Schmitt, S. M.; Kochar, M. S. *Clinical Chemistry (Washington, D. C.)* **1997**, 43, 1764-1770.
- (17) Nulens, E.; Bodeus, M.; Bonelli, F.; Soleti, A.; Goubau, P. *Clinical and Diagnostic Laboratory Immunology* **2000**, 7, 536-539.
- (18) Bizzaro, N.; Bonelli, F.; Tonutti, E.; Tozzoli, R.; Villalta, D. *Clinical and Diagnostic Laboratory Immunology* **2001**, 8, 922-925.
- (19) Elshal, M. F.; McCoy, J. P. *Methods (San Diego, CA, United States)* **2006**, 38, 317-323.
- (20) Rao, R. S.; Visuri, S. R.; McBride, M. T.; Albala, J. S.; Matthews, D. L.; Coleman, M. A. *Journal of Proteome Research* **2004**, 3, 736-742.
- (21) Pickering, J. W.; Martins, T. B.; Schroder, M. C.; Hill, H. R. *Clinical and Diagnostic Laboratory Immunology* **2002**, 9, 872-876.
- (22) Ortega-Vinuesa, J. L.; Bastos-Gonzalez, D. *Journal of Biomaterials Science, Polymer Edition* **2001**, 12, 379-408.
- (23) Molina-Bolivar, J. A.; Ortega-Vinuesa, J. L. *Langmuir* **1999**, 15, 2644-2653.
- (24) Molina-Bolivar, J. A.; Galisteo-Gonzalez, F.; Hidalgo-Alvarez, r. *Colloids and Surfaces, B: Biointerfaces* **1996**, 8, 73-80.
- (25) Cram, L. S. *Methods in Cell Science* **2002**, 24, 1-9.
- (26) Kellar, K. L.; Iannone, M. A. *Experimental Hematology (New York, NY, United States)* **2002**, 30, 1227-1237.
- (27) Kellar, K. L.; Douglass, J. P. *Journal of Immunological Methods* **2003**, 279, 277-285.
- (28) Kellar, K. L.; Kalwar, R. R.; Dubois, K. A.; Crouse, D.; Chafin, W. D.; Kane, B.-E. *Cytometry* **2001**, 45, 27-36.
- (29) Molina-Bolivar, J. A.; Galisteo-Gonzalez, F. *Journal of Macromolecular Science, Polymer Reviews* **2005**, C45, 59-98.
- (30) Molina-Bolivar, J. A.; Galisteo-Gonzalez, F.; Ortega-Vinuesa, J. L.; Schmitt, A.; Hidalgo-Alvarez, R. *Journal of Biomaterials Science, Polymer Edition* **1999**, 10, 1093-1105.
- (31) Nolan, J. P.; Mandy, F. *Cytometry, Part A* **2006**, 69A, 318-325.
- (32) Bonetta, L. *Nature Methods* **2005**, 2, 785-795.
- (33) Chapman, G. V. *Journal of Immunological Methods* **2000**, 243, 3-12.
- (34) Michael, K. L.; Taylor, L. C.; Schultz, S. L.; Walt, D. R. *Analytical Chemistry* **1998**, 70, 1242-1248.
- (35) Song, L.; Ahn, S.; Walt, D. R. *Analytical Chemistry* **2006**, 78, 1023-1033.

- (36) Epstein, J. R.; Lee, M.; Walt, D. R. *Analytical Chemistry* **2002**, 74, 1836-1840.
- (37) Walt, D. R. *Science (Washington, D. C.)* **2000**, 287, 451-452.
- (38) Rodriguez, W. R.; Christodoulides, N.; Floriano, P. N.; Graham, S.; Mohanty, S.; Dixon, M.; Hsiang, M.; Peter, T.; Zavahir, S.; Thior, I.; Romanovicz, D.; Bernard, B.; Goodey, A. P.; Walker, B. D.; McDevitt, J. T. *PLoS Medicine* **2005**, 2, 663-672.
- (39) Gottschalk, I.; Gustavsson, P.-E.; Ersson, B.; Lundahl, P. *Journal of Chromatography, B: Analytical Technologies in the Biomedical and Life Sciences* **2003**, 784, 203-208.
- (40) Gruber, H. E.; Hoelscher, G. L.; Leslie, K.; Ingram, J. A.; Hanley, E. N. *Biomaterials* **2006**, 27, 371-376.
- (41) Hjerten, S. *TrAC, Trends in Analytical Chemistry* **1984**, 3, 87-90.
- (42) Hjerten, S.; Eriksson, K. O. *Analytical Biochemistry* **1984**, 137, 313-317.
- (43) Makino, K.; Matsumoto, T.; Nakatsuji, Y.; Nagahara, S.; Takeuchi, T. *Chromatographia* **1987**, 23, 909-914.
- (44) Makino, K.; Ozaki, H.; Imaishi, H.; Takeuchi, T.; Fukui, T.; Hatano, H. *Chromatographia* **1987**, 23, 247-253.
- (45) Liao, J.-L.; Li, Y.-M.; Hjerten, S. *Analytical Biochemistry* **1996**, 234, 27-30.
- (46) Li, Y.-M.; Liao, J.-L.; Nakazato, K. i.; Mohammad, J.; Terenius, L.; Hjerten, S. *Analytical Biochemistry* **1994**, 223, 153-158.
- (47) Yao, K.; Hjerten, S. *Journal of Chromatography* **1987**, 385, 87-98.
- (48) Cuatrecasas, P. *Journal of Biological Chemistry* **1970**, 245, 3059-3065.
- (49) Cuatrecasas, P. *Nature* **1970**, 228, 1327-1328.
- (50) Labrou, N. E. *Journal of Chromatography, B: Analytical Technologies in the Biomedical and Life Sciences* **2003**, 790, 67-78.
- (51) Mondal, K.; Gupta, M. N. *Biomolecular Engineering* **2006**, 23, 59-76.
- (52) Winzor, D. J. *Journal of Biochemical and Biophysical Methods* **2001**, 49, 99-121.
- (53) Porath, J.; Carlsson, J.; Olsson, I.; Belfrage, G. *Nature (London, United Kingdom)* **1975**, 258, 598-599.
- (54) Mondal, K.; Gupta, M. N.; Roy, I. *Analytical Chemistry* **2006**, 78, 3499-3504.
- (55) Robinson, B. S.; Monis, P. T.; Dobson, P. J. *Applied and Environmental Microbiology* **2006**, 72, 5857-5863.
- (56) Ma, Z.-Y.; Guan, Y.-P.; Liu, H.-Z. *Reactive & Functional Polymers* **2006**, 66, 618-624.
- (57) Wang, J.; Peng, X.; Liu, D.; Bao, Y.; An, L. *Separation and Purification Technology* **2006**, 50, 141-146.
- (58) Denizli, A.; Piskin, E. *Journal of Biochemical and Biophysical Methods* **2001**, 49, 391-416.

- (59) Dufner, P.; Jermutus, L.; Minter, R. R. *Trends in Biotechnology* **2006**, *24*, 523-529.
- (60) Padoa, C. J.; Crowther, N. J. *Diabetes Research and Clinical Practice* **2006**, *74*, S51-S62.
- (61) Mallikaratchy, P.; Stahelin, R. V.; Cao, Z.; Cho, W.; Tan, W. *Chemical Communications (Cambridge, United Kingdom)* **2006**, 3229-3231.
- (62) Djordjevic, M.; Sengupta, A. M. *Physical Biology* **2006**, *3*, 13-28.
- (63) Goring, H. U.; Homann, M.; Lörger, M. *International Journal for Parasitology* **2003**, *33*, 1309-1317.
- (64) Garret-Flaudy, F.; Freitag, R. *Biotechnology and bioengineering* **2000**, *71*, 223-234.
- (65) Ghose, S.; Forde, G. M.; Slater, N. K. H. *Biotechnology Progress* **2004**, *20*, 841-850.
- (66) Lamla, T.; Stiege, W.; Erdmann, V. A. *Molecular and Cellular Proteomics* **2002**, *1*, 466-471.
- (67) Rao, S.; Zydner, A. L. *Journal of Membrane Science* **2006**, *280*, 781-789.
- (68) Chapman, M. D.; Keir, G.; Petzold, A.; Thompson, E. J. *Journal of Immunological Methods* **2006**, *310*, 62-66.
- (69) Ma, Z.; Kotaki, M.; Ramakrishna, S. *Journal of Membrane Science* **2005**, *265*, 115-123.
- (70) Hollman, A. M.; Christian, D. A.; Ray, P. D.; Galey, D.; Turchan, J.; Nath, A.; Bhattacharyya, D. *Biotechnology Progress* **2005**, *21*, 451-459.
- (71) Ding, Z.; Fong, R. B.; Long, C. J.; Stayton, P. S.; Hoffman, A. S. *Nature (London, United Kingdom)* **2001**, *411*, 59-62.
- (72) Hoffman, A. S. *Clinical Chemistry (Washington, D. C.)* **2000**, *46*, 1478-1486.
- (73) Teotia, S.; Lata, R.; Gupta, M. N. *Journal of Chromatography, A* **2004**, *1052*, 85-91.
- (74) Sharma, A.; Roy, I.; Gupta, M. N. *Biotechnology Progress* **2004**, *20*, 1255-1258.
- (75) Hilbrig, F.; Freitag, R. *Journal of Chromatography, B: Analytical Technologies in the Biomedical and Life Sciences* **2003**, *790*, 79-90.
- (76) Davalos-Pantoja, L.; Ortega-Vinuesa, J. L.; Bastos-Gonzalez, D.; Hidalgo-Alvarez, R. *Colloids and Surfaces, B: Biointerfaces* **2001**, *20*, 165-175.
- (77) Song, D.; Forciniti, D. *Journal of Colloid and Interface Science* **2000**, *221*, 25-37.
- (78) Ahmed, F.; Cole, K. D. *Separation and Purification Methods* **2000**, *29*, 1-25.
- (79) Wang, J.; Bhattacharyya, D.; Bachas, L. G. *Biomedical Diagnostic Science and Technology* **2002**, 381-392.
- (80) Vikholm-Lundin, I.; Albers, W. M. *Biosensors & Bioelectronics* **2006**, *21*, 1141-1148.

- (81) Kellar, K. L.; Oliver, K. G. *Methods in Cell Biology* **2004**, 75, 409-429.
- (82) Porath, J. O.; Janson, J. C.; (Exploaterings Aktiebolag T.B.F.). Application: DE, 1971, pp 26 pp.
- (83) Rees, D. A. *Biochemical Journal* **1972**, 126, 257-273.
- (84) Arnott, S.; Fulmer, A.; Scott, W. E.; Dea, I. C.; Moorhouse, R.; Rees, D. A. *Journal of molecular biology* **1974**, 90, 269-284.
- (85) Labropoulos, K. C.; Niesz, D. E.; Danforth, S. C.; Kevrekidis, P. G. *Carbohydrate Polymers* **2002**, 50, 393-406.
- (86) Lai, M. F.; Lii, C. *Int J Biol Macromol FIELD Full Journal Title:International journal of biological macromolecules* **1997**, 21, 123-130.
- (87) Mohammed, Z. H.; Hember, M. W. N.; Richardson, R. K.; Morris, E. R. *Carbohydrate Polymers* **1998**, 36, 15-26.
- (88) Pernodet, N.; Maaloum, M.; Tinland, B. *Electrophoresis* **1997**, 18, 55-58.
- (89) Maaloum, M.; Pernodet, N.; Tinland, B. *Electrophoresis* **1998**, 19, 1606-1610.
- (90) Normand, V.; Lootens, D. L.; Amici, E.; Plucknett, K. P.; Aymard, P. *Biomacromolecules* **2000**, 1, 730-738.
- (91) Hermanson, G. T.; Mallia, A. K.; Smith, P. K. *Immobilized Affinity Ligand Techniques*; Academic Press, Inc.: San Diego, CA, 1992.
- (92) Kusakawa, N.; Ostrovsky, M. V.; Garner, M. M. *Electrophoresis FIELD Full Journal Title:Electrophoresis* **1999**, 20, 1455-1461.
- (93) Labropoulos, K. C.; Niesz, D. E.; Danforth, S. C.; Kevrekidis, P. G. *Carbohydrate Polymers* **2002**, 50, 407-415.
- (94) Kohn, J.; Wilchek, M. *Biochem Biophys Res Commun FIELD Full Journal Title:Biochemical and biophysical research communications* **1982**, 107, 878-884.
- (95) Ayers, J. S.; Bethell, G. S.; Hancock, W. S.; Hearn, M. T. W.; (Development Finance Corp. of New Zealand, N. Z.). Application: DE 1978, pp 31 pp.
- (96) Gustavsson, P.-E.; Mosbach, K.; Nilsson, K.; Larsson, P.-O. *Journal of Chromatography, A* **1997**, 776, 197-203.
- (97) Gustavsson, P.-E.; Axelsson, A.; Larsson, P.-O. *Journal of Chromatography, A* **1999**, 830, 275-284.
- (98) Qing-Hong, S.; Xin, Z.; Yan, S. *Biotechnology and Bioengineering* **2005**, 92, 643-651.
- (99) Hjerten, S. *Biochimica et biophysica acta* **1964**, 79, 393-398.
- (100) <http://www.bioscience-beads.com>.
- (101) Rodriguez, M. D. Doctoral Dissertation, The University of Texas at Austin, 2003.
- (102) Porath, J.; Laas, T.; Janson, J. C. *Journal of chromatography* **1975**, 103, 49-62.

- (103) Hjerten, S.; Wu, B.; Liao, J. *Journal of Chromatography* **1987**, 396, 101-113.
- (104) Devlin, K. *Mathematics: The Science of Patterns*; Scientific American Library, 1994.
- (105) Sloane, N. J. A. *Nature (London)* **1998**, 395, 435-436.
- (106) Szpiro, G. G. *Kepler's Conjecture*; Wiley, 2003.
- (107) Afeyan, N. B.; Fulton, S. P.; Regnier, F. E. *Journal of Chromatography* **1991**, 544, 267-279.
- (108) Gustavsson, P.-E.; Larsson, P.-O. *Journal of Chromatography, A* **1996**, 734, 231-240.
- (109) Benson, J. R. *American Laboratory (Shelton, CT, United States)* **2003**, 35, 44-46, 48-52.
- (110) Li, N.-h.; Benson, J. R.; Kitagawa, N.; (Biopore Corporation, USA). Application: US, 1997, pp 17 pp, Cont -in-part of U S 15,583,162.
- (111) Hayashi, A.; Kanzaki, T. *Food Hydrocolloids* **1987**, 1, 317-325.
- (112) Cohen, A. L. *Scanning Electron Microscopy* **1977**, 10, 525-536.
- (113) Porakishvili, N.; Fordham, J. L. A.; Charrel, M.; Delves, P. J.; Lund, T.; Roitt, I. M. *Journal of Immunological Methods* **2000**, 234, 35-42.
- (114) Cammann, K.; Chemnitius, G.; Meusel, M.; Ross, B. *NATO ASI Series, Series 2: Environment* **1997**, 38, 185-194.
- (115) Natoli, L. *American Laboratory (Shelton, CT, United States)* **1993**, 25, 10.
- (116) Paitan, Y.; Biran, I.; Shechter, N.; Biran, D.; Rishpon, J.; Ron, E. Z. *Analytical Biochemistry* **2004**, 335, 175-183.
- (117) Savoy, S.; Lavigne, J. J.; Yoo, J. S.-J.; Wright, J.; Rodriguez, M.; Goodey, A.; McDoniel, B.; McDevitt, J. T.; Anslyn, E. V.; Shear, J. B.; Ellington, A.; Neikirk, D. P. *Proceedings of SPIE-The International Society for Optical Engineering* **1998**, 3539, 17-26.
- (118) Gustavsson, P.-E.; Larsson, P.-O. *Journal of Chromatography, A* **1999**, 832, 29-39.
- (119) Fulton, S. P.; Meys, M.; Varady, L.; Jansen, R.; Afeyan, N. B. *BioTechniques* **1991**, 11, 226-231.
- (120) Afeyan, N. B.; Gordon, N. F.; Mazsaroff, I.; Varady, L.; Fulton, S. P.; Yang, Y. B.; Regnier, F. E. *Journal of Chromatography* **1990**, 519, 1-29.
- (121) Shainoff, J. R. *Biochemical and biophysical research communications* **1980**, 95, 690-695.
- (122) Borch, R. F.; Bernstein, M. D.; Durst, H. D. *Journal of the American Chemical Society* **1971**, 93, 2897-2904.
- (123) Gu, W. Y.; Yao, H.; Huang, C. Y.; Cheung, H. S. *Journal of biomechanics* **2003**, 36, 593-598.
- (124) Tamada, Y.; Ikada, Y. *Nippon Kagaku Kaishi* **1985**, 2066-2072.
- (125) Kaufmann, M. *Journal of Chromatography, B: Biomedical Sciences and Applications* **1997**, 699, 347-369.

- (126) Cui, S. T. *Journal of Chemical Physics* **2005**, *123*, 054706/054701-054706/054704.
- (127) Barak-Shinar, D.; Rosenfeld, M.; Abboud, S. *Journal of the Electrochemical Society* **2004**, *151*, H261-H266.
- (128) Bard, A. J.; Faulkner, L. R. *Electrochemical Methods: Fundamentals and Applications*, 2nd Edition ed., 1980.
- (129) Chen, S.; Kucernak, A. *Journal of Physical Chemistry B* **2002**, *106*, 9396-9404.
- (130) Huang, J.-C. *International Journal of Polymeric Materials* **2004**, *53*, 577-586.
- (131) Crank, J. *The Mathematics of Diffusion*. 2d Ed, 1975.
- (132) Elaissari, A. *Colloidal Polymers: Synthesis and Characterization*. [In: *Surfactant Sci. Ser.*, 2003; 115], 2003.
- (133) Ali, M. F. Doctoral Dissertation, The University of Texas at Austin, Austin, 2006.
- (134) Gregory, S. G.; Barlow, K. F.; McLay, K. E.; Kaul, R.; Swarbreck, D.; Dunham, A.; Scott, C. E.; Howe, K. L.; Woodfine, K.; Spencer, C. C. A.; Jones, M. C.; Gillson, C.; Searle, S.; Zhou, Y.; Kokocinski, F.; McDonald, L.; Evans, R.; Phillips, K.; Atkinson, A.; Cooper, R.; Jones, C.; Hall, R. E.; Andrews, T. D.; Lloyd, C.; Ainscough, R.; Almeida, J. P.; Ambrose, K. D.; Anderson, F.; Andrew, R. W.; Ashwell, R. I. S.; Aubin, K.; Babbage, A. K.; Bagguley, C. L.; Bailey, J.; Banerjee, R.; Beasley, H.; Bethel, G.; Bird, C. P.; Bray-Allen, S.; Brown, J. Y.; Brown, A. J.; Bryant, S. P.; Buckley, D.; Burford, D. C.; Burrill, W. D. H.; Burton, J.; Bye, J.; Carder, C.; Chapman, J. C.; Clark, S. Y.; Clarke, G.; Clee, C.; Clegg, S. M.; Cobley, V.; Collier, R. E.; Corby, N.; Coville, G. J.; Davies, J.; Deadman, R.; Dhimi, P.; Dovey, O.; Dunn, M.; Earthrowl, M.; Ellington, A. G.; Errington, H.; Faulkner, L. M.; Frankish, A.; Frankland, J.; French, L.; Garner, P.; Garnett, J.; Gay, L.; Ghorri, M. R. J.; Gibson, R.; Gilby, L. M.; Gillett, W.; Glithero, R. J.; Grafham, D. V.; Gribble, S. M.; Griffiths, C.; Griffiths-Jones, S.; Grocock, R.; Hammond, S.; Harrison, E. S. I.; Hart, E.; Haugen, E.; Heath, P. D.; Holmes, S.; Holt, K.; Howden, P. J.; Hunt, A. R.; Hunt, S. E.; Hunter, G.; Isherwood, J.; James, R.; Johnson, C.; Johnson, D.; Joy, A.; Kay, M.; Kershaw, J. K.; Kibukawa, M.; Kimberley, A. M.; King, A.; Knights, A. J.; Lad, H.; Laird, G.; Langford, C. F.; Lawlor, S.; Leongamornlert, D. A.; Lloyd, D. M.; Loveland, J.; Lovell, J.; Lush, M. J.; Lyne, R.; Martin, S.; Mashreghi-Mohammadi, M.; Matthews, L.; Matthews, N. S. W.; McLaren, S.; Milne, S.; Mistry, S.; Moore, M. J. F. M.; Nickerson, T.; O'Dell, C. N.; Oliver, K.; Palmeiri, A.; Palmer, S. A.; Pandian, R. D.; Parker, A.; Patel, D.; Pearce, A. V.; Peck, A. I.; Pelan, S.; Phelps, K.; Phillimore, B. J.; Plumb, R.; Porter, K. M.; Prigmore, E.; Rajan, J.; Raymond, C.; Rouse, G.; Saenphimmachak, C.; Sehra, H. K.; Sheridan, E.; Shownkeen, R.; Sims, S.;

- Skuce, C. D.; Smith, M.; Steward, C.; Subramanian, S.; et al. *Nature (London, United Kingdom)* **2006**, *443*, 1013.
- (135) Hirschhorn Joel, N. *Pediatr Res FIELD Full Journal Title:Pediatric research* **2005**, *57*, 74R-77R.
- (136) McDermott, D. H.; Yang, Q.; Kathiresan, S.; Cupples, L. A.; Massaro, J. M.; Keaney, J. F.; Larson, M. G.; Vasan, R. S.; Hirschhorn, J. N.; O'Donnell, C. J.; Murphy, P. M.; Benjamin, E. J. *Circulation* **2005**, *112*, 1113-1120.
- (137) Silverman, E. S.; Liggett, S. B.; Gelfand, E. W.; Rosenwasser, L. J.; Baron, R. M.; Bolk, S.; Weiss, S. T.; Drazen, J. M. *Pharmacogenomics Journal* **2001**, *1*, 27-37.
- (138) Pearce, C. L.; Hirschhorn, J. N.; Wu, A. H.; Burt, N. P.; Stram, D. O.; Young, S.; Kolonel, L. N.; Henderson, B. E.; Altshuler, D.; Pike, M. C. *Journal of the National Cancer Institute* **2005**, *97*, 51-59.
- (139) Kwok, P. Y.; Gu, Z. *Molecular Medicine Today* **1999**, *5*.
- (140) Drazen, J. M.; Yandava, C. N.; Dube, L.; Szczerback, N.; Hippensteel, R.; Pillari, A.; Israel, E.; Schork, N.; Silverman, E. S.; Katz, D. A.; Drajesk, J. *Nat Genet FIELD Full Journal Title:Nature genetics* **1999**, *22*, 168-170.
- (141) Bailey, D.; Zanders, E.; Dean, P. *Pharmacogenomics Journal* **2001**, *1*, 38-47.
- (142) Landegren, U.; Nilsson, M.; Kwok, P. Y. *Genome Res FIELD Full Journal Title:Genome research* **1998**, *8*, 769-776.
- (143) Dunbar, S. A. *Clinica Chimica Acta* **2006**, *363*, 71-82.
- (144) Wang, J.; Chatrathi, M. P. *Analytical Chemistry* **2003**, *75*, 525-529.
- (145) Effenhauser, C. S.; Paulus, A.; Manz, A.; Widmer, H. M. *Analytical Chemistry* **1994**, *66*, 2949-2953.
- (146) Taton, T. A.; Lu, G.; Mirkin, C. A. *J Am Chem Soc FIELD Full Journal Title:Journal of the American Chemical Society* **2001**, *123*, 5164-5165.
- (147) Peterson, A. W.; Heaton, R. J.; Georgiadis, R. M. *Nucleic Acids Res FIELD Full Journal Title:Nucleic acids research* **2001**, *29*, 5163-5168.
- (148) Tsourkas, A.; Behlke, M. A.; Bao, G. *Nucleic Acids Research* **2002**, *30*, 4208-4215.
- (149) Tomiyama, T.; Lake, D.; Masuho, Y.; Hersh, E. M. *Biochem Biophys Res Commun FIELD Full Journal Title:Biochemical and biophysical research communications* **1991**, *177*, 279-285.

Vita

Jorge Wong was born in Lima, Perú on October 24, 1970, the third child of Elena Chong and Juan José Wong. He spent most of his childhood in Quito, Ecuador where he finished high school at Colegio La Salle. He moved back to Perú, attended the Pontificia Universidad Católica del Perú and graduated with a Science Bachelor degree in Chemistry. He joined the research laboratory of Professor John T. McDevitt at the University of Texas at Austin towards a doctoral degree in Chemistry.

Permanent address: 5809 N. 1st Lane, McAllen, TX 78504

This dissertation was typed by the author.